ISSN 0503-1540

Tome 38 *December 2000* Numéro 4

La mer

うみ

The Proceedings of the 5th International Marine Science Symposium
on the Physical, Biological, Chemical and Geological Processes
in the Pacific Ocean and Asian Marginal Seas
(The tenth PAMS/JECSS Workshop)
7-9 October 1999, Kagoshima, Japan

2000年12月

日仏海洋学会

La Société franco-japonaise
d'océanographie
Tokyo, Japon

SOCIETE FRÀNCO-JAPONAISE D'OCEANOGRAPHIE

Cimité de Rédaction

(de o'exercice des années de 2000 et 2001)

Note pour la présentation des manuscrits

La mer, organe de la Sociét franco-japonaise d'océanographie, publie des articles et notes originaux, des articles de synthèse, des analyses d'ouvrages et des informations intéressant les membres de la société. Les sujets traités doivent avoir un rapport direct avec l'océanographie générale, ainsi qu'avec les sciences halieutiques.

Les manuscrits doivent étre présentés avec un double, et dactylographiés, en *double interligne*, et au recto exclusivement, sur du papier blanc de format A4 (21×29.7 cm). Les tableaux et les légendes des figures serount regroupés respectivement sur des feuilles séparées à la fin du manuscrit.

Le manuscrit devra étre présenté sous la forme suivante:

1° Il sera écrit en japonais, français ou anglais. Dans le cadre des articles originaux, il comprendra toujours le résumé en anglais ou français de *200 mots* environs. Pour les textes en langues européennes. il faudra joindre en plus le résumé en japonais de *500 letters* environs. Si le manuscrit est envoyé par un non-japonophone, le comité sera responsable de la rédaction de ce résumé.

2° La présentation des articles devra étre la méme que dans les numéros récents; le nom de l'auteur précédé du prénom *en entier*, en minuscules; les symboles et abréviations standards autorisés par le cometé; les citations bibliographiques seront faites selon le mode de publication: article dans une revue, partie d'un livre, livre entier, etc.

3° Les figures ou dessins originaux devront étre parfaitement nettes en vue de la réduction nécessaire. La réduction sera faite dans le format 14.5×20.0 cm.

La premiére épreuve seule sera envoyée à L'auteur pour la correction.

Les membres de la Société peuvent publier 7 pages imprimées sans frais d'impression dans la mesure à leur manuscrit qui ne demande pas de frais d'impression excessift (pour des photos couleurs, par exemple). Dans les autres cas, y compris la présentation d'un non-membre, tous les frais seront à la charge de l'auteur.

Cinquante tirés-à-part peuvent étre fournis par article aux auteurs à titre gratuit. On peut en fournir aussi un plus grand nombre sur demande, par 50 exemplaires.

Les manuscrits devront étre adressés directement au directeur de publication de la Société: Y. YAMAGUCHI, Université des Péches de Tokyo, Konan 4-5-7, Minato-ku, Tokyo, 108 Japon; ou bien au rédacteur étranger le plus proche: H. J. CECCALDI, EPHE, Station marine d'Endoume, rue Batterie-des-Lions, 13007 Marseille, France; E. D. GOLDBERG, Scripps Institution of Oceanography, La Jolla, California 92093, Etats-Unis; ou T. R. PARSONS, Institute of Ocean Sciences, P.O.Box 6000, 986OW, Saanich Rd., Sidney, B. C., V8L 4B2, Canada.

The Proccedings of

the 5th International Marine Science Symposium on

the Physical, Biological, Chemical and Geological Processes

in the Pacific Ocean and Asian Marginal Seas

(the tenth PAMS／JECSS Workshop)

7-9 October 1999, Kagoshima, Japan

Guest Editors:

Akio Maeda(Faculty of Engineering, Kagoshima University)

Hiroshi Ichikawa(Faculty of Fisheries, Kagoshima University)

Associate Editors:

Venkataramana Katta, Hiroyuki Kikukawa, Hirohiko Nakamura, Ayako Nishina,

Kimihiko Ohki, Masahito Sakurai, Michio Sato, and Katsutoshi Tomita

Preface

Akio MAEDA and Hiroshi ICHIKAWA

The proceedings contains selected papers of the Tenth PAMS (Pacific Asian Mariginal Seas) and JECSS (Japan and East China Seas Studies) Workshop, held on 7–9 October 1999 at the Inamori Auditorium, Kagoshima University, Kagoshima, Japan, as a part of the 5th International Marine Science Symposium on the Physical, Biological, Chemical and Geological Processes in the Pacific Ocean and Asian Marginal Seas. The workshop was organized by Profs. Akio MAEDA (chairperson), Hiroshi ICHIKAWA(Secretary General), Toshihiro ICHIKAWA, Kimihiko OHKI, Takakazu OZAWA, and Masahito SAKURAI of Kagoshima University, and Profs. Tetsuo YANAGI and Jong-Hwan YOON of Kyushu University. The workshop was sponsored by Kagoshima University, Japan Marine Science Foundation, Japan Marine Science and Technology Center, Ministry of Education, Science, Sport and Culture, Japan, and Kawatetsu Techno-Construction Co., LTD. Efforts of the local committee successfully organizing both the scientific and social programmes were greatly appreciated by all participants.

A book of extended abstracts of ninety papers (fourty five for oral sessions, thirty six for poster sessions, and nine for extended abstract only) was distributed at the workshop. These papers reflect the growing interests in physical, biological, chemical and geological oceanography of the Pacific Asian marginal seas and the Pacific Ocean. Participants at the tenth workshop submitted thirteen papers to this Proceedings and ten papers were finally accepted after peer reviews. We are very thankful to fifteen referees, whose comments and criticism were so helpful to improve most of papers in this volume.

We express our thanks to Prof. H. SUDOU, the president of Société franco-japonaise d'océanographie, and Prof. Y. YAMAGUCHI, the Editor-in-Chief of La mer, for their help to publish this volume in La mer.

(Guest Editors, Kagoshima University)

La mer 38 : 167-172, 2000
Société franco-japonaise d'océanographie, Tokyo

Introduction: the Physical, Biological, Chemical and Geological Processes in the Pacific Ocean and Asian Marginal Seas

Hiroshi ICHIKAWA* and Akio MAEDA**

Since the first Japan and East China Sea Studies(JECSS) Workshop was convened on 1-4 June 1981 at Tsukuda University by joint convenership of Dr. Kenzo TAKANO (Prof. Emeritus of the University at persent) and late Prof. Takashi ICHIYE of Taxas A&M University, JECSS Workshop has been held once in every two years. Its purposes were initially to exchange knowledge on research activity and to discuss research results on the physical aspects of the Japan and East China Seas under the unfortunate political circumstances among countries around the Japan and East China Seas. For responding to increase in demand for better understanding of global change of marine environment, its scope was expanded to include the physical, biological, chemical and geological aspects of the Pacific Asian Marginal Seas, and the name of the workshop has been changed to PAMS / JECSS Workshop since 1993 at Qingdao, China. Succeeding the ninth PAMS/JECSS Workshop held on 22-24 September 1997 at Taipei, Taiwan, the tenth PAMS/JECSS Workshop was held on 7-9 October 1999 at the Inamori Auditorium, Kagoshima University, Kagoshima, Japan, as a part of the 5th Internatinal Marine Science Symposium on the Physical, Biological, Chemical and Geological Processes in the Pacific Ocean and Asian Marginal Seas of Japan Marine Science Foundation.

It is an urgent task to fix the plans for keeping the marine environment appropriate for whole future human beings. Materials discharged locally into coastal seas, are spreading globally after passing through the marginal seas. In order to predict the global change of marine environment, it is crucial to estimate the amount of materials discharged into coastal seas and elucidate the physical, biological, chemical and geological processes in the marginal seas. The objectives of this workshop was to provide a forum to review the status of oceanographic research on the various processes in the Pacific Ocean and Asian marginal seas and their role in the global change of marine environment.

A total of one hundred and two persons participated in the workshop. Among them, 47 were from Japan, 29 from Korea, 8 from U.S.A, 7 from China (Beijing), 7 from China (Taipei), 2 from Indonesia, 1 from Malaysia, and 1 from Russia. The workshop consisted of 11 sessions for oral presentations together with 2 poster sessions. Number of papers on the Tushima Starit, South Sea of Korea, and Japan (East) Sea including oral and poster presentations was the maximum of twenty one, followed by 13 papers on the Kuroshio in the regions from near Taiwan to south of Japan, and 11 papers on the coastal ocean.

It is our pleasure that this workshop contributed largely to improvements of our understanding of spatial and temporal variation processes of marine environment in each of the Asian marginal seas as mentioned in the following summary reports.

Session 1. South China Sea

South China Sea (SCS) is the largest marginal sea in the world. Its water interacts with the Kuroshio and the surrounding seas,

* Faculty of Fisheries, Kagoshima University, 4-50-20 Shimoarata, Kagoshima, 890-0056, Japan
** Faculty of Engineering, Kagoshima University, 1-21-40 Korimoto, Kagoshima, 890-0065, Japan

including the Philippines Sea, the East China Sea, the Sulu Sea and the Jawa Sea, etc. Recently there have been some studies on their interaction and the water exchange. In the 10th PAMS/JECSS workshop, the first session was devoted to the studies of the SCS with four oral presentations. (1) Y. HSUEH presented a model to calculate the topography-forced current difurcation. The model explained dynamically the formation of the perennial South China Sea Warm Current (SCSWC). (2) T. YANAGI used the satellite altimetric data to estimate the horizontal distribution of sea surface dynamic topography and obtained the eddies and the seasonally averaged circulation patterns in the SCS. (3) Based on the water mass analysis, T. NAMBA discussed the circulation in the SCS in winter and summer. (4) A. K. LIU discussed the nonlinear internal waves in the SCS, based mainly on synthetic aperture radar observations and mooring measurements.

The following are some of the unsolved problems, which should be studied further in the future. (1) On the Kuroshio intruded into the SCS through Bashi Channel, there are different views. Some scientists considere that there is a branch of the Kuroshio intruding into the SCS, which is called to be as the South China Sea Branch of the Kuroshio. However, other scientists consider that the Kuroshio has no direct branch intruding into the SCS and there is a stronger southwestward flow near the Dongsha Islands, which is a part of the circulation in the north eastern part of the SCS. (2) There is a seasonal change in the circulation in the SCS. We must elucidate their dynamic mechanism. (3) There are a lot of warm and cold eddies with seasonal change in the SCS. We must show the dynamical causes of their change. (4) In contrast with the upper circulation in the SCS, there have been few studies on the deep circulation in the SCS which differs from that in the upper layer.

(reported by Y. YUAN, Second Institute of Oceanography, SOA)

Session 2. Kuroshio near Taiwan

C. T. LIU presented results from 11 hydrographic and acoustic Doppler current profiler (ADCP) surveys for measuring the volume transport of the Kuroshio through the East Taiwan Channel. These results provide the first definitive estimations of Kuroshio transport in the area. The variability in the transport detected in the ADCP monitoring program across PCM-1 of WOCE suggests the influence of open ocean eddies. The eddy/Kuorshio interaction is invoked to explain the migration path of sea turtles. YUAN *et al.* perform inverse calculation on density sections from a number of hydrographic surveys in an expanded area east of Taiwan and west of the Ryukyu Islands. The Kuroshio transport estimates east of Taiwan are generally 10 Sv or more greater than that through the East Taiwan Channel. Those west of the Ryukyu Islands are similar to those reported by C. T. LIU, suggesting the diversion of part of the Kuroshio transport to east of the Ryukyu Islands. LIU and YUAN, in the fourth paper in the session, show that a northeastward flow of 12 Sv is indeed found east of the Ryukyu islands. Multiple current cores with alternating directions are also present. Xinyu GUO uses a series of nested numerical (POM) models of the North Pacific Ocean to focus on the volume transport through the Taiwan Strait, a parameter of strategical importance in the oceanography of the marginal seas around Taiwan. The average for 1992-98 is 1.9 Sv northward with a root-mean-square value of 1 Sv. In view of a prolonged absence of any measurement due to the difficult political situations in the Taiwan Strait, this result can be considered as the best estimate to date and points to the value of numerical models.

Of the four poster papers, MANDA *et al.* describe upwelling of subsurface Kuroshio water onto the East China Sea shelf. The concentration of seeded (350-450 m) particles in the lower half of the shelf water column seems to suggest a general foreshortening of water column in the meander. Anticyclonic vorticity must be generated. Isobe performs interesting numerical experiments to show that the branching of the Kuroshio southwest of Kyushu depends upon the amount of water allowed to leave the East China Sea through the Tokara Strait. NAKAMURA *et al.* provide evidence for a cyclonic circulation in the deep layers in the northern part of the Okinawa Trough, just

below the anticyclonic flow of the Kuroshio. YAMASHIRO *et al.* examine the flow and temperature distibution in the Tokara Strait and relate them to the path fluctuations of the Kuroshio.

All in all, except for the flow in the Luzon Strait, a paradigm of the Kuroshio flow around Taiwan appears to emerge. The diversion to the east of Ryukyu seems to make sense. Meanders of the Kuroshio allows the subsurface Kuroshio water to encroach onto the shelf. It is hopeful that, the next time around, a complete picture of the Kuroshio around Taiwan may be a possibility.

(reported by Y. HSUEH, Florida State Univ.)

Session 3. Kuroshio in the East China Sea

There are two oral and six poster presentations in this session. The oral presentations are on the spatial and temporal variation of Kuroshio in the East China Sea. From the data of surface drifter and hydrographic surveys, H. -J. LIE concluded that the eddies and Kuroshio frontal movements are closely related, and that the shoreward cyclonic movement is associated with the upwelling of the slope water. He also found that the downstream propagation speed is 20 km/day for meander of wavelength 100 km and amplitude 15 km. S. MIZUNO used two years long moored current meter data combined with hydrography and wind forcing analysis to conclude that the Ekman dynamics is the controlling mechanism on the shoaling of the mixed layer of Kuroshio in the Summer and Fall. Both above conclusions were also reached by Taiwanese oceanographers on the study of Kuroshio near Taiwan.

In the poster session, six more papers related to the above topics : (1)The upwelling associated with Kuroshio was verified with diagnostic models by A. MANDA *et al.* ; (2) A. ISOBE also used diagnostic models to discuss the generation mechanism on the branching of Kuroshio near Japan that started near Taiwan ; (3) H. NAKAMURA *et al.* studied the variation of the deep water in the Northern Okinawa Trough and found that its variation is strongly related to the variation of Kuroshio water near the surface layer ; (4) the Kuroshio variation influences the coastal water movement further downstream in the Tokara Strait by T. YAMASHIRO *et al.*, southwest of Tokara Strait by H. ICHIKAWA *et al.*, and south of Shikoku by M. KASHIMA *et al.*

All of these papers demonstrated that the phenomena on the Kuroshio variation is similar from Taiwan to Japan and Korea, and the physics that governs the Kuroshio variation should be very similar. PAMS/JECSS provided an unique opportunity for the local oceanographers to exchange their findings and research ideas on oceanography of this region.

(reported by C. -T. LIU, National Taiwan Univ.)

Session 4: Yellow and East China Seas

The session composed of two oral presentations (one invited) and four posters, dealing with tide and tidal current, circulation and biogeochemical aspects in the continental shelf area of the Yellow and East China Seas: two papers for tide and tidal current, two for circulation, one for biogeochemical process.

Invited speaker, B. H. CHOI, has evaluated modification of the Yellow Sea tidal regime by tidal barrier construction in the western coastal area of Korea. Significant perturbations of the order of 20 cm in sea level and 10 cm/s in current were expected in the neighbourhood of the barrier and they affect not only the whole Yellow Sea tidal regime, but also the marine environmental system related to the tide such as sediment distribution and suspended matters. J. -J. HUNG presented recycling of organic matters using intensive data collected in the southwestern East China Sea.

In the poster session, new findings and methods were presented ; (1) M2 current of the Yellow Sea was estimated from Lagrangian drifter, (2) annual cycling motion of fresh coastal water in the southern Yellow Sea was clearly suggested based on intensive hydrographic data, (3) Stratified tidal current in summer was numerically investigated, (4) a 3-D circulation model was applied to simulate basic oceanographic features in the Yellow and East China Seas.

Number of presentation is limited, compared to previous PAMS/JECSS Workshops. However, scientific level and understanding are much improved, with many new findings.

(reported by H. J. LIE, KORDI)

Session 5: Tushima Strait and South Sea of Korea

Recent obervations of CTD and direct currents in the sea between the Cheju Strait and the western channel of the Korea/Tsushima Strait indicate a large fluctuation of water propeties and currents on various time scales. However, all observations show that the eastward transport through the Cheju Starit accounts for a significant portion of the transport in the western channel of the Korea/Tsushima Strait. A coastal current along the Korean coast is uncertain as observations do not agree in its direction. A continuous program is neccessary in future to understand the variability of the current system in this system in this area, which determine the inflow condition for the Tsushima Current.

(reported by K. KIM, Seoul National Univ.)

Session 6 and 7. Japan/East Sea I and II

The analysis of satellite and modern and historical field data and numerical simulations provided new insight into the variability of the JES circulation (flow and mass fields) on time scales ranging from the atmospheric mesoscale and synoptic scale to seasonal, interannual, and interdecadal. For example, K. -H. CHO simulated the interaction of the Korean seabreeze/landbreeze system with coastal topography and the coastal marine boundary layer, resulting in strong atmospheric forcing of coastal waters. C. N. MOOERS forced JES-POM with Siberian cold-air-outbreaks simulated by a mesoscale atmospheric model (MM5) to study synoptic scale, event-driven wintertime convection, and additionally found that basin-scale sea surface height and transport oscillations were generated. A. MORIMOTO used several years of satellite altimeter data to describe the space-time evolution of JES currents and mesoscale variability in several subdomains, finding a common spectural peak of 50 days and typical eddy lifetimes of 9 months. H. HASE examined 27 years of monthy hydrographic transects to describe the seasonal evolution of the thermal wind and, thus, map the pathway of the First and Second Branches of the TWC, finding that the First(Nearshore) Branch flows inside the 200 m isobath from the eastern T/K Strait to Tsugaru Statit, the Second(Middle) Branch flows from the western T/K Strait seaward of the 200m isobath, presumably to Soya Strait, and the First Branch has a summer maximum that translates downstream at the rate of 7 km/d. Y. H. SEUNG simulated intrinsic interannual variability (due to dynamical instability of the subpolar jet sytem) on time scales of several years, finding, with steady throughflow-forcing plus no-wind-forcing versus wind-forcing cases, that wind-forcing drastically changed the character of the Subpolar Jet meanders and eddy-shedding and reduced the intensity of internnual variability.

K. KIM used high quality and high resolution CTD and DO data from CREAMS winter cruises off Vladivostok to demonstrate that low salinity, low temperature water was present in the outcrop zone in the western Japan Basin for low salinity Intermediate Water formation and sinking beneath the Subpolar Front to 200 to 400 m, while high salinity Intermediate Water was formed in the eastern Japan Basin. C.-W. SHIN analyzed MMO&KORDI historical hydrographic data to trace the wintertime formation off Vlaidvostok and North Korea, summertime spreading to Ulleung Basin, and autumnal dissipation of the salinity minimum of the low salinity Intermediate Water. H. KAWAMURA simulated the influence on JES of global atmospheric warming that began 50 years ago and found that JES swiched from Deep to Intermediate Water formation about 40 years ago, and that cyclonic wind stress curl off Vladivostok, together with low salinity, low temperature water from the Amur River, plays an important role in cyclonic circulation generation and Intermediate Water formation there. S. IKEDA simulated the JES marine ecosystem and biogeochemistry, taking into account organic carbon loading from land and regional economic development and global warming scenarios, and finding that the transport of organic carbon to the middle and deep layers may decrease, which would decrease the DO in the upper layer, but longer computations are needed for better confidence. Overall, new and old data, and complex and simple models,

are addressing overlapping questions in the JES, whose answers have major implications for the design of future monitoring and modeling systems, scientific research and societal policy agendas.

(reported by C. N. MOOERS, Univ. of Miami)

Session 8. Instruments

Five papers were presented in Section 8 on the applications of advanced technology in studying the Pacific Asian Marginal Sea. W. T. LIU presented an invited paper on using various combinations of spacebased sensors, including Quik SCAT, TRMM, Topex/Poseidon, SSMI, and AVHRR. These data were used to study the interplay between the dynamics and hydrologic parameters in typhoons Olga which landed on Korea, the monsoons in the South China Sea and their relation with ENSO, and El Niño modification of decadal anomalies in the North Pacific. He also used an image of the evolving typhoon Dan to introduce an information system, which processes, displays, and disseminates data in near real-time. Two papers on H. F. Radar were presented. S. FUJII developed a long-range instrument that can observe the Kuroshio from land. D. BARRICK presented a compact, low-cost, and easy-to-deploy radar, and S. RAMP discussed its scientific application at a number of locations around the world. There were also two papers on acoustic tomography. S. OH presented an experiment using explosive charge in deep water and a vertical line array as receiver to map the profile of temperature perturbation. H. YAMAOKA presented a system composed of five moored acoustic transcevers and a ship monitor, and the measurement of the tidal vortex. The result suggest powerful new technology in future scientific pursue in the PAMS/JECSS Program.

(reported by W. T. LIU, JPL)

Session 9. North Pacific Ocean and its Marginal Sea

Three papers by oral presentation relating to simulation of ocean circulation using GFDL Modular Codes were made in session 9. First invited paper by Y. MASUMOTO deals with the simulation of internnual variations of the Indonesian through flow using the dataset of ERS scatterometer and NOAA/NESDIS for surface heat flux during 1992–1997 with model coverage of the Indian and Pacific Oceans. Despite a raised question regarding the suitability of a half-degree horizontal grid resolution of the model for resolving the complex geometry and narrow passages for flow through the Indonesian Archipelgago, simulated interannual variations were consistent with observation. Author suggested further observations and additional modeling studies with fine grid resolution models of various kinds. Second paper by D. XU *et al.* deals with simulation of the seasonal change of the Kuroshio using climatological dataset of Hellerman and Levitus. Model simulations were performed prognostically as temperature and salinity restored for the surface boundary condition. Last paper by Z. WEI *et al.* deals with a diagnostic circulation study on the world ocean circulation. There were suggestions to carefully examine the restoring time scale for diagnostic experiments.

There were also seven poster presentations. M. KUBOTA and H. TOMITA: Satellite derived turbulent heat flux extimation over western North Pacific with satellite data, SSM/I and NCEP and also COADS and results had higher resolution on time and space. B. H. CHOI *et al.* indicated further necessity of establishing global tidal current dataset to improve regional and global dissipation of the M2 tide to complete the balancing of energy in the model. Paper by Z. YUAN *et al.* have dealt the ADCP measurement from VOS. C. -T. A. CHEN documents a 20-year seawater temperature at Nanwan, where there is heat-discharge from a coastal Power Plant. M. MATSUYAMA presented a result on direct ADCP measurement at Soya Strait, of which the summer transport is about 1.2 SV. K. ICHIKAWA's poster deals with T / P, ERS altimetry-derived SSH anomaly in the Bungo Channel, and correlated with mesoscale eddies east of Ryukyu Islands.

(reported by B. H. CHOI, Sungkyunkwan Univ.)

Session 10 and 11. Coastal Ocean

The research on Coastal Ocean in the early time of its development neglected the research on the Oceanography. A few measurements of coastal hydrography were carried out due to

engineering requirements. We in the oceanography community know the importance of the Kuroshio, the major current in the world ocean. But the most poeple outside the oceanography community, are not aware of the importance of the ocenography in relation to our daily lives. Coastal Oceanography, however, has its role related to people's daily lives, especially to the coastal area.

In the session of coastal oceanography, there are five oral presentations. Two of which by C. -T. A. CHEN and D. -L. TANG are related to nuclear power plant. The other two by A. ATMADIPOERA and I. MURIPTO discuss the coastal hydrography of Jakarta Bay and its fisheries. The last one by J. NA discusses tidal flat in the western coast of Korea. I believe the issue will play on important role for the land utilization of coastal area in future.
(reported H. -W. LI, National Taiwan Ocean Univ.)

Acknowledgements

This workshop was organized successfully due to the geneous contributions from many organizations. Financial supports were provided by the Ministry of Education, Science, Sports and Culture, Japan, Japan Marine Science Foundation, Kawatetsu Techno-Constrution Co. LTD. and others. We greatly appreciate their kind support. We are also grateful to the Chief of International Affairs Section of Kagoshima University and the Administration office-staff of the Faculty of Engineering of Kagoshima University for their cooperation and assistance in arranging this Warkshop. We appreciate the clear summaries reported by the session chairpersons.

Received and accepted on November 30, 2000

La mer 38 : 173–178, 2000
Société franco-japonaise d'océanographie, Tokyo

The Kuroshio east of Taiwan and in the East China Sea in July 1997

Yaochu YUAN*, Yonggang LIU*, Huiqun WANG*, Jilan SU* and Arata KANEKO**

Abstract : On the basis of hydrographic data obtained from two cruises by R/V Xiangyanghong No.14 and R/V Chofu-Maru in July 1997, a modified inverse method, and three dimensional diagnostic, semidiagnostic and prognostic models are applied to examine the Kuroshio east of Taiwan and in the East China Sea. Conclusive remarks on the Kuroshio in July 1997 are as follows: 1) The net northward volume transport (VT) of the Kuroshio through Section K_2 southeast of Taiwan was about 37.5×10^6 m^3/s. It was much smaller than those in early summer of 1985, October 1995 and May–June 1996. 2) There was no branch of the Kuroshio east of Taiwan flowing northeastward to the region east of Ryukyu Islands. 3) There were an anticyclonic eddy east of the Kuroshio and southeward flow east of this anticyclonic eddy. 4) There was an anticycloninc recirculating eddy south of Miyako Island and southeast of Okinawa Isand. 5) The net northward VT of the Kuroshio through Section PN in the East China Sea was about 23.0×10^6 m^3/s.

Key words : *Kuroshio, East of Taiwan, East China Sea, Numerical study, 1997 El-Niño*

1. Introduction

The region east of Taiwan is very important for understanding the Kuroshio, the Kuroshio Countercurrent and other subgyres in Western North Pacific because all western ends of the subgyres merge together there, as pointed out by HASUNUMA and YOSHIDA(1978). YUAN *et al.* (1998b) gave a remark in explanation of some studies on the Kuroshio east of Taiwan. The Kuroshio has some important current characteristics in the area east of Taiwan and its adjacent region. For example, YUAN *et al.* (1998a, b) pointed out that there was an eastern branch of the Kuroshio east of Taiwan, flowing northeastward to the region east of Ryukyu Islands and occupying a part of the western boundary current east of Ryukyu Islands in October 1995 and early summer of 1996. However, no branch of the Kuroshio flowed into the region east of Ryukyu Island in early summer of 1985 (YUAN *et al.*, 1996). YUAN *et al.* (1996, 1998a, 1998b) further pointed out that the above Kuroshio current patterns are closely related to the strengths and positions of cyclonic and anticyclonic gyres in the adjacent region.

In this paper, on the basis of hydrographic data obtained in summer of 1997, a modified inverse method, and three dimensional and nonlinear diagnostic, semidiagnostic and prognostic models are applied to examine the Kuroshio east of Taiwan and in the East China Sea during summer of 1997. The current features of the Kuroshio east of Taiwan and in the East China Sea, and those in its adjacent region are also discussed. Furthermore, we make a comparison of results in 1997 with the previous cruises, and a comparison of the computed results with ADCP current data.

2. Numrical Models and Data

The hydrographic data were obtained from two cruises, i. e., a cruise of China–Janpan

* Second Institute of Oceanography, Key Lab of Ocean Dynamic Processes and Satellite Oceanography, State Oceanic Administration, Hangzhou 310012, China
(e-mail: yuanyc@zgb.com.cn)
** Department of Environmental Sciences, Faculty of Engineering, Hiroshima University, Higashi-Hiroshima 739, Japan

Cooperative Research on the subtopical gyre during July 3–20, 1997 (hereafter called cruise 1) and another cruise during July 16–22, 1997 by R/V Chofu-Maru (hereafter called cruise 2) in the East China Sea (Fig. 1). The modified inverse method proposed by YUAN *et al.* (1992) is applied to calculate the current structure, volume transport (VT) and stream function in the regions east of Taiwan, southeast of the Ryukyu Islands and in the East China Sea (hereafter called computation 1). All of the three dimensional and nonlinear diagnostic, semidiagnostic and prognostic σ -coordinate models (WANG and YUAN, 1997) are used to compute the circulation east of Taiwan and southeast of the Ryukyu Islands (hereafter called computation 2). For computation 1, seven boxes are selected in the regions east of Taiwan and southeast of Ryukyu Islands, and one box in the East China Sea.

3. Major results of computation 1

In this section, major features of the Kuroshio east of Taiwan and in the East China Sea, and distributions of eddies east of Taiwan estimated by computation 1 are discussed. We compare the computed results with the ADCP measurement also.

3.1 The velocity distributions at Sections K_2 and PN

We discuss only the velocity distributions at Section K_2 southeast of Taiwan (Fig. 2) and Section PN in the East China Sea (Fig. 3) due to limitation of pages.

1) Section K_2 southeast of Taiwan

Section K_2 is located southeast of Taiwan (Fig. 1). In Fig. 2, there are two current cores in the Kuroshio. The main branch of the Kuroshio is near the southern tip of Taiwan, i. e., at the computational points 1 and 2. The maximum velocity at Section K_2 is about 112 cm/s at the sea surface of the computational point 2. It is much smaller those in early summer of 1985 (YUAN *et al.*, 1996), October 1995 (YUAN *et al.*, 1998a) and early summer of 1996 (YUAN *et al.*, 1998b). The second core is located at the computational points 4 and 5 with its maximum velocity of about 49 cm/s at the surface of the computational point 4. There are southward flows in the upper 800 m of the computational point 3, in the upper 75 m of the computational point 6, in the lower 50 m of the computational point 7, at the computational points 8 and 9, and below the Kuroshio. The comparison be-

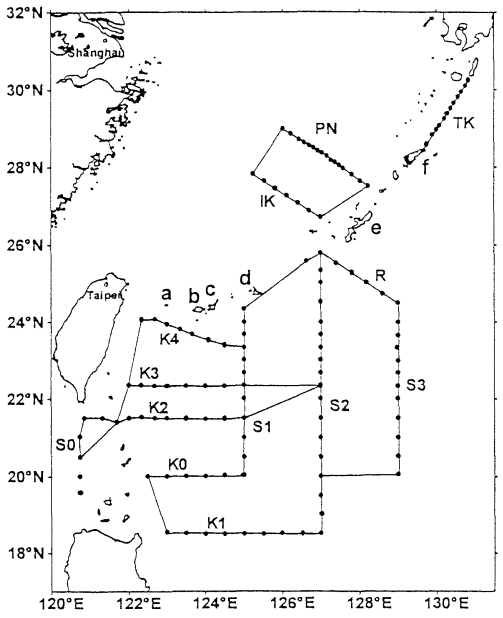

Fig. 1. Location of hydrographic stations and sections, and computation boxes in July 1997 (a : Yonakuni I., b : Iriomote I., c : Ishigaki I., d : Miyako I., e : Okinawa I., f : Amami-Oshima I.)

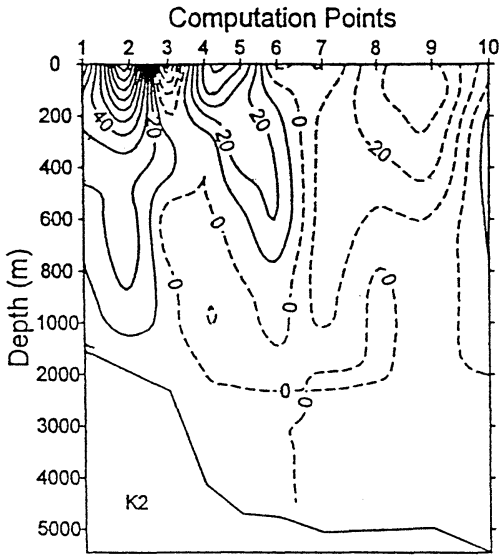

Fig. 2. Velocity distribution at Section K_2 in July 1997 (positive: northward, : unit: cm/s)

tween the current calculated above (Fig. 2) and the ADCP current observed at Section K_2 in July 1997 (Fig. 6) shows that they coincide qualitatively to each other.

2) Section PN in the East China Sea

Section PN is a familiar section in the East China Sea (Fig. 1). Fig. 3 shows the velocity distributions at Section PN in July 1997. In Fig. 3, there are two current cores in the Kuroshio. Its main current core is located near the coutinental slope, the computational points 6 and 7 (Fig. 3), with its maximum velocity of 141 cm/s at the sea surface of the computational point 6. The second core is located at the computational points 9 and 10 with its maximum velocity of 91 cm/s at the 125 m of the computational point 9. There are southward flows in the upper layer of the computational points 11 and 12, and below the Kuroshio. Northward flows also exist below southward flows of the computational points 11 and 12, and the computational points 13 and 14.

3.2. Stream function and volume transport

Fig. 4 and Table 1 show the distribution of stream function and total volume transport in July 1997. In Table 1, the net northward volume transport (VT) of the Kuroshio through Section K_2 is about 37.5×10^6 m^3/s in July 1997. It is much smaller than those in early summer of 1985, October 1995 and May-June 1996 (e.g. YUAN *et al.*, 1998a, 1998b). In Fig. 4, the Kuroshio is located west of 123° E at Section K_2 then flows northward through Section K_4. There is no branch of the Kuroshio east of Taiwan flowing northastward to the region east of Ryukyu Islands. The distributions of stream function, total volume transport, and temperature in Fig. 4 show that: (1) There is an anticyclonic eddy in the east of the Kuroshio, of which center is located at 22°20′ N, 123° E; (2) There is a southward flow, which probably comes from a southwestward flow at the northern part of Section S_3, in the aree east of the adove-mentioned anticyclonic eddy; (3) There is a cold eddy C_1 in the area east of a southward flow, of which center is located at 22°20′ N, 124°30′ E. There is also a cold eddy C_2 in a southeastern part of the computed region; (4) There is an anticyclonic eddy in the region south of Miyako and southeast of Okinawa Island. Comparing the computed results in Fig. 4 with the ADCP current averaged in the layer from 25 m to 75 m depths in Fig. 6 in July 1997, we find that they agree qualitatively to each other.

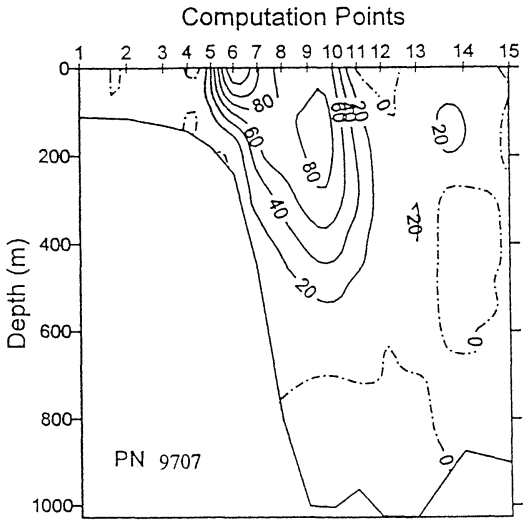

Fig. 3. Velocity distribution at Section PN in July 1997 (positive: northward, unit: cm/s)

The decrease of the Kuroshio VT through Section K_2 in July 1997 may be due to the following two reasons. (1) The North Equatorial Current (NEC) weakens during El-Niño event suggested by XU *et al.* (1987). They showed that the phase of seasonal variation of the NEC at 130° E and that of the Kuroshio VT were the same phase. As the year 1997 is the strong El-Niño year, the Kuroshio VT at Section K_2 may have decreased with the weakening of NEC. (2) KAGIMOTO and YAMAGATA (1997) pointed out that the role of the anticyclonic eddy activity in the Kuroshio VT along the Nansei Islands. Comparing the strength of the anticyclonic recirculating eddy east of the

Table 1. Volume transport(VT)and position of the Kuroshio at Section K_2 during some cruises

Cruises	VT (10^6 m^3/s)	Its position
Early summer of 1985	45.0	West of 123° E
October 1995	57.8	West of 123°20′ E
Early summer of 1996	44.6	West of 123°40′ E
July 1997	37.5	West of 123° E
December 1997	27.6	West of 124° E

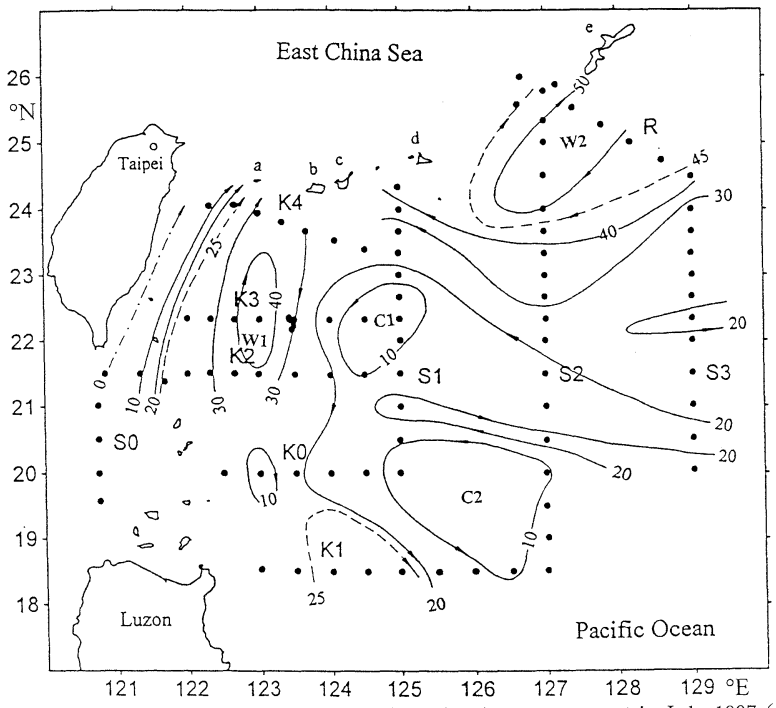

Fig. 4. The distribution of stream function and total volume transport in July 1997 (unit: 10^6 m^3/s)

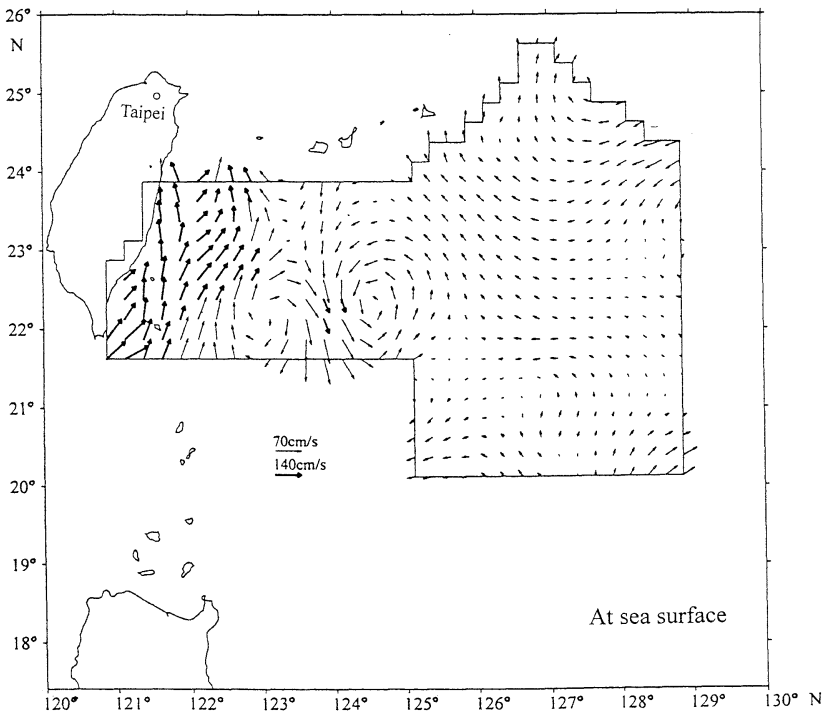

Fig. 5. The horizontal velocity distribution at the sea surface for the diagnostic calculation in July 1997

Ryukyu Islands in July 1997 with that in the other year such as May–June 1996 in YUAN *et al.* (1998b), the decrease of the Kuroshio VT through Section K_2 may be associated with the weakening of the anticyclonic recirculating eddy east of the Ryukyu Islands.

It is warthy to note that the classical Sverdrup relation is not valid in the region of the Kuroshio. However, it is still valid in the broad ocean interior east of the Kuroshio Countercurrent (KAGIMOTO and YAMAGATA, 1997). This means that we can not explain the above seasonal variation of the Kuroshio VT from the classical Sverdrup relation.

In July 1997 the net northward VTs of the Kuroshio through Sections IK and PN in the East China Sea (see Fig. 1) are 26.3×10^6 and 23.0×10^6 m^3/s, respectively, and that through the Tokara strait across Section TK (see Fig. 1) is 23.3×10^6 m^3/s, The average net northward VT of the Kuroshio through Section PN in other cruises are as follow: (1) 28.6×10^6 m^3/s during ten cruises from 1987 to 1990 (YUAN *et al.*, 1994); (2) 28.0×10^6 m^3/s in the four cruises of 1992 (LIU and YUAN, 1999) and 27.1×10^6 m^3/s during the eight cruises of 1993 and 1994 (LIU and YUAN, 1999); (3) 26.7×10^6 m^3/s October 1995 (YUAN *et al.*, 1998a) and 27.2×10^6 m^3/s in early summer of 1996 (YUAN *et al.*, 1998b). This means that VT of the Kuroshio at Section PN was smaller slightly in July 1997 than in other cruises.

4. Major results of computation 2

In this section we first discuss the horizontal velocity distibutions at the sea surface, 200 m, 500 m and 1000 m depeths, which are deduced from the diagnostic calculation. Due to the limitation of pages, only the horizontal velocity distribution at the surface (Fig. 5) is shown. The following main results are obtained. (1) The Kuroshio east of Taiwan flows northeastward, and makes a cyclonic meander and truns to flow northward. Its maximum velocity at (or near) the southern boundary is about 147.4, 123.1, 98.5 and 42.8 cm/s at the sea surface, 100

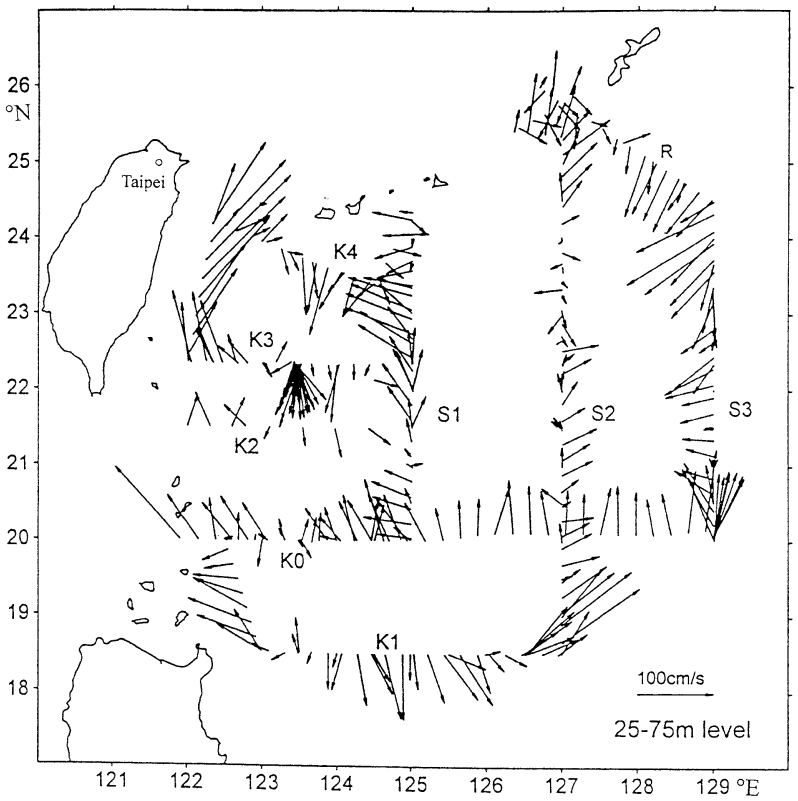

Fig. 6. The average ADCP current vectors in the layers from 25 to 75m depths in July 1997

Table 2. Volume transports (VT) of the Kuroshio through Section PN in the East China Sea during some cruises

Cruises	Average VT of the Kuroshio ($10^6 m^3/s$)
Ten cruises from 1987 to 1990	28.6
Four cruises of 1992	28.0
Eight cruises of 1993 and 1994	27.1
October 1995	26.7
Early summer of 1996	27.2
July 1997	23.0
November 1997	25.9

m, 200 m and 500 m levels, respectively. (2) There is no branch of the Kuroshio flowing northward to the region east of the Ryukyu Islands. (3) As pointed out by the computation 1, there are an anticyclonic eddy (W_1) and a cold eddy (C_1) in the east of the Kuroshio. Their locationas are at 22° 20′ N, 123° 10′ E, respectively. There is a southward flow between the above two eddies of W_1 and C_1. An anticyclonic recirculating eddy appears in the northeastern part of the computational region.

Comparing the results of computation 2 with those of computation 1 and the average ADCP current (Fig. 6), it can be said that the distributions of horizontal velocity deduced from the diagnostic calculation agree quite with the results of computation 1 and the average ADCP current.

Comparing the results of diagnostic calculation with those of semidiagnostic and prognostic calculations, they are coincident qualitatively to each other while there are some differences between them in quantity. For example, the maximum velocities of the Kuroshio east of Taiwan for the semidiagnostic calculation are about 164.9, 147.6, 132.7 and 46.7 cm/s at the sea surface, 100 m, 200 m and 500 m levels, and those for the prognostic calculations are about 164.6, 147.6, 132.3 and 40.0 cm/s at the sea surface, 100 m, 200 m and 500 m levels. This means that the Kuroshio east of Taiwan is strengthened for the semidiagnostic and prognostic calculations. Therefore, we should consider the interaction among the density field, velocity field and bottom topography when the density field and so on have been adjusted.

Acknowledgement

This project was supported by both the National Natural Science Foundation of China under contract No. 49736200 and No. 49776287, and the Major State Basic Research Program, No. G1999043802.

References

HASUNUMA, K. and K. YOSHIDA (1978): Splitting of the Subtropical Gyre in the Western North Pacific. J. Oceanogr. Soc. Japan, **34**, 160–172.

KAGIMOTO, T. and T. YAMAGATA (1997): Seasonal transport variation of the Kuroshio: An OGCM Simulation. J. Phys. Oceanogr., **27** (**3**), 403–418.

LIU, Y. and Y. YUAN (1999): Variability of the Kuroshio in the East China Sea in 1992. Acta Oceanological Sinica, **18** (**1**), 1–15.

LIU, Y. and Y. YUAN (1999): Variability of the Kuroshio in the East China Sea in 1993 and 1994. Acta Oceanologica Sinica, **18** (**1**), 17–36.

WANG, H. and Y. YUAN (1997): Calculation of current in the Taiwan strait during summer Ⅱ. Three dimension semidiagnostic and prognostic calculation. Acta Oceanologica Sinica, **19** (**3**), 10–20.

XU B., T. FANG, C. LING, J. JIANG and S. LI (1987): The variational character of North Equatorial Current in West Pacific Ocean during 1964–1983. Acta Oceanologica Sinica, **9** (**3**), 286–293.

YUAN, Y., J. SU and Z. PAN (1992): Volume and heat transports of the Kuroshio in the East China Sea in 1989. La mer, **30**, 251–262.

YUAN, Y., Z. PAN, I. KANEKO and M. ENDOH (1994): Variability of the Kuroshio in the East China Sea and the currents east of the Ryukyu Islands. Proceedings of China–Japan Joint symposium of the Cooperative Research on the Kuroshio, Qingdao, China, 27–29 October 1992, China Ocean Press, Veijing 121–144.

YUAN, Y., C.-T. LIU, Z. PAN and S. ZHENG (1996): Circulation east of Taiwan and in East China Sea and east of Ryukyu Island during early summer 1985. Acta Oceanologica Sinica, **15** (**4**), 423–435.

YUAN, Y., Y. LIU, C.-T. LIU and J. SU (1998a): The Kuroshio east of Taiwan and the currents east of the Ryukyu-gunto during October of 1995. Acta Oceanologica Sinica, **17** (**1**), 1–13.

YUAN, Y., A. KANEKO, J. SU, X. ZHU, Y. LIU, N. GOHDA and H. CHEN (1998b): The Kuroshio east of Taiwan and in the East China Sea and the Currents east of Ryukyu Islands during early summer of 1996. Journal of Oceanography, **54**, 217–226.

Received on February 10, 2000
Accepted on October 10, 2000

La mer 38 : 179–184, 2000
Société franco-japonaise d'océanographie, Tokyo

Variation of the currents east of the Ryukyu Islands in 1998

Yonggang LIU* and Yaochu YUAN**

Abstract : Based on the CTD and wind data east of the Ryukyu Islands obtained in three cruises abroad by R/V Chofu Maru in 1998, the current velocities and volume transports are calculated by the modified inverse method. The northeastward Ryukyu Current over the slope east of the Okinawa Island and a southwestward current east of the Ryukyu Current are recognized to exist in February, April and July of 1998. There is a weaker southwestward countercurrent in the deep layer under the Ryukyu Current in February and July of 1998. Some warm or cold eddies in different scales, having direct influence on the Ryukyu Current, appear east of the Ryukyu Current in all the three cruises of 1998. The maximum velocity of the Ryukyu Current at Section OK is stronger in July, but weaker in February and April of 1998. The northeastward volume transports of the Ryukyu Current in February, April and July of 1998 are about 10×10^6, 3×10^6 and 8×10^6 m^3/s, respectively. The volume transport is smaller in April, partially due to the influence of a cyclonic eddy east of the Okinawa Islands. The calculated current velocities are in good agreement with those measured with vessel-mounted ADCP.

Key words : *Ryukyu Current, eddies*

1. Introduction

Hydrographic observation at OK line southeast of the Okinawa Island has been carried out by R/V Chofu Maru three (or four) times a year since 1993. The currents east of the Ryukyu Islands during 1992–1997 had been computed by use of the modified dynamic method and the modified inverse method in order to examine the seasonal and interannual variations of the Ryukyu Current before 1997 by LIU *et al.* (1998) and LIU *et al.* (2000). The northward Ryukyu Current often lies over the eastern slope of the Ryukyu Islands, while its velocity and volume transport (hereafter VT) have temporal variability. Weak current cores of the Ryukyu current can be identified still in the velocity distribution of OK line when the southward current east of the Ryukyu Islands was very strong in April of 1995 (LIU *et al.*, 1998). The Ryukyu Current was also found in all the three cruises (April, July and October) in 1997 (LIU *et al.*, 2000). The Ryukyu Current is stronger in summer and autumn, but weaker in spring, according to the statistical average of its maximum velocity (hereafter V_{max}) in 11 cruises during 1993–1996 (LIU *et al.*, 1998). Similar seasonal variation of the Ryukyu Current was also found in 1997 (LIU *et al.*, 2000). On the other hand, some eddies east of the Ryukyu Islands have direct influence on the Ryukyu Current, e.g., the stronger northward currents in summer and autumn of 1997 were partially attributed to the activities of warm eddies east of the Ryukyu Islands (LIU *et al.*, 2000).

The influence of eddies east of the Ryukyu Islands was much emphasized by NAKANO *et al.* (1998). They examined the temporal fluctuation of the geostrophic transport across the OK line from 1993 through 1997 and made a conclusion that no steady northeastward current was found in the east of the Ryukyu Islands. The structure of geostrophic velocity field varied correspondingly with the location of eddies (NAKANO *et al.*, 1998).

To examine the variation of the Ryukyu

* Second Institute of Oceanography, State Oceanic Administration, Hangzhou 310012, China, (e-mail: yliu@marine.usf.edu)
** Key Lab of Ocean Dynamic Processes and Satellite Oceanography, SOA, Hangzhou 310012, China

Table 1. Information about the observed data southeast of the Ryukyu Islands

Cruise	Sections	Observation period	Wind Speed(m/s)	Wind Direction(–)
9801	OK, L1, L2	1998.02.02–22	3.0	71
9804	OK, OE, OS	1998.04.26–29	3.4	146
9806	OK, OE, KR	1998.07.19–23	9.7	229

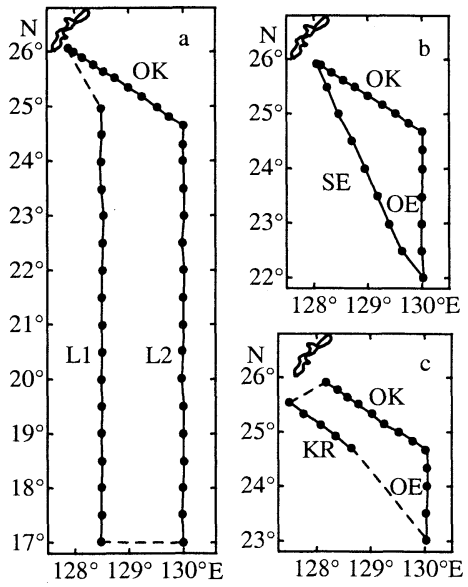

Fig. 1. Locations of CTD stations, sections and computation boxes in February (a), April (b) and July (c) cruises of 1998

Current and the effect of its adjacent eddies in 1998, we analyzed in this paper the CTD, ADCP and wind data east of the Ryukyu Islands obtained by R/V Chofu Maru in cruises 9801, 9804 and 9806 (see Table 1 and Fig. 1). Velocities and VTs of the currents east of the Ryukyu Islands are computed by the modified inverse method. Variation of the Ryukyu Current in 1998 is discussed in this paper, as well as interaction between the Ryukyu Current and its adjacent eddies.

2. Numerical computation and parameters

The modified inverse method (YUAN *et al.*, 1998) has made the following four important modifications for the previous inverse model, i.e., (1) vertical eddy viscosity term in momentum equations, i.e., the flow is non-geostrophic, (2) vertical eddy diffusion term in the density equation, (3) an inequality constraint of heat transfer between atmosphere and ocean, and (4) β-effect. Computation boxes are shown in Fig. 1. In the computation by the modified inverse model mentioned above, each computation box is divided into five vertical layers with $\sigma_{t,p}$ values of 24.8, 26.0, 27.0 and 27.6 at the four interfaces. Due to lack of detailed wind data, a uniform wind field is assumed for each cruise and an average wind speed is obtained by vector averaging wind data observed at each CTD station during each cruise (see Table 1). Due to lack of heat flux data in this area, the heat inequality constraints will not be performed in the present study. Vertical eddy viscosity coefficient Az and vertical eddy diffusion coefficient K_v are taken to be 100 cm^2/s and 10 cm^2/s, respectively. An optimum reference level (ORL) of 2000 m is selected for the three cruises according to the empirical search method (FIADEIRO and VERONIS, 1983). In these computations, the following shallow water correction is adopted in the determination of the reference level: if the water depth of the station (H) is larger than the ORL, it is taken to be ORL, else it is taken to be H.

3. Computed results and discussion

3.1 Velocity distribution

The OK line is a northwest–southeastward section located southeast of the Okinawa Island. Hydrographic observations were conducted on February 2–4, April 26–27, and July 19–20, 1998. Velocity distribution at each section can be calculated by the modified inverse model. However, due to the limited pages, we will discuss the velocity distribution at Section OK only in these three cruises as follows.

In Fig. 2a (February, cruise 9801), there is a northeastward current (the Ryukyu Current) in the western part of Section OK. Its two current cores are located in the subsurface layer of computation points 4 and 5 and the middle layer of computation point 3. The two V_{max}

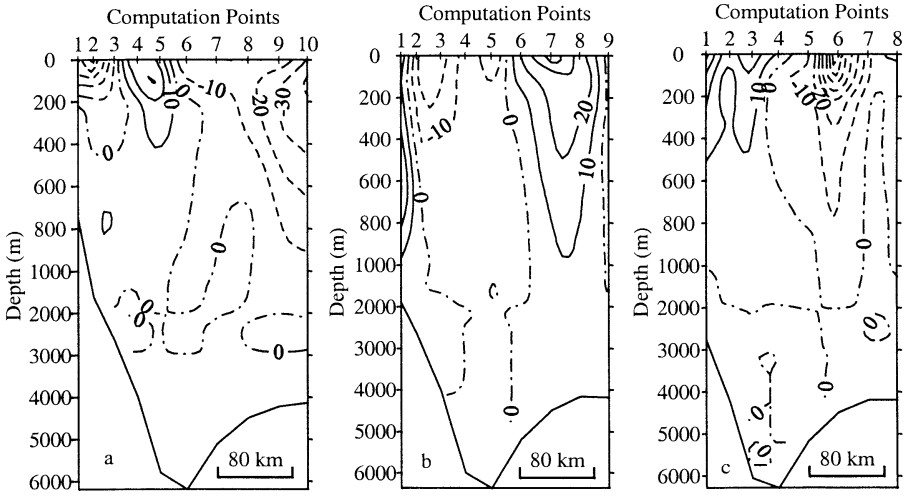

Fig. 2. Velocity distribution at Section OK in February (a), April (b) and July (c) of 1998 (cm/s; positive value: northeastward, negative value: southwestward)

values are 34 cm/s at 125 m level of computation point 5 and 15 cm/s at 700 m level of computation point 3, respectively. West of the Ryukyu Current, there is a stronger southward current in the surface layer west of computation point 3 near the Okinawa Island with its V_{max} of 59 cm/s in the subsurface layer of computation point 2. The area in the eastern part of Section OK is dominated mainly by a southward current. Distributions of geopotential anomaly referred to 1500 db show that there is an anticyclonic circulation southeast off the Okinawa Island (Figs. 3a, 3b, 3c). So both part of the Ryukyu Current and the eastern southwestward current make up a part of the anticyclonic circulation. The V_{max} of the southwestward current at computation point 3 and the northeastern current at computation point 7 are 28 and 43 cm/s in the surface layer, respectively. Both the velocities calculated by the modified inverse method and the geopotential anomalies are in good agreement with the currents measured with vessel mounted ADCP (Figs. 3a, 3b).

In Fig. 2b (April, cruise 9804), the Ryukyu Current is located at computation point 1 of Section OK near the Okinawa Island, with V_{max} of 31 cm/s at 600 m level. A southward current lies between computation points 2 and 5, and a northward current is located between

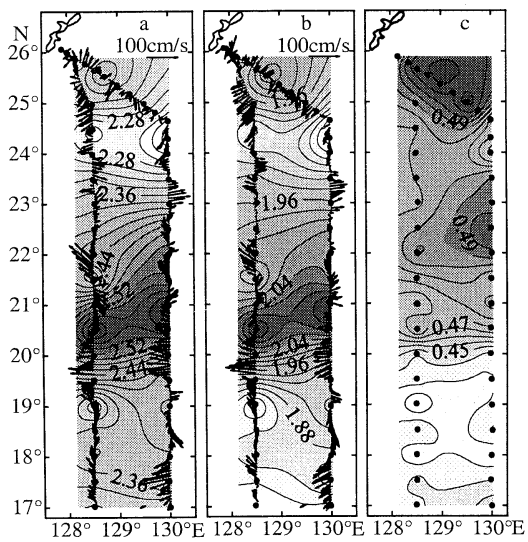

Fig. 3. Geopotential anomaly ((10^{-2} m^2/s^2), ref. to 1500 db) and the currents measured with ADCP at 3 m (a), 97 m (b) and 800 m (c) levels in February of 1998

computation points 6 and 8. Both of them make up the southern part of a cyclonic eddy, which can be identified from distributions of geopotential anomaly (Figs. 4a, 4b, 4c). This eddy has a large vertical extent, ranging from the surface to 1500 m depth or so. It seems that there is also an anticyclonic eddy at the southern part of Section SE south of Section OK.

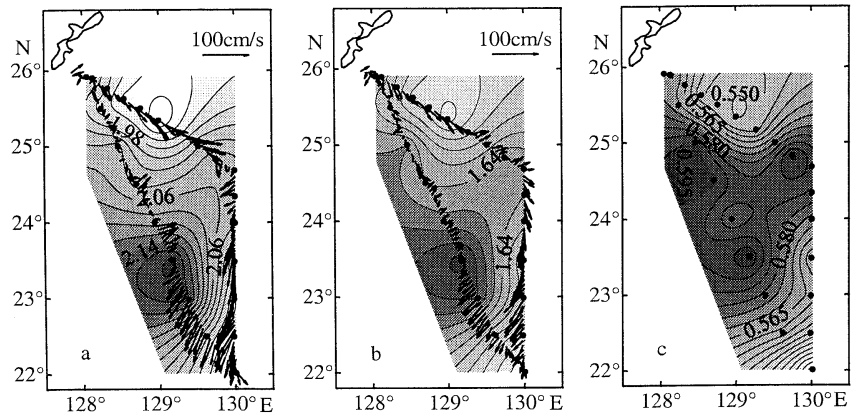

Fig. 4. Geopotential anomaly ($(10^{-2}\ m^2/s^2)$, ref. to 1000 db) and the currents measured with ADCP at 3 m (a), 97 m (b) and 800 m (c) levels in April of 1998

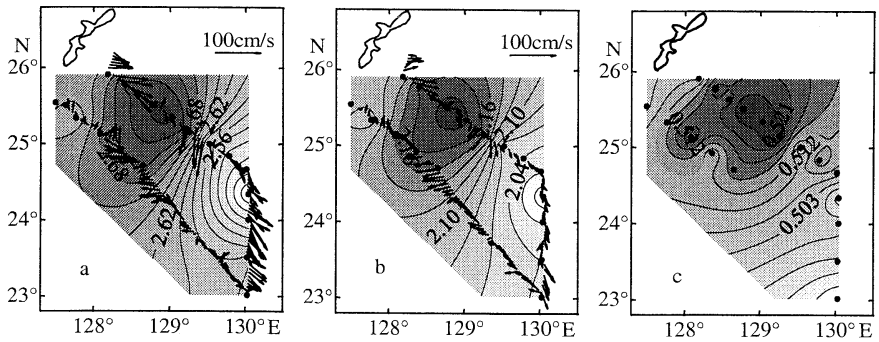

Fig. 5. Geopotential anomaly ($(10^{-2}\ m^2/s^2)$, ref. to 1500 db) and the currents measured with ADCP at 3 m (a), 97 m (b) and 800 m (c) levels in July of 1998

Temperature and salinity distributions (figures are not shown here) show that there are cold and warm water cores corresponding to the locations of the cyclonic and anticyclonic eddies mentioned above, respectively. Currents measured with ADCP at both 3 m and 97 m levels also confirm the above-mentioned two eddies and the Ryukyu Current (Figs. 4a, 4b). NAKANO *et al.* (1998) showed that a part of the high Sea Surface Dynamic Height (anticyclonic eddy) moved westward along 22° N and 25° N, and reached the area southeast of the Okinawa Island. These eddies affect the structure of geostrophic velocity field.

In Fig. 2c (July, cruise 9806), northeastward currents dominate the western part of Section OK. There are two northward current cores with V_{max} values of 42 and 29 cm/s at the surface layer of computation points 1 and 3, respectively. The eastern part of Section OK is dominated by a stronger southward current with V_{max} of 80 cm/s at 50m level of computation point 8. These two currents make up an anticyclonic eddy southeast off the Okinawa Islands, which can be identified from distributions of geopotential anomaly and ADCP currents (Figs. 5a, 5b, 5c). Horizontal temperature and salinity distributions (figures are not shown here) also show that there is a warm eddy southeast of Okinawa. This warm eddy shifts a little to the east in the deeper layer, and still exists at a depth of 1800 m or so. From Figs. 5 a, 5 b, 5 c, there is also a cyclonic flow in the eastern part of the computation area, which is to the southeast of the anticyclonic eddy mentioned above.

3.2 Variation of the Ryukyu Current

Calculated results indicate that there is a northeastward Ryukyu Current over the slope

east of the Ryukyu Islands. Its V_{max} varies between 31~42 cm/s during the 3 cruises, which is similar to that in 1997 (LIU *et al.*, 2000). A southwestward current exists east of the Ryukyu Current in February, April and July of 1998, and a weaker southwestward countercurrent also exits in the deep layer under the Ryukyu Current in February and July of 1998. Some mesoscale warm/cold eddies appear east of the Ryukyu Islands in February, April and July of 1998, and they have direct influence on the Ryukyu Current. An anticyclonic eddy east of the Ryukyu Current strengthens the northward current, while a cyclonic eddy, weakens it. It is worthy to note that the sea surface height revealed by the altimetry data also show that there are active mesoscale eddies east of the Ryukyu Islands (NAKANO *et al.*, 1998).

The values of V_{max} of the Ryukyu Current at Section OK in February, April and July of 1998 were 34, 31 and 42 cm/s, respectively. As mentioned above, the Ryukyu Current may be weakened by the adjacent cyclonic eddy in April. The existence of the anticyclonic eddy east of the Ryukyu Current may partially account for the strengthening of the Ryukyu Current in July. However, the observed stations are far away from the Okinawa Island, and only a part of the Ryukyu Current near Okinawa is observed in both cruises 9804 and 9806. That is to say, the V_{max} values of the Ryukyu Current may be underestimated in the spring and summer cruises. Seasonal variation of the Ryukyu Current from spring to summer in 1998 is similar to that in 1997. The Ryukyu Current is also stronger in summer and weaker in spring of 1997. V_{max} at Section OK in spring and summer of 1997 were 25 and 47 cm/s, respectively (LIU *et al.*, 2000). It needs further investigation to identify whether the meso-scale eddies did cause the same seasonal variations of V_{max} in 1997 and 1998 or did not.

3.3 Volume transport

In the modified inverse computation, the total VTs flowing into and out from a computation box must be equal to each other. We will discuss the VT through Section OK and pay a special attention to the VT of the Ryukyu Current in each cruise as follows.

In February, the northeastward and southwestward VTs through Section OK are 12.0×10^6 and 21.8×10^6 m^3/s, respectively. It is very difficult to tell precisely the VT of the Ryukyu Current from the northward VT of the adjacent warm eddy, since it is not so simple as to draw a dividing line between the Ryukyu Current and the adjacent warm eddy. For a rough estimation, let's define the Ryukyu Current area in this cruise as the area between computation points 1 and 5 at Section OK in Fig. 2a, then the northward VT of the Ryukyu Current is about 10×10^6 m^3/s.

In April, the northeastward and southwestward VTs through Section OK are 19.3×10^6 and 11.2×10^6 m^3/s, respectively. The northward VT of the Ryukyu Current is about 3×10^6 m^3/s, which is smaller than that of 5×10^6 m^3/s in spring of 1997 (LIU *et al.*, 2000). The VT of the Ryukyu Current is a little underestimated due to the following two aspects: The observed stations are far away from the Okinawa Island, and only a part of the Ryukyu Current near Okinawa is observed in April. The small VT of the Ryukyu Current in spring can be also attributed to the influence of the cyclonic eddy east of the Okinawa Islands.

In July, the northeastward and southwestward VTs through Section OK are 11.7×10^6 and 15.9×10^6 m^3/s, respectively. The northeastward VT of the Ryukyu Current is about 8×10^6 m^3/s, which is smaller than that of 16×10^6 m^3/s in the summer cruise of 1997 (LIU *et al.*, 2000). This VT is also underestimated because only a part of the northeastward Ryukyu Current is observed due to the limited locations of the observed stations at the western end of Section OK near the Okinawa Island in this cruise as mentioned above.

4. Conclusions

Based on the CTD and wind data obtained by R/V Chofu Maru east of the Ryukyu Islands in 1998, the velocities and VTs of the currents east of the Ryukyu Islands are computed by the modified inverse method.

The calculated results indicate that the northeastward Ryukyu Current lies over the slope east of the Okinawa Island in February,

April and July of 1998. A southwestward current also exists east of the Ryukyu Current in the three cruises of 1998, and a weaker southwestward countercurrent exits in the deep layer under the Ryukyu Current in February and July of 1998. Some warm or cold eddies in different scales appear east of the Ryukyu Current in all the three cruises of 1998, and they have direct influence on the Ryukyu Current.

The Ryukyu Current is stronger in July, but weaker in February and April of 1998 according to the maximum velocity of the Ryukyu Current at Section OK. The northeastward VT of the Ryukyu Current in February, April, and July of 1998 are about 10×10^6, 3×10^6 and 8×10^6 m^3/s, respectively.

Both the current velocities calculated by the modified inverse method and the distributions of the geopotential anomaly are in good agreement with the currents measured with vessel mounted ADCP.

Acknowledgement

This project was supported by the Youth Marine Science Foundation of State Oceanic Administration, China (No.98202), the National Natural Science Foundation of China (No. 49776287), and the Major State Basic Research Program of China (No. G1999043802). Gratitude is due to the Nagasaki Marine Observatory for providing the hydrographic data.

References

FIADEIRO, M. E., and G. VERONIS (1982): On the determination of absolute velocities in the ocean. J. Mar. Res., **40**(Suppl.), 159–182.

LIU Y., Y. YUAN, T. NAKANO and M. AMINO (1998): Variability of the currents east of the Ryukyu Islands during 1995～1996. In Proceedings of Japan China Joint Symposium of Cooperative Study on Subtropical Circulation System. Seikai National Fisheries Research Institute, Fisheries Agency of Japan, Nagasaki, P. 221–232.

LIU Y., Y. YUAN, T. SHIGA, H. YAMAMOTO, S. TSUBAKI and M. IMAI (2000): Circulation southeast of the Ryukyu Islands. In Proceedings of Second Workshop on China–Japan Joint Research of Subtropical Circulation System, Xiamen, November 1998 (accepted).

NAKANO T., T. KURAGANO and Y. LIU (1998): Variations of oceanic conditions east of the Ryukyu Islands. In Proceedings of Japan–China Joint Symposium of Cooperative Study on Subtropical Circulation System. Seikai National Fisheries Research Institute, Fisheries Agency of Japan, Nagasaki, P.129 –140.

YUAN Y., A. KANEKO, J. SU, X. ZHU, Y. LIU, N. GOHDA and H. CHEN (1998): The Kuroshio east of Taiwan and in the East China Sea and the currents east of Ryukyu Islands during early summer of 1996. J. Oceanogr., **54**, 217–226.

Recived on February 13, 2000
Accepted on November 15, 2000

La mer 38 : 185–188, 2000
Société franco-japonaise d'océanographie, Tokyo

Study on the free oscillations in the Yellow Sea

Chengchun QIAN*

Abstract : The free oscillations in the Yellow Sea triggered by atmospheric forcing had been revealed from the tidal record. The period of free oscillation is estimated to be about 22 hours by power spectrum via maximum entropy method. The phase delays among the free oscillations at selected three tidal stations show that the free oscillation propagates from north to south along the west coast of the Yellow Sea. The numerical modeling gives almost the same results.

Key words : *free oscillations, Yellow Sea, period*

1. Introduction

In the Yellow Sea, there should be free oscillations triggered by atmospheric process; their period are estimated by the geometry of the Yellow Sea, using J. R. MERIAN's fromula (SVERDRUP, 1946) as follows.

For enclosed rectangle bay:

$$T = \frac{2l}{\sqrt{gh}}.$$

For semienclosed rectangle bay:

$$T = \frac{4l}{\sqrt{gh}}.$$

Here T is period of free oscillation, l and h are the length and the average depth of the bay respectively, and g is the gravity acceleration. For the Yellow Sea, the west–eastward length is about 500 km, the south–northward length is also about 500 km, and the average depth is about 50 m. By using above formulae and parameters, the period of the free oscillations occurring in the Yellow Sea is estimated to be about 12.55 hours and 25.1 hours. These periods are nearly equal to the semidiurnal and diurnal tidal periods. However their phases should be different from the astronomic tides, because the free oscillations are generated by storms at a random time. Therefore these free oscillations should be extracted from the tidal record in order to estimate their period.

To determine the existence of free oscillation in the Yellow Sea and to calulate its period, in this paper, the free oscillation components are derived from tidal records and their periods are estimated by power spectrum. In order to examine the driving mechanism of observed free oscillations, the numerical modeling was also done.

2. Observational results in the Yellow Sea

To extract the free oscillation components from tidal records, firstly the astronomic tides are calculated by using the harmonic constants obtained from tidal records by harmonic analysis method, secondly the astronomic tides are wiped off from tidal records. The remains containing free oscillation components are analyzed by intrinsic mode function (IMF) method (HUANG, 1998), this method is also called EMD (Empirical Mode Decomposition) and used to decompose a numerical signal series into several modes; as a result, the free oscillation systems can be found in the data series of some modes of IMF.

The tidal records measured at Lianyungang, Qingdao and Rushan during 1981 to 1985 had been analyzed by the method described above. The positions of the three tide gauge stations are shown in Fig. 1. From the above results, four typical free oscillation components are selected and shown in Fig. 2 to Fig. 9. Figures 2, 4, 6, and 8 show the free oscillation at the three stations, Figures 3, 5, 7, and 9 show the water elevations from which the free oscillation had

* Ocean University of Qingdao, 5 Yushan Road, Qingdao, China

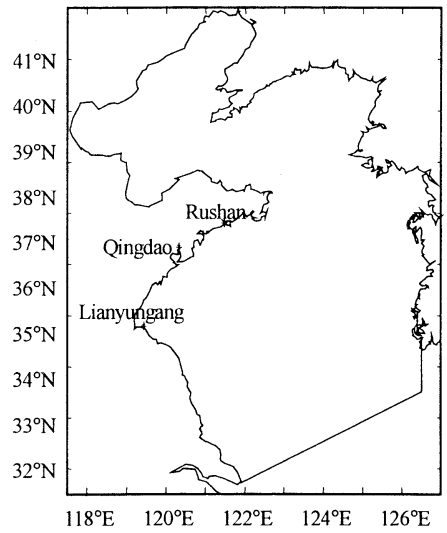

Fig. 1. The tide gauge stations and calculating field

been extracted.

The free oscillation during 17 to 25 August 1985 was triggered by the typhoon named Mamie. The maximum wind speed at the center of Mamie reached 34 m/s; it crossed the Yellow Sea during 17 to 20 August 1985 (Fig. 10 shows Mamie's path), and triggered the free oscillation in the Yellow Sea. Another three during 25 April to 1 May 1983, 12 to 20 November 1983, and 4 to 9 October 1985, were triggered by three extratropical cyclones respectively. The three extatropical cyclones had similar characteristicsl; they moved eastward over the East Asia Continent along the 40°N latitude with a cold front extended southwestward from their centers; before the attack of cold fronts, the Yellow Sea was controlled by southwest wind; when the fronts crossed the Yellow Sea, the northwest wind controlled the Yellow Sea.

All these free oscillations have the amplitude exceeding 10 cm, and their periods are about 20–22 hours extimated by power spectrum via maximum entropy method. The oscillation phases at the three stations have obvious relationship (see figures 2, 4, 6 and 8) from Rushan to Lianyungang with phase delay of about one hour. This result indicates that the free oscillations should propagate from north to south along the west shore of the Yellow Sea.

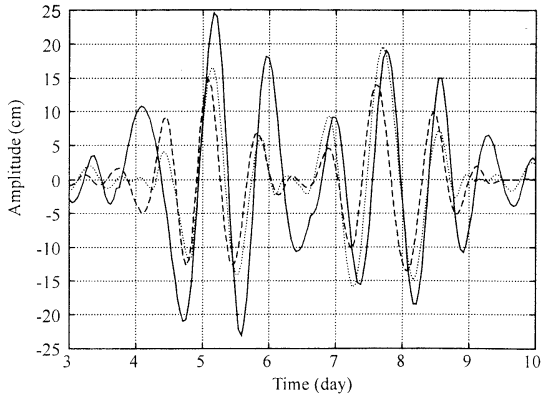

Fig. 2. The free oscillations derived from observation data, 25 April to 1 May 1983 (Dot line: Qingdao, solid line: Lianyungang, dash line: Rushan)

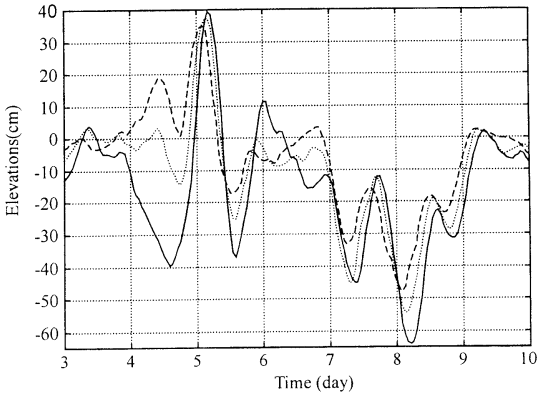

Fig. 3. The water elevations derived from tide data, 25 April to 1 May 1983 (Dot line: Qingdao, solid line: Lianyungang, dash line: Rushan)

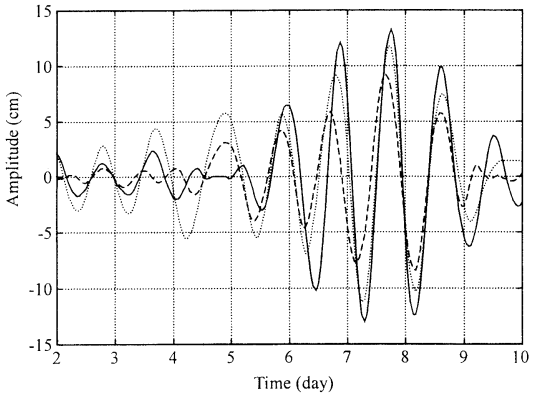

Fig. 4. The free oscillations derived from observation data, 12 to 20 November 1983 (Dot line: Qingdao, solid line: Lianyungang, dash line: Rushan)

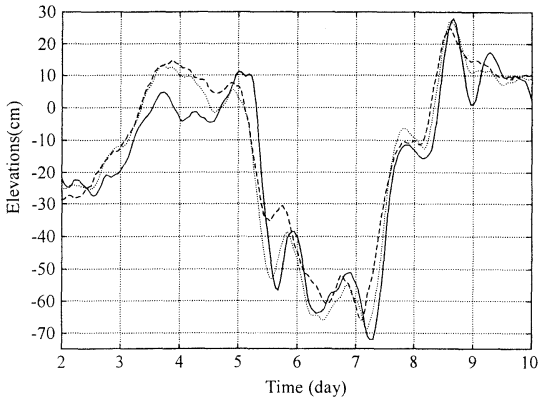

Fig. 5. The water elevations derived from tide data, 12 to 20 November 1983 (Dot line: Qingdao, solid line: Lianyungang, dash line: Rushan)

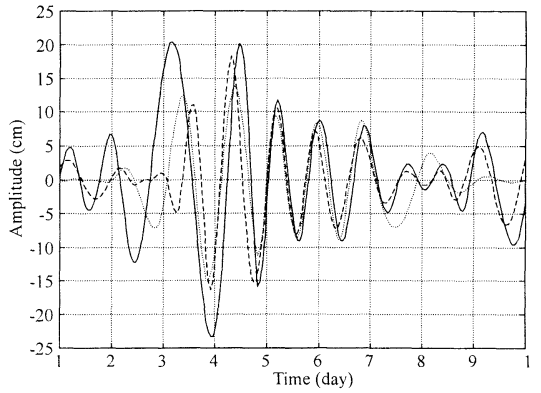

Fig. 6. The free oscillations derived from observation data, 17 to 25 August 1985 (Dot line: Qingdao, solid line: Lianyungang, dash line: Rushan)

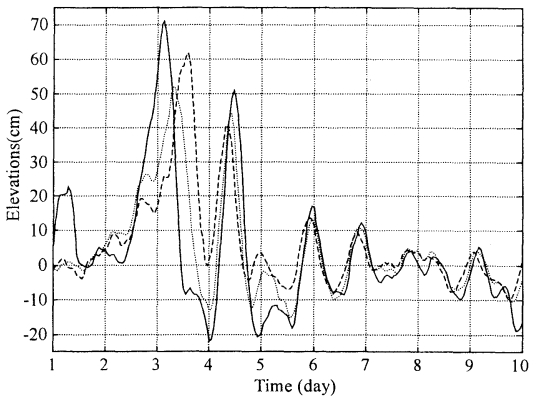

Fig. 7. The water elevations derived from tide data, 17 to 25 August 1985 (Dot line: Qingdao, solid line: Lianyungang, dash line: Rushan)

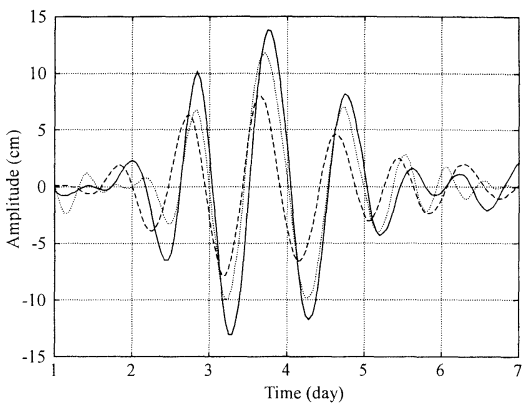

Fig. 8. The free oscillations derived from observation data, 4 to 9 October 1985 (Dot line: Qingdao, solid line: Lianyungang, dash line: Rushan)

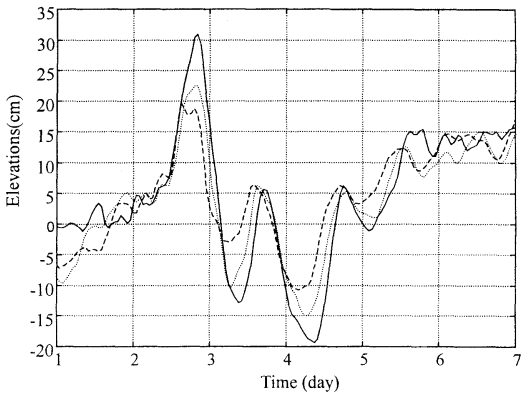

Fig. 9. The water elevations derived from tide data, 4 to 9 October 1985 (Dot line: Qingdao, solid line: Lianyungang, dash line: Rushan)

3. Numerical simulating of free oscillations in the Yellow Sea

The depth integrated two-dimentional long wave equations are employed for simulating the free oscillations in the Yellow Sea. The finite-difference mesh is used. At the land boundaries, the velocity components in the direction perpendicular to the coastline are set to be vanished. At the open boundaries, radiation types of conditions are adopted. The calculating field includes the Yellow Sea and the Bohai Sea (see Fig. 1); the grid spacing is 1/12 degree (longitude and latitude); the time step length is 5 minutes; the bottom friction coefficient is 0.0016 (due to the slightly variation with location and the lack of observation, generally the

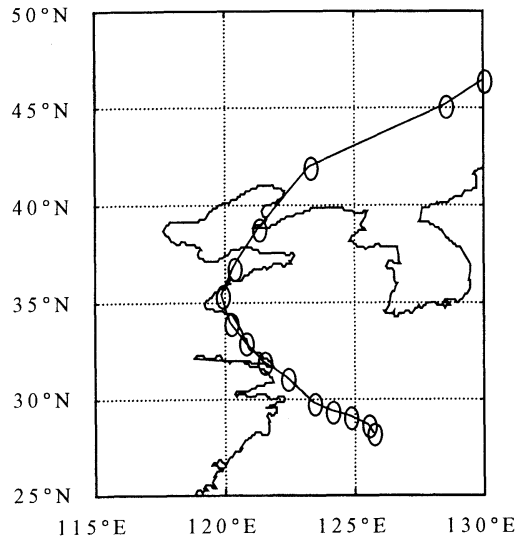

Fig. 10. The path of typoon Mamie (the circles indicate the center positions every 6 hours from 02:00, 17 August 1985)

bottomo friction coefficient is selected to be 0.001–0.003 in numerical simulating). The initial conditions for all the calculated points are as follow: the water level increases from 0 cm to 300 cm in south–north direction, in west–east direction the water level is constant; there is no motion of water.

The model runs for 7 days and outputs the water level at the three points Lianyungang, Qingdao and Rushan. The model's results are analyzed by IMF method; the obtained free oscillations (see Fig. 11 and Fig. 12) have the period about 18.5 hours estimated by power spectrum via maximum entropy method.

The results of numerical simulation are little different from those derived from the tidal records due to inadequate selection fo coefficient of bottom friction. If the coefficient of bottom friction is increased from 0.0016 to 0.0026, the period increased to 20.5 hours.

4. Conclusions

In the Yellow Sea, when there is a storm affecting this sea area the free oscillation will be triggered and propagate from north to south along the west shore of the Yellow Sea with the period of about 20–22 hours.

The numerical simulation showed that free oscillation can be generated and it can propagate in the Yellow Sea.

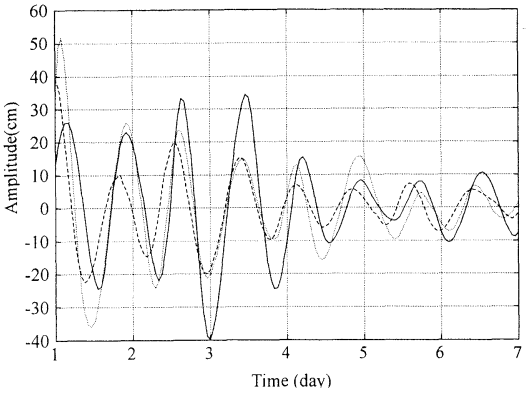

Fig. 11. The free oscillations derived from numerical simulation (Dot line: Qingdao, solid line: Lianyungang, dash line: Rushan)

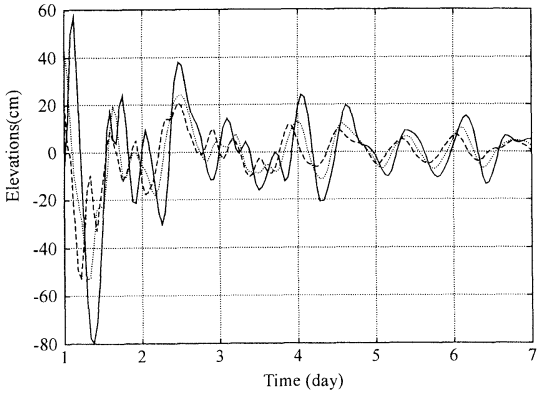

Fig. 12. The water elevations derived from numerical simulation (Dot line: Qingdao, solid line: Lianyungang, dash line: Rushan)

References

HUANG, N. E.(1998): The Empirical Mode Decomposition and the Hilbert Spectrum for nonlinear and nonstationary time series analysis. Proceedings of the Royal Society: Mathematical, Physical and Engineering Sciences, **A454**, pp903–995.

SVERDRUP, H. U., M. W. JOHNSON and R. H. FLEMING (1946): The Oceans: Their Physics, Chemistry and General Biology, Prentice–hall, INC. New York, pp. 472–474.

Received on January 11, 2000
Accepted on October 23, 2000

La mer 38 : 189–198, 2000
Société franco-japonaise d'océanographie, Tokyo

Circulation patterns of the Japan Sea

Vladimir PONOMAREV* and Olga TRUSENKOVA*

Abstract : The current system and characteristic circulation patterns in the Japan Sea are simulated using the MHI numerical layered model (Marine Hydrophysical Institute, Sebastopol, Ukraine) which can treat features of the large/synoptic scale dynamic processes over the irregular bottom topography. The model is forced mainly by heat and buoyancy fluxes through the straits and sea surface. Numerical experiment is performed from Levitus climatology temperature initial conditions. In model spin-up from the smooth initial density distribution, the system of jet currents and fronts is formed due to layer outcropping. Principal circulation features such as the Liman Current, East Korean Warm Current, Offshore and Nearshore Tsushima Current Branches, known from observation and simulations performed earlier by many authors are simulated. The numerical result obtained on 1/16° grid is characterized by current branching in the northwest sea area and multiple structure of the Subarctic Front. The synoptic scale features in the main pycnocline such as meandering, cyclonic/anticyclonic eddies and streamers are simulated.

Key words : *Japan Sea, sea circulation, numerical simulation, synoptic dynamic structures*

1. Introduction

The Japan Sea is a weakly stratified deep marginal sea connected to the Pacific Ocean, East China Sea and Sea of Okhotsk by shallow straits. The transformed subtropical water is directly transported through the Japan Sea to the oceanic transitional area between the subtropic and subarctic gyres and to the Sea of Okhotsk by inflow into the Tsushima (Korean) Strait and outflow to the Tsugaru and Laperus (Soya) Straits.

The Japan Sea is characterized by shallow pycnocline (down to 250–300 m in the southern sea and only seasonal one down to 50 m in the northern sea) and an almost homogeneous cold deep water mass known as the Japan Sea Proper Water underneath. The Subarctic (Polar) Front at about 39°–40°N separates the southern and northern areas.

More than 100 years of oceanographic observations in the Japan Sea established the principal features of the sea circulation. There is a cyclonic gyre in the northern Japan Sea formed by the East Korean Warm Current (EKWC) flowing north- and northeastward and by the North Korean Cold Currents flowing south- and southwestward Liman and North Korean Cold Currents. The circulation is mostly anticyclonic in the southern Japan Sea, characterized by the three current branches entering the sea through the Tsushima Strait. They are baroclinic EKWC, baroclinic unstable Offshore Tsushima Branch flowing mostly along 1000 m isobath with countercurrent in lower layer and barotropic Nearshore Branch along 200 m isobath (YOON, 1991).

In the recent decades, satellite and high-accuracy CTD and ADCP observations have emphasized the important role of synoptic scale processes in the Japan Sea. Meandering and branching of the main currents, quasi-stationary and moving eddies have been revealed in the southwestern and southeastern sea areas, over the Yamato Rise, and in Northwestern Japan Sea (ICHIYE and TAKANO, 1988; OSTROVSKII and HIROSE, 1994; DANCHENKOV *et al.*, 1997).

Recent numerous numerical simulations based on different models reproduced most of the large scale flow patterns in the Japan Sea mentioned above. Some mechanisms were

* Pacific Oceanological Institute, 43 Baltiyskaya, Vladivostok, 690041, Russia
e-mails: archer@stl.ru, ponom@t.kanazawa-t.ac.jp, trolia@ocean.poi.dvo.ru

revealed such as wind stress curl or/and buoyancy forcing, and topographical control (YOON, 1991; SEUNG and KIM, 1993; HOLLOWAY *et al.*, 1995; HOGAN and HURLBURT, 1997; MOOERS and KANG, 1997). The frequently arising problems, such as overshooting of EKWC, absence of one of the Tsushima Current branches, and modeling of deep water circulation were also discussed. Features of the synoptic scale dynamics were also simulated by high-resolution models (RO, 1999). The crucial factor is parameterization of horizontal and vertical friction/turbulent diffusion which is accounted for different manner among various models, such as reduced gravity models, Holloway's model, Princeton University model (POM), and layered models.

The goal of this study is to demonstrate the circulation patterns in the Japan Sea simulated by a layered model which allows substantial isopycnal turbulent momentum/heat/salt exchange while diapycnal turbulent fluxes between inner layers are set up low or negligible. Vertical change of baroclinic component of horizontal velocity may be expected to be more realistic.

2. MHI hydrodynamic model and setup of the numerical experiment

The MHI numerical layered model of sea circulation is developed by MIKHAILOVA and SHAPIRO, (1992), SHAPIRO (1998) in the Marine Hydrophysical Institute (MHI), Sebastopol, Ukraine. It is based on the primitive equations under the hydrostatic and Boussinesq approaches. The MHI model consists of a turbulent upper mixed layer (UML) and any number of inner layers with temperature and salinity integrated vertically within layers but being functions of time and horizontal coordinates. UML approximation is, mostly, similar to that employed in BLECK *et al.* (1989). Parameterizations of buoyancy, heat and salt fluxes on the sea surface, bottom of UML and other layer interfaces have been comprehensively described in MIHAYLOVA and SHAPIRO, (1992) and SHAPIRO (1998). Both entrainment and detrainment (subduction) regimes are allowed for UML. Note, that employing non-homogeneous inner layers makes easier subduction approximation in the MHI model compared to most isopycnal models, such as BLECK *et al.* (1989). Buoyancy variations in inner layers are limited by the so-called "base" stratification:

$$b^{\sigma}{}_{k} \leq b_{k} < b^{\sigma}{}_{k-1} \qquad \text{for } k \geq 2, \tag{1}$$

where $b^{\sigma}{}_{k}$ is the kth layer base buoyancy ($b^{\sigma}{}_{k} > b^{\sigma}{}_{k+1}$) and b_{k} is the kth layer buoyancy, and $b^{\sigma}{}_{n} = 0$, $b^{\sigma}{}_{0} = \infty$. If buoyancy of an inner layer gets out of its "base" limits, the layer outcrops, acquiring zero thickness and becoming dynamically inactive and transparent for mass, heat and salt fluxes.

As for boundary conditions, normal components of velocity, heat and salt fluxes are equal to zero at the sea bottom. Bottom friction and friction between layers are set up as square functions of horizontal velocity shear. At lateral walls, no slip condition is imposed, and no heat or salt flux is allowed. In inflow/outflow ports, volume transport, temperature, salinity, and inflow-outflow layers thickness are given in an annual cycle. At the sea surface, kinematic boundary condition for vertical velocity, wind stress, and equations of heat and salt balance are given (SHAPIRO, 1998). Annual cycle of air temperature, incoming short-wave solar radiation, wind velocity, cloudiness, and precipitation is taken into account to calculate buoyancy flux through the sea surface. The model can be forced by climatic or synoptic winds. The model equations, conditions at layer interfaces, finite difference approximation and methods of the numerical solution are described in MIKHAILOVA and SHAPIRO, (1992) and SHAPIRO (1998).

Bottom topography used in the model run is introduced by scaling initial sea depth:

$$Z_{n}'(x,y) = Z_{m} + \alpha \cdot [Z_{n}(x,y) - Z_{m}], \tag{2}$$

where $Z_{n}(x,y)$, $Z_{n}'(x,y)$, are initial and scaled sea depth and Z_{m} is mean sea depth. Scaling factor α is equal to 0.7, scaled sea depth is further smoothed by 9-point filter.

We performed the initial spin-up simulation with horizontal resolution of 1/16° (5-7 km) to obtain temperature, salinity, layer interfaces, and horizontal velocity fields adapted to the summer external conditions including weak climatic wind and bottom topography. Vertical

resolution of 7 layers including UML and 6 inner layers is chosen so that the 2nd layer corresponds to a layer of subtropical water, 3rd – 5th layers represent the main pycnocline, and 6th –7th layers describe deep waters of the Japan Sea (Japan Sea Proper Water).

Initial condition of summer Levitus climatology is chosen for temperature in layers 1 – 6 referenced to the layer middle depth, while a constant value of 0.06°C is accepted for the lowest 7th layer. Horizontally homogeneous initial salinity is set up as 33.5, 33.7, 34.00, 34.02, 34.05, 34.06, and 34.077 psu. Flat initial interfaces between layers are defined at 5, 50, 100, 150, 250, and 500m depth. As density gradient is supported mostly by temperature gradient in the Japan Sea, initial condition as described is chosen intentionally with the purpose to study the simulated field adaptation, especially of salinity and layer interfaces started from homogeneous state. Base buoyancy is chosen as 10 (∞), 2.1, 1.3, 1, 0.83, 0.72, and 0.

The subtropical water enters into the Japan Sea through the Tsushima Strait (of 100 m depth, layers 1–3), with temperature of 26/20 ℃, salinity of 34.4/34.6 psu and total volume transport of 1.5 Sv. The entered water volume flows out from the Japan Sea through the Tsugaru and Laperus (Soya) Straits (of 100 and 50 m depth) divided between them in ratio of 2:1. The simulation is performed under forcing of weak summer climatic wind. Starting date is the 1st of June. The following coefficients are used in the simulation: 2.5×10^{8} m^4/s for bi-harmonic isopycnal viscosity, 25 m^2/s for isopycnal harmonic viscosity and diffusion, and 5×10^{-8} m^2/s for diapycnal mixing. Note, that bi-harmonic viscosity is applied, while harmonic viscosity is switched on only when needed to suppress checkerboard noise.

3. Simulation of the circulation patterns in the Japan Sea

Spin-up simulation started from Levitus climatology generally describes main current systems of the northern and southern Japan Sea as early as in 40 days of integration (Figs. 1–2). Temperature, horizontal velocity, initially homogeneous salinity and layer interfaces become adapted to each other and to the bottom topography, total kinetic energy reaches quasi-stationary state in 10–12 days. Sea surface height developed in 40 days of integration shows cyclonic gyre in the northern Japan Sea and anticyclonic circulation in the southern sea (not shown). The pattern is similar to that simulated by other authors, such as YOON, (1991), SEUNG and KIM, (1993), HOLLOWAY *et al.* (1995), MOOERS and KANG, (1997), HOGAN and HURLBURT (1997), and RO (1997). Sea surface height difference of about 20 cm between northern and southern sea areas is similar to that derived from altimetry data assimilation (HIROSE and OSTROVSKII, 1994).

In the Northern Japan Sea, Primorye (Liman) Current is obtained as an irregular stream intensified along the Primorye coast to the south of 44°30′ N with general cyclonic circulation in the Peter the Great Bay near Vladivostok. It reaches southward as far as 40° N where it becomes the coastal countercurrent in relation to the northeastern branch of the East Korean Warm Current (EKWC) flowing along the continental slope and turning eastward from the slope (Fig. 1).

The Shrenk (Liman) Current is obtained in the Northern Tatar Strait from 52° to 49° N with general cyclonic circulation in the Strait (Figs. 1–2). There exists northeastward stream from 45° to 49° N along the Siberian coast from sea surface down to 500 m (1st – 5th layers). That is coincident with the observation in summer described by YURASOV and YARICHIN (1991). They explained the northward and northeastward surface currents along the Northern Primorye coast to be caused by the summer monsoon. On the contrary, Primorye Current along the most areas of the northwestern sea coast is intensified under forcing of winter synoptic wind conditioned by the winter monsoon as shown in PONOMAREV and YURASOV (1994), and PONOMAREV and TRUSENKOVA (2000a).

The northern EKWC branch carries transformed subtropical water to the north to the Laperus (Soya) and Tatar Straits and is usually associated with the Northern Front (Fig. 1) of the interfrontal zone between 38°–40°30′ N. The 2nd layer outcrops in the north of this jet, where UML comes into contact with the 3rd layer and the water from the 2nd layer gets

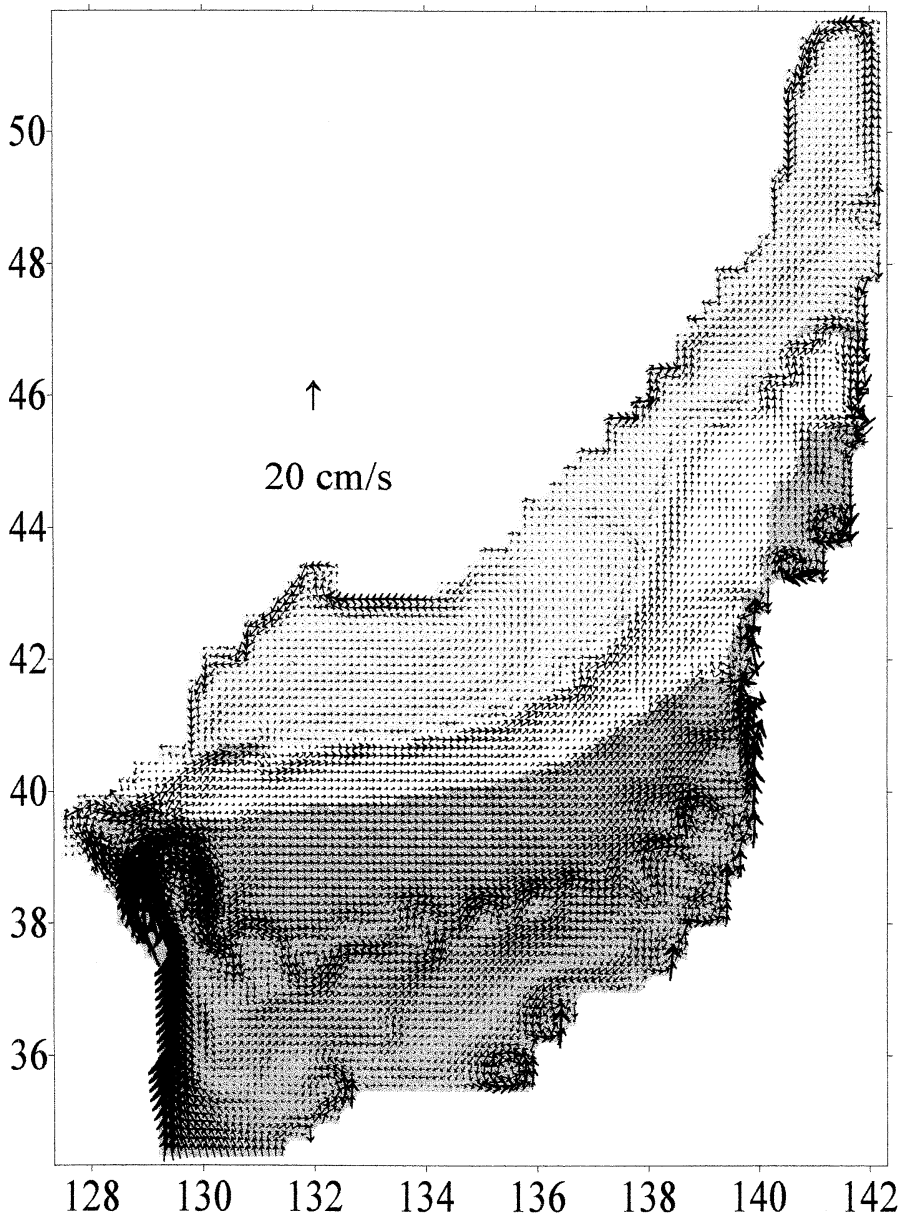

Fig. 1. Horizontal velocity in the UML in every 4th grid point. The northern area where the 2nd layer outcrops, is filled with smoke-grey; the interfrontal zone, where the 3rd layer outcrops but the 2nd layer does not, is filled with white, and the southern area, where the layers do not outcrop, is painted with charcoal grey.

involved into the 3rd layer. The 3rd layer outcrops in the interfrontal zone where the 2nd layer contacts the 4th layer with water from the 3rd layer entering the 2nd layer (Figs. 1 and 2). Two main, northern and southern fronts and a subsurface intermediate front between them are clearly seen in slopes of interface depth between 2nd and 3rd layers and 3rd and 4th layers (Fig. 3a, b). The northern front manifests itself in UML velocity (Fig. 1),

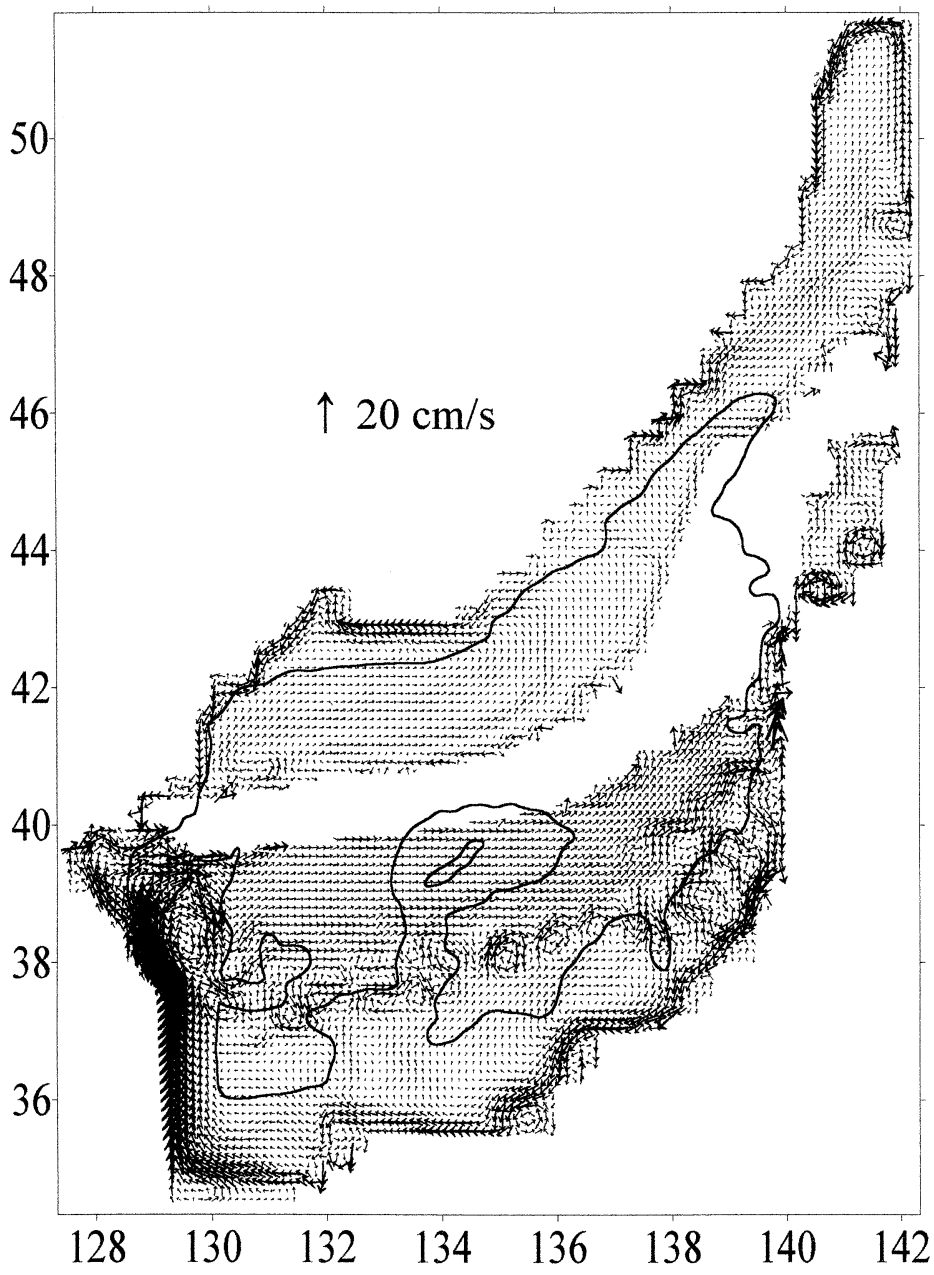

Fig. 2. Horizontal velocity in the 3rd layer. Velocity vectors are shown in every 4th grid location. The layer outcrops in the interfrontal zone where there is no arrows. 1500 m contour of bottom topography is shown.

temperature and in less extent salinity (not shown). The southern front can be seen in UML, 2nd and 3rd layers temperature, salinity, horizontal velocity and depths of interfaces between layers (Figs. 1–3).

Figure. 2 shows countercurrents in the main pycnocline of the interfrontal zone, with an eastward and northeastward current along the southern edge of 3rd layer outcropping area and a westward and southwestward current

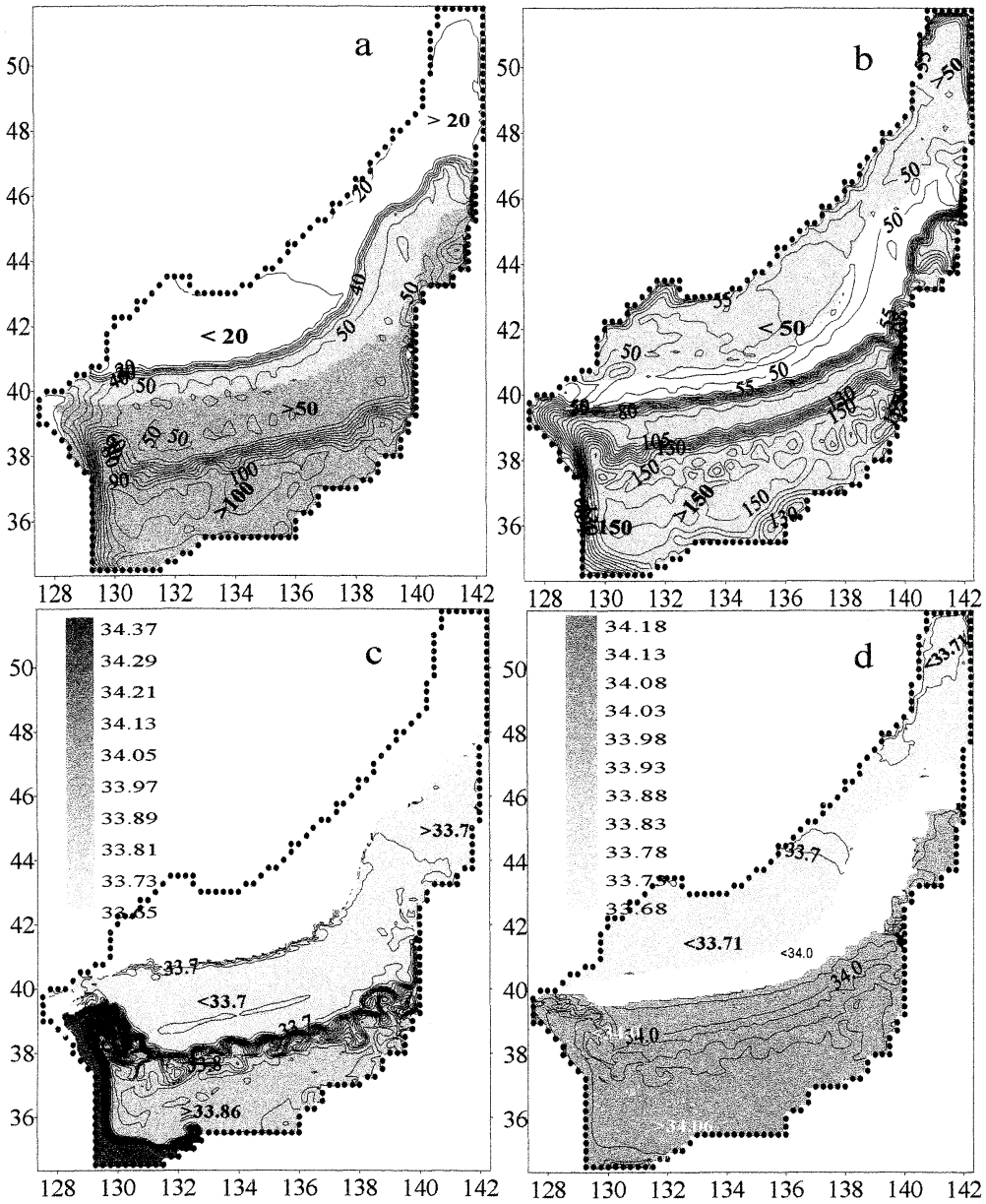

Fig. 3. Topography (contours every 5 m) of lower interfaces (a, b) and salinity (c, d) in the 2nd (a, c) and 3rd (b, d) layers (salinity contours every 0.01 psu in (c) and 0.005 psu in (d)). In (a, c) the northern area where the 2nd layer outcrops, and in (b, d) the interfrontal zone where 3rd layer outcrops are white. In (a, d) the southern area where both the 2nd and 3rd layers do not outcrop is filled with charcoal grey.

along its northern edge. There is a countercurrent at the northern/northwestern edge of the Northern Front in UML (Fig. 1). Countercurrents and convergence/divergence areas were earlier reported in the interfrontal zone, based on observation data (YURASOV and YARICHIN, 1991).

The subsurface intermediate front is well

pronounced in the 3rd layer temperature (not shown) and salinity (Fig. 3d). The 3rd layer temperature (8–9 ℃) is higher in the north of the outcropping area than that to the south (7–8℃). This should be attributed to the fact that in this area the 3rd layer carries warmer water mass from the initial 2nd layer.

Initial salinity is taken constant in layers, unlike Levitus climatological initial temperature. Nevertheless, salinity field formed in the upper layers during 40-days spin-up reveals lower values in the north and, especially, in the northwest Japan Sea. The intermediate front separates the subtropical high salinity water in the south (34 psu and more) from the low salinity waters in the north (33.71 psu and less; Fig. 3c). Moreover, starting from vertically increasing initial salinity, a belt of lower salinity is formed along this front in the southern area just in 40 days of integration, although the difference is very small (33.99 psu versus 34.00 psu; Fig. 3c). It is a result of anti-entrainment (subduction) from the upper layers, i.e., the temporal variable process which would form salinity minimum layer in the southern sea. Intermediate layer of lower salinity is a feature of the water structure in the Southern Japan Sea, well known from observations (YURASOV and YARICHIN, 1991).

The northern and southern fronts were earlier revealed from oceanographic observations (Zuenko, 1999). The simulation performed in this study shows that the Subarctic Frontal Zone in the Japan Sea should be associated with the multiple front system.

As for the southern current system, the three known branches (YOON, 1991) are obtained in this simulation, namely, EKWC (western branch), central (the Offshore Branch) and eastern coastal (Nearshore Branch) Tsushima Current branches.

EKWC flows as an intensified western boundary current along the Korean continental slope as far north as 39°–40° N where it bifurcates with separating off the slope. Similar double branch structure of EKWC was found based on trajectories of drift bottles (MIITA and KAWATATE, 1986). It is known from observations (YURASOV and YARICHIN, 1991) that EKWC separates from the coast at 37° – 38° N, so our simulation shows an "overshooting" of EKWC (Figs. 1 and 2). In some studies overshooting is explained by insufficient horizontal grid resolution and high coefficients of isopycnal mixing. For example, overshooting occurs on 1/8° – 1/16° grids but disappears on 1/32° grid in HOGAN and HURLBURT, (1997). However, it seems in our simulation that it is due to insufficient time of integration from the initial Levitus temperature fields interpolated from the coarse 1° grid to the fine 1/16° grid. When started from horizontally homogeneous initial conditions, we obtained EKWC separating from the coast at 37° N even on 1/4° grid (PONOMAREV and TRUSENKOVA, 2000 b). Cyclonic gyre in the Northwest Japan Basin area adjacent to the Primorye and North Korea is clearly seen in Figs. 1 and 2.

While separating from the slope, the southern EKWC branch forms a strong anticyclonic meander over the top of the Korean Plateau centered at 38° 20′ N, 129° 30′ E. The similar meander and eddy was reported in KATOH (1994) based on ADCP and hydrographic data although it was positioned to be at about 1° southward. In the east of the meander, the EKWC joins with the Offshore Branch of the Tsushima Current.

The Tsushima Offshore Branch associated with the southern front of the Subarctic Frontal Zone is the current meandering over the eastern slope of the Yamato Basin pronounced in UML, 2nd and 3rd layers (Figs.1, 2 and 4). It is characterized by a chain of baroclinic eddies generated in pycnocline due to baroclinic instability. According to the vertical velocity profile at the edge of an anticyclonic eddy (38° 6′ N, 134° 50′ E; location shown as a black dot in Fig. 4b) in Fig. 5a, velocity in UML, 2 nd, 3rd, 4th, 6th and 7th layers has values of 13.4, 15.2, 10.4, 3.4, 0.7 and 0.5 cm/s, respectively (the 5th layer outcrops to the 4th layer in this grid location). Velocity is more than 10 cm/s down to 145m (interface between 3rd and 4th layers), with maximum (15.2 cm/s; Fig. 5 a) in the 2nd layer. Vertical velocity profile averaged over the sea also has its maximum (34 cm/s; Fig. 5b) in the 2nd layer corresponding to depth of highest vertical gradient of buoyancy. Subsurface velocity maximum can be associated with

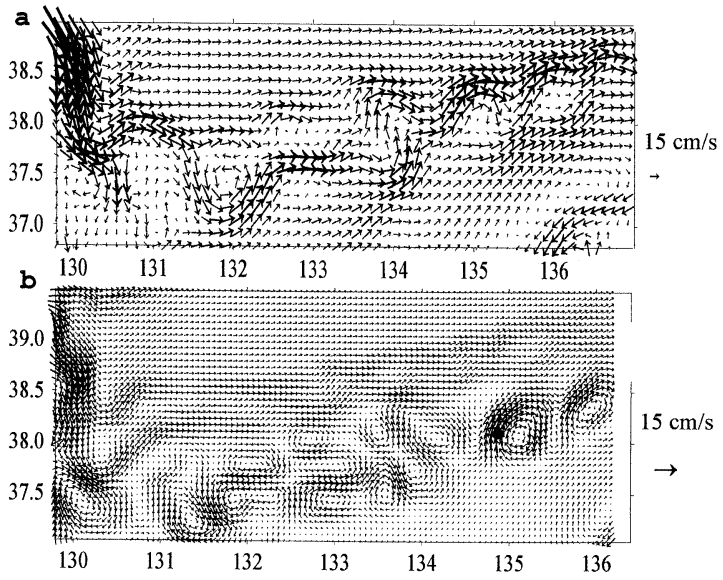

Fig. 4. A chain of baroclinic eddies in the Offshore Tsushima Branch as seen in horizontal velocity in the 2nd (a) and 3rd (b) layers. A black dot denotes location of the velocity vertical profile from Fig. 5a.

synoptic scale dynamics. However, in this area there is no immediate trace of pycnocline eddies in the 6th and 7th thick layers of deep waters, where another kind of synoptic scale circulation develops, mostly controlled by bottom topography.

Figure 4 shows some features of synoptic scale dynamics in the area of the Offshore Tsushima Current, namely branches, meanders, streamers, mushroom-like structures, cyclonic and anticyclonic eddies packed in pairs, quadruples and chains. Between 130° E and 134° E the synoptic scale current bifurcates in the 2nd layer (Fig. 4a) and a complicated eddy structure in the pycnocline in the 3rd layer (Fig. 4b) is formed. In the east of 134°30′ E, with periodic in space meanders and jet streams (streamers) in UML and 2nd layer, there are three anticy-clonic eddies in the 3rd layer with a diameter of 60–70 km.

Warm eddies with such scale were observed also in the southern Japan Sea (ICHIYE and TAKANO, 1988; DANCHENKOV *et al.*, 1997 and others). Different flow patterns in UML, 2nd and 3rd layers should be attributed mostly to low coefficient of diapycnal mixing.

The meandering Offshore Branch can be clearly traced at the depth of interface between the 2nd–3rd and 3rd–4th layers (Fig. 3a, b). Both temperature and salinity in UML, 2nd, and 3rd layers reveal meandering and spiral patterns along the Offshore Branch path an the 37°–38° N band (Fig. 3c, d).

The Nearshore Tsushima Branch is not very well pronounced in our results. It occupies 4 grid points adjacent to the Japanese coast in UML (Fig. 1) and also in the 2nd, upper inner layer, with its lower interface at the depth of about 100 m. Poor development of the coastal branch in the initial spin-up experiment should be attributed to the same reasons as overshooting of EKWC, namely to short time of integration and coarse resolution of initial temperature field.

4. Conclusions

The MHI circulation model successfully simulates the general circulation of the Japan Sea in initial 40-day spin-up from the climatological (Levitus) density distribution with 1/16° horizontal resolution under forcing of weak summer climatic wind. It coincides with numerous oceanographic observations in the sea and many previous simulations based

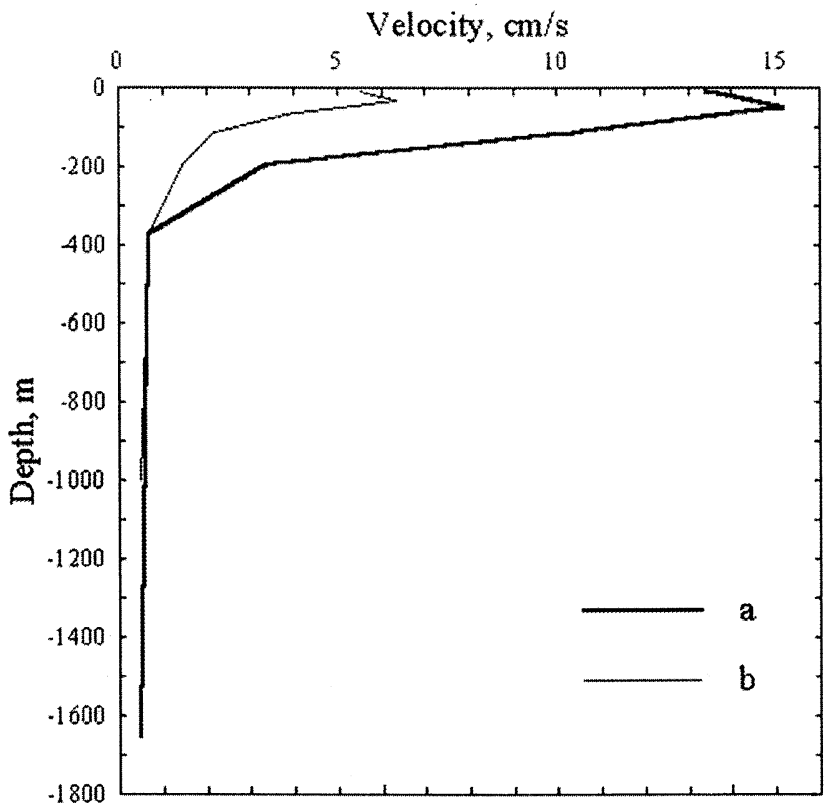

Fig. 5. Vertical profiles of horizontal velocity at the (38°6′N, 134°50′E) grid location (a) and averaged over the sea (b).

on different models. Two faults of our spin-up simulation are overshooting of EKWC and poor development of the Nearshore Tsushima Current Branch. However, these deficiencies are avoided in 40-year model run from horizontally homogeneous initial condition despite the coarse resolution of 1/4° grid (PONOMAREV and TRUSENKOVA, 2000b).

Subduction algorithm provided by coupling of non-homogeneous both UML and inner layers allows formation of a belt of lower salinity and, later, salinity minimum layer in the main pycnocline, starting from vertically increasing initial salinity distribution.

By allowing layer outcropping, the MHI model realistically reproduces frontal interfaces.

The numerical result is characterized by the branching of current in the northwest sea and multiple structure of the Subarctic Front. The synoptic scale features are simulated in the main pycnocline such as meandering, cyclonic /anticyclonic eddies and streamers. These synoptic scale patterns are due to baroclinic instability in the area of the Southern Subarctic Front characterized by well pronounced main pycnocline. Application of bi-harmonic rather than harmonic isopycnal viscosity as well as of low coefficient of diapycnal mixing and non-linear interface friction favors different flow patterns in UML, 2nd and 3rd layers.

References

BLECK, R., H. P. HANSON, D. HU, and E. B. KRAUS (1989): Mixed layer-thermocline interaction in a three dimensional isopicnic coordinate model. J. Phys. Oceanogr., **19**, 10: 1417-1439.

DANCHENKOV, M. A., V. B. LOBANOV, and A. A. NIKITIN (1997): Mesoscale eddies in the Japan Sea. Their role in circulation and heat transport. Proc. of the CREAMS'97 Int. Symp., Fukuoka, Japan, 28-30 Jan. 1997, 81-84.

HOGAN, P. J., and H. E. HURLBURT (1997): Sea of Japan

circulation dynamics via the NRL layered ocean model. Proc. of the CREAMS'97 Int. Symp., Fukuoka, Japan, 28–30 Jan. 1997, 109–112.

HOLLOWAY, G., T. SOU, and M. EBY (1995): Dynamics of circulation of the Japan Sea. Journal of Marine Research, **53**, 539–569.

ICHIYE, T., and K. TAKANO (1988): Physical structure of eddies in the Southwestern East Sea. La mer, **26**, 69–75.

KATOH, O. (1994): Tsushima Current in the south-western Japan Sea, J. Phys. Oceanogr., **50**, 317–338.
MIITA, T. And K. KAWATATE (1986): Trajectories of drift bottles released in the Tsushima Strait. Progress of Oceanography, **17**, 255–263.

MIKHAYLOVA, E. N., and N. B., SHAPIRO, (1992): Quasi-isopycnal multilayer model of large-scale ocean circulation. Morskoy Gidrophysicheskiy Journal Sebastopol, USSR, **4**, 3–13, (in Russian).

MIITA, T., and K. KAWATATE (1986): Trajectories of drift bottles released in the Tsushima Strait. Progress of Oceanography, **17**, 255–263.

MOOERS, C. N. K., and H. S. KANG (1997): On the 26 sigma level POM model for Japan (East) Sea circulation. Proc. of the CREAMS'97 Int. Symp., Fukuoka, Japan, 28–30 Jan. 1997, 15–17.

OSTROVSKII, A., and Y. HIROSE (1994): The Japan Sea circulation as seen in satellite infrared imagery in autumn 1993. Proc. CREAMS 94, 24–26 Jan. 1994, Fukuoka, Japan, 129–133.

PONOMAREV, V. I., and O. O. TRUSENKOVA (2000a): The dynamic response to the wind and buoyancy forcing in the Sea of Japan. Proc. of Int. Conf. on coastal ocean., Moscow, Russia, Sep. 1998, 99–108.

PONOMAREV, V. I., and O. O. TRUSENKOVA (2000b): Simulation of the Japan Sea circulation in summer 1999 using the MHI layered model. Proceedings of CREAMS–2000 Fourth Int. Symp., May 15–16, 2000, Vladivostok, Russia (in press).

PONOMAREV, V. I., and G. I. YURASOV (1994): The Tartar (Mamiya) Strait Currents. Journal of the Korean Society of Coastal and Ocean Engineers, **6**, 335–339.

RO, Y.J. (1999): Numerical experiments of the meso scale eddy activities in the East (Japan) Sea. Proc. of the CREAMS'99 Int. Symp., Fukuoka: 116–119.

SEUNG, Y. H., and K. KIM (1993): A numerical modeling of the East Sea circulation. Journal of the Oceanological Society of Korea, **28**, 292–304.

SHAPIRO, N. B. (1998): Formation of the Black Sea general circulation considering stochastic wind stress. Morskoy Gidrophysicheskiy Journal, Sebastopol, Ukraine, **4**, 12–24 (in Russian).

YOON J.-H. (1991): The branching of the Tsushima Current/ Rep. Res. Inst. Appl. Mech. Kyushyu Univ., **38**, 1–21.

YURASOV G. I., and V. G. YARICHIN (1991): Currents of the Japan Sea. Vladivostok, 173 pp (in Russian).

ZUENKO, Yu. (1999): Two decades of Polar Front large-scale meandering in the North-western Japan Sea. Proc. of the CREAMS'99 Int. Symp., Fukuoka: 68–71.

Recived on February 10, 2000
Accepted on November 2, 2000

La mer 38 : 199-203, 2000
Société franco-japonaise d'océanographie, Tokyo

The SeaSonde HF radars for coastal current mapping with recent oceanographic applications

Donald E. BARRICK*, Laura A. PEDERSON* and Steven R. RAMP**

Abstract : HF radar technology in the U. S. has evolved away from large phased arrays and conventional high-power pulsed waveforms in two respects: (1) the large cumbersome phased arrays are replaced by compact crossed-loop systems that can be mounted on a single post or building rooftop; (2) an efficient digitally synthesized, PC-processed waveform is used that greatly reduces radiated power levels while achieving longer ranges. These improvements lead to both lower initial prices and operating costs. Called the SeaSonde, variations on this family of products can achieve ranges to 300 km in certain cases, or fine spatial resolutions to 100 m suitable for smaller-scale bays and harbors. Many comparisons with other sensors have validated system function and show accuracies equal to or better than the older, conventional, larger phased array systems. Ongoing research includes real-time assimilation of the HF radar data into numerical models for nowcasting and forecasting ocean conditions. The Rutgers University Regional Ocean Model System (ROMS) showed dramatic improvement in nowcast skill during a coastal upwelling event off New Jersey when the HF radar current vectors, or even single-site current radial components, were included in the assimilation.

Key words : *HF radar, ocean currents, remote sensing, circulation modeling*

1. Evolution of HF coastal current-mapping radars in the U. S.

The HF/VHF part of the radio spectrum is used to map surface currents from shore because the interaction of the radar signals with the ocean waves is well understood and leads to simple interpretations of the echo. An additional advantage is the ability of vertically polarized signals at these frequencies to propagate well beyond the visible horizon over the highly conducting sea. The more familiar and ubiquitous microwave radars cannot map currents because they do not possess these advantages. The distinctive resonant peaks seen in HF echo from the sea were discovered experimentally 45 years ago (CROMBIE, 1955). The underlying theoretical nature of these dominant spectral echoes was shown (BARRICK, 1972) to be first-order Bragg scatter; he also derived expressions for the lower-level second-order spectral continuum surrounding these peaks. The Doppler shift of the first-order Bragg peaks is employed to obtain the radial velocities of the surface currents, while the secondorder continuum provides information about the sea state (e. g., waveheights, directions, etc.). Because a single radar detects only the radial component of the horizontal current velocity, two or more radars are normally deployed to synthesize a total current vector at each point on their common map area.

While conventional beam-forming techniques were well understood at microwave frequencies, the application of these same techniques to the HF band leads to quite large antenna sizes, as its lateral dimension must be many radio wavelengths in extent. Called phased arrays, these antenna systems combine signals from many array elements in software to form and scan their beams across bearing angle. Using large phased-array antennas on San Clemente Island, CA, BARRICK, CROMBIE and their colleagues established the utility of HF

* CODAR Ocean Sensors, Ltd, 1000 Fremont Avenue, Suite K, Los Altos, CA 94024, U. S. A.
don@codaros.com; laura@codaros.com
** Oceanography Department, Naval Postgraduate School, Monterey, CA 93943, U. S. A.

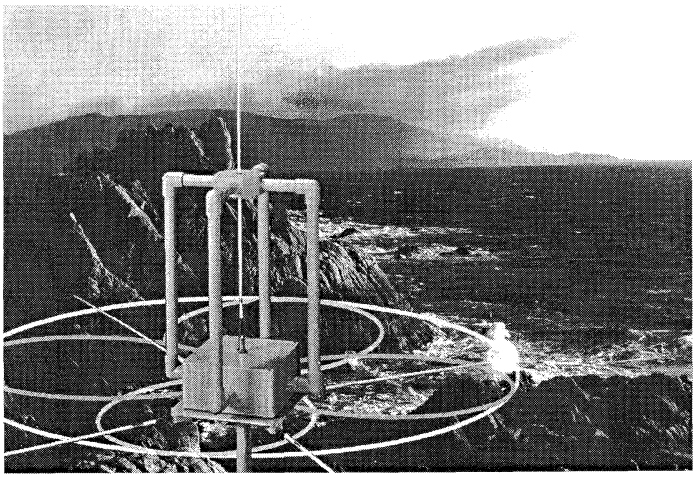

Fig. 1. Photo of SeaSonde crossed airloop receive antenna unit on post, with patterns sketched below.

radars for coastal surface-current mapping over 25 years ago (BARRICK *et. al.*, 1974; STEWART and JOY, 1974).

The major impediment to widespread HF radar use has been this large phased-array antenna size, demanding at least 100 meters of coast per site, not including their transmit antennas. Besides their large costs, this is a major inconvenience factor that often limits access to coastal points with desirable views, not to mention operation from offshore platforms. This obstacle was overcome by inventions at U. S. NOAA's research laboratories headed by BARRICK in the 1970s (BARRICK *et. al.*, 1977). Compact antennas replaced the large phased arrays, made possible by application of direction-finding (DF) principles instead of deam forming (LIPA and BARRIC, 1983; BARRIC and LIPA,1997). The SeaSonde family of products is its commercial culmination. Their compact antennas are kept out of reach, either on posts, building rooftops, or the derrick of an oil rig. Along with the introduction of a unique highly efficient waveform and its digital generation and processing, this low-powered compact system allows unmanned real-time operation. Some sites have continued for over six years uninterrupted. Its compact nature and ease of setup also makes it also well suited to quick-response deployments.

These breakthroughs-with resulting lower costs-increased the utility of HF radar, and may be responsible for the recent proliferation of SeaSondes. Although HF radar current mapping was demonstrated nearly 30 years ago, this revolutionary technology did not begin making its way into the oceanographic and user communities until the early 1990s. Over 50 units of the SeaSonde family have been built and sold since 1993 (most still operating today). These include standard systems with ranges of ~50 km, high-resolution versions for ports and harbors, and long-range units that can see beyond 200 km.

2. Accuracies achieved with direction-finding SeaSondes

One of the questions frequently asked is: how is it possible to get accuracies from compact radars that are equivalent to those from the large, conventional phased-array systems? The typical SeaSonde receive antenna is a crossed-loop/monopole unit mounted on a post, as shown in Fig. 1. Sketched underneath the antenna photo are plots of the idealized antenna patterns: two orthogonal cosine patterns(from the loops) and an omni-directional pattern (from the vertical monopole). When the antennas truly have these idealized patterns, a simple four-quadrant arctangent function will resolve the angle of the echo signal over 360° of bearing. In practice, the patterns are somewhat distorted by their environment, and measured patterns obtained during the initial system

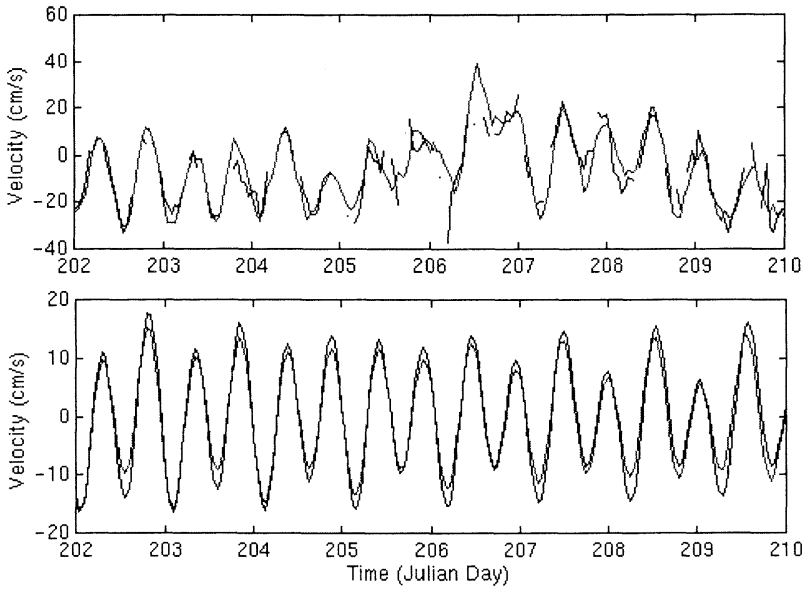

Fig. 2. Plots of raw radial current vector comparison (upper panel) for South site SeaSonde at Rutgers LEO-15 and ADCP bin 4.5 m below surface for one week; 6.7 cm/s rms difference. Lower is plot of radial tidal time series comparison for same week, with 2.3 cm/s rms difference. [From KOHUT *et al.*, 1999]

calibration are used in the DF algorithm to extract unbiased bearing angle. Bearing angle (DF) determination is done for each of the radial-velocity-shifted Doppler signals that comprise the first-order Bragg peaks.

Establishing accuracy with any HF surface-current mapping radar is difficult: no other instrument measures exactly the same thing. The HF radar senses the mean current within the upper meter, averaged over a horizontal radar cell. Multiple Lagrangian drifters have been tracked in Monterey Bay, CA for such comparisons. Perhaps the most frequently invoked comparison employs bottom-mounted acoustic Doppler current profilers (ADCPs), selecting their cell closest to the surface that is not contaminated by sidelobe reverberations; this is typically 3-5 meters deep. The water layer depth above this bin can also vary with tide height, being significant in some areas. Thus the ADCP output is essentially an Eulerian, point measurement that is then compared with an area average at different water depths. In additon, HF radar feels the Stokes drift (wave-induced current), whereas the ADCP does not. Nevertheless, this instrument comparison is probably the best available.

One recent such comparison was done with the Rutgers University SeaSondes deployed off New Jersey. Located 29 km from the southern SeaSond, the radials (i. e., current components at the ADCP pointing toward the radar) were compared hourly for one month, a typical week's data being shown in Fig. 2 (KOHUT *et al.*, 1999). The closest ADCP bin to the surface that could be used was 4.5 m deep. The rms difference in the raw, hourly time series over one month was 6.7 cm/s. The radial tidal components that were extracted from the month time series are shown in the lower panel of Fig. 2 for the same week, their rms difference is 2.3 cm /s. Not all of these differences are errors in one or the other instrument, but it can be said with certainty that any instrumental error did not exceed these amounts. These differences are comparable to (slightly better than) those observed with the OSCR 100-m phased array operated by U. of Miami(CHAPMAN and GRABER, 1997).

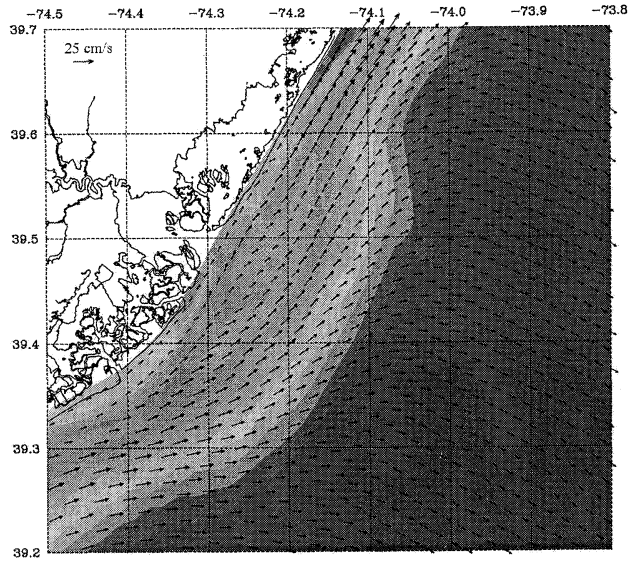

Fig. 3a. Ocean numerical circulation model outputs for July 17, 1998 without SeaSonde data assimilation. [From KOHUT *et al.*, 1999]

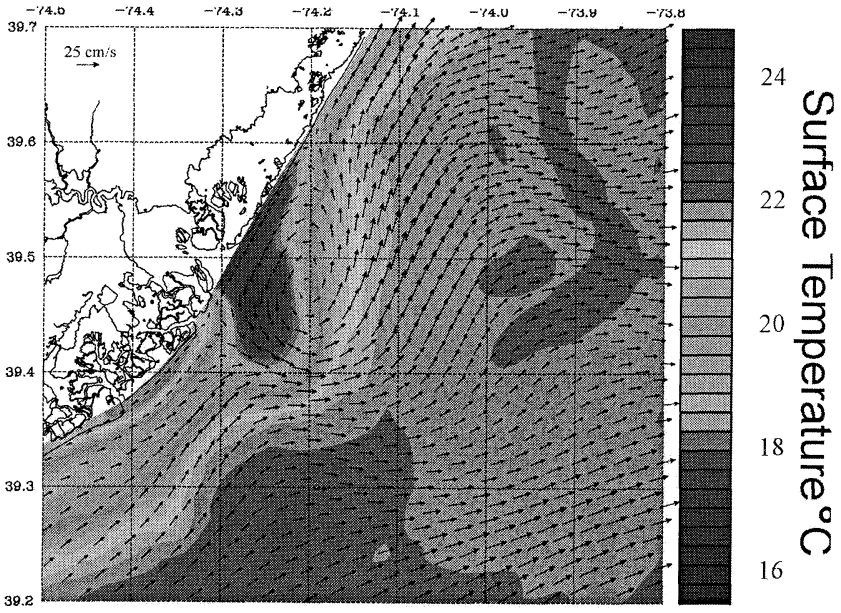

Fig. 3b. Ocean numerical circulation model outputs for July 17, with SeaSonde data assimilation. The assimilation dramatically improves the model's capability to forecast the observed eddy and upwelling center, as confirmed by independent observations. [From KOHUT *et al.*, 1999]

3. Benefits of assimilation of SeaSond current maps into circulation models

Variations of the Princeton Ocean model (POM) developed by Mellor and Blumberg in the 1970s(BLUMBERG and MELLOR, 1987) have been widely used for nowcasting and forecasting oceanographic conditions in coastal regions and marginal seas around the world. Like all numerical models, the POM's forecast skill depends on obtaining the best possible initial

conditions and can be improved by data assimilation. Some work has already been done on assimilation of HF radar current data into the POM model in the Monterey Bay (LEWIS *et al.*, 1998). The results are encouraging, but indicate that additional smoothing of the radar data may be necessary for use with mass-conserving numerics. This work is continuing in the bay under the auspices of the National Ocean Partnership Program (NOPP). Recently, the Rutgers University Regional Ocean Modeling System (ROMS) has also been used to assimilate the CODAR SeaSond data. A key feature of the summertime oceangraphic situation off the New Jersey coast is the evolution of anticyclonic eddies that accompany upwelling events. Without SeaSonde surface current map data the ROMS model consistently omitted these essential features. The model was subsequently initiated both with and without the SeaSonde surface current information. The non-assimilative model did not reveal the development of an upwelling eddy on July 17, 1998 (Figure 3a), while the assimilative model clearly shows this feature (Figure 3b). The eddy's existence was confirmed by subsequent in-situ and satellite AVHRR observations. The assismilation in turn led to better forecasts that were useful in planning vessel sampling operations associated with LEO-15 (KOHUT *et al.*, 1999).

4. Conclusions

HF radars for coastal and offshore current mapping have found acceptance and are rapidly proliferating in recent years. Part of this may be due to the availability of compact, low-cost, easy-to-deploy and use SeaSonde-type radar designs since 1993. This makes both long-term deployments-as well as short several-week field campaigns-much easier to implement. Accuracies are demonstrably comparable to or better than those of the older larger phased array designs. Among the oceanographic and marine applications of radar current maps, we highlight here the improvement offered in numerical circulation forecasting based on their assimilation into these models.

References

BARRICK D. E. (1972): Remote sensing of sea state by radar, *In*: Remote Snsing of the Troposhphere, DERR, V.E(ed), U.S. Government Printing Office, Washington, D. C.

BARRICK, D. E., J. M. HEADRICK, R. W. BOGLE and D. D. CROMBIE (1974): Sea backscatter at HF: Interpretation and utilization of the echo, Proc. IEEE, **62(6)**, 673-680.

BARRICK, D. E., M. W. EVANS and B. L. WEBER (1977): Ocean surface currents mapped by radar, Science, **198**, 138-144.

BARRICK, D. E. and B. J. LIPA (1997): Evolution of bearing determination in HF current mapping radars, Oceanography, **10(2)**, 72-75.

BLUMBERG, A. F. and G. L. MELLOR (1987): A description of a three-dimensional coastal ocean circulation model. *In*: Three Dimensional Coastal Models, Coastal and Estuarine Sciences, **4**, HEAPS, N. S. (ed), Amer. Geophys. Union Geophysical Monograph Board, 1-16.

CHAPMAN, R. D. and H. C. GRABER (1997): Validation of HF radar measurenments, Oceanography, **10(2)**, 76-79.

CROMBIE, D. D. (1995): Doppler spectrum or sea echo at 13.56 Mc/s, Nature, **175**, 681-682.

KOHUT, J., S. GLENN and D. BARRICK (1999): SeaSonde is integral to coastal flow model development, Hydro International, **3(3)**, 32-35.

LEWIS, J. K., I. SHULMAN and A. F. BLUMBERG (1998): Assimilation of Doppler radar current data into numerical ocean models. Cont. Sh. Res., **18**, 541-559.

LIPA, B. J. and D. E. BARRICK (1983): Last-squares methods for the extraction of surface currents from CODAR crossed-loop data: Application at ARSLOE, IEEE J. Oceanic Engr., **OE-8**, 226-253.

STEWART, R. H. and J. W. JOY(1974): HF radio measurements of ocean surface currents, Deep Sea Research, **21**, 1039-1049.

Received on January 11, 2000
Accepted on August 31, 2000

La mer 38 : 205-210, 2000
Société franco-japonaise d'océanographie, Tokyo

Seasonal changes of circulation in North Pacific by a MOM2 simulation

Dongfeng XU* Yaochu YUAN* Noriya YOSHIOKA** and Yasushi YOSHIKAWA**

Abstract : A Modular Ocean Model (MOM2) is used to simulate the circulation of the North Pacific, which is driven by climatological wind stress from HERLLERMAN and ROSENSTEIN (1983). The climatological temperature and salinity data (LEVITUS, 1982) is used as initial condition. After 8-years integration for annual forcing, monthly forcing is used to integrate the model for another 4-years.

The model results show that: (1) The Volume Transport (VT) of Kuroshio changes in the East China Sea from 27.5×10^6 m^3/s(SV) in winter to 32.9×10^6 m^3/s(SV) in summer, which is in contrast with that derived from Sverdrup relation. The North Equatorial Current (NEC) bifurcates at northernmost latitude in October and southernmost latitude in May, which influence the Kuroshio VT on PN section (near the Ryukyu Islands). This is caused by the seasonal shift of zeroline of wind stress curl over the southern part of the subtropical North Pacific. The vertical velocity difference is larger in summer, which also results in the a little larger VT of the Kuroshio on PN section in summer. (2) The Kuroshio bifurcates into two branches at the east of Taiwan. The main one flows northward into the East China Sea, and the other one flows northeastward to the region east of Ryukyu Islands. (3) There exists a permanent anti-cyclonic eddy south of Japan.

Key words : *Kuroshio, North Equatorial Current (NEC), seasonal change, wind stress curl*

1. Introduction

The seasonal change of the Kuroshio has been extensively studied, especially on PN section (near the Ryukyu Islands). About the Volume Transport (VT) of the Kuroshio across PN section, YUAN *et al.* (1994), using 11 cruises data from 1987 to 1994, got the result of 28.6×10^6 m^3/s. On average, the VT is strong in summer than in autumn. ICHIKAWA and BEARDSLEY (1993) used the hydrographic data from 1986 to 1989 and found that the VT of the Kuroshio west of the Ryukyu Islands equaled $27.6\pm3.7\times10^6$ m^3/s. Numerical models have also been used to explain the reason of a little larger VT of the Kuroshio on PN section in summer than that in winter, which is out of phase predicted by the Sverdrup Balance. KAGIMOTO and YAMAGATA (1997) used the POM model and found that the JEBAR (Joint Effect of BAroclinity and bottom Relief) effect is the main reason. By a 2-layer model SAKAMOTO and YAMAGATA (1996) proved that the role of JEBAR makes the total transport of the Kuroshio relatively insensitive to seasonal changes of winds as observed. Also by a 2-layer model SEKINE and KUTSUWADA (1994) proposed that some part of VT of western boundary current passes the eastern side of Nansei Islands in winter. In fact, the change in the Kuroshio VT is much influenced by the variation at the upstream side. Using a reduced gravity model and 20-years wind data, QIU and LUKAS (1996) found that the Kuroshio (at 20°N) has a seasonally minimum (maximum) VT in fall when the North Equatorial Current (NEC) bifurcates seasonally at the northernmost (southernmost) latitude which is influenced by the shift of wind stress curl of the North Pacific.

* Second Institute of Oceanography, Key Lab of Ocean Dynamics Processes and Satellite Oceanography ,SOA , Hangzhou 310012, China
(e-mail: df__xu@263.net)
** Japan Marine Science and Technology Center, Yokosuka, 237, Japan
(e-mail: yoshikaway@jamstec.go.jp)

The motivation of this paper is to find the influences of the seasonal shift of wind stress curl over the subtropical region to the seasonal change in VT of the Kuroshio on PN section. By a MOM2 simulation with seasonal wind and stratification, we found that the shift of the NEC bifurcation position caused change in the Kuroshio VT not only in the low-latitude but also in the mid-latitude such as on PN section. The summer stratification is also the reason of the larger Kuroshio VT on PN section in summer than in winter.

2. Ocean Model

A Modular Ocean Model (MOM2) is used to simulate the circulation of the North Pacific. The model domain is from 1° N to 61° N and from 120° E to 90° W. The grid size changes from 0.25 to 1 degree both in meridional and zonal directions, most fine in the Northwest Pacific. The model has 7 layers in vertical direction. The depths at the bottom of each level are 30 m, 60 m, 192.2 m, 694.0 m, 1794.0 m, 3492.1 m, 5560 m, respectively. All the four boundaries are closed. The ETOPO5, 1/12° world topography data set from the *National Oceanic and Atmospheric Administration* (1988), is smoothed to our model grid. On the north and south boundaries, sponge layers are adapted in which temperature and salinity are restored to the climatological values with the restoring time changing from 25 days outside to 75 days in the interior. Temperature and salinity are also restored on the surface boundary. Climatological wind stress data from HERLLERMAN and ROSENSTEIN (1983) is used. The climatological temperature and salinity data (LEVITUS, 1982) is used as the initial condition. The annual forcing is used to integrate the model from the rest state during 8-years. After that, monthly forcing is used to integrate the model for another 4-years. A seasonal equilibrium has reached for the upper layers. We have compared the results between hrizontal eddy viscosity (SMAGORINSKY, 1963) and constant eddy viscosity. Our result shows that the SMAGORINSKY scheme is more capable to simulate the mesoscale phenomena.

3. Computed results and discussion

3.1. Variation of NEC bifurcation position

Figure 1a and 1b show that the zeroline of wind stress curl shifts toward the southernmost latitude in May and northernmost latitude in October. By the Sverdrup relation, the NEC shifts seasonally (Figs.1c and 1d), and the shift of the NEC causes the seasonal change in the NEC bufurcation position at the western boundary (Fig.2a). QIU and LUKAS (1996) used the FSU (Florida State University) wind data and got the similar result. XU and YUAN (1995) used the TOGA data from 1986 to 1989 and found the same seasonal changes in the NEC bifurcation at the 130° E section.

3.2 East of Taiwan

The Kuroshio east of Taiwan separates into the two branches: the main brabch flows through the ridge northeastern of Taiwain and then flows along the continental slope of the East China Sea, and the other eastern branch flows east of the Ryukyu Islands. The two branches confluence together in the region south of Japan. Figures 3a and 3b show the velocity structure across the 23.125° N section in May and October at the 12th model years. The depth of 20cm/s velocity isoline reaches 600m in May but only 400 m in October. The maximum velocity reaches 92.1 cm/s in May and 69.0 cm/s in October. This means that the Kuroshio is intensified in the upper layer and the vertical difference is larger in summer than in winter. This is caused by the stratification effect in summer. SUN and KANEKO (1994) reported the similar measured phenomena. LIU *et al.* (1992) have pointed out that in winter the Ekman effect of the northeasterly monsoon caused the shallowing of the thermocline.

3.3. East China Sea

Figure 2b shows the variation of monthly mean VT of the Kuroshio on PN section. It is larger in May than in October. The VT in PN section is 31.0, 31.9, 32.1, 27.5×10^6 m^3/s in January, April, July and October respectively. KAGIMOTO and YAMAGATA (1997) got the similar result by POM simulation. Figures. 4a and 4b are the stream function of May and October

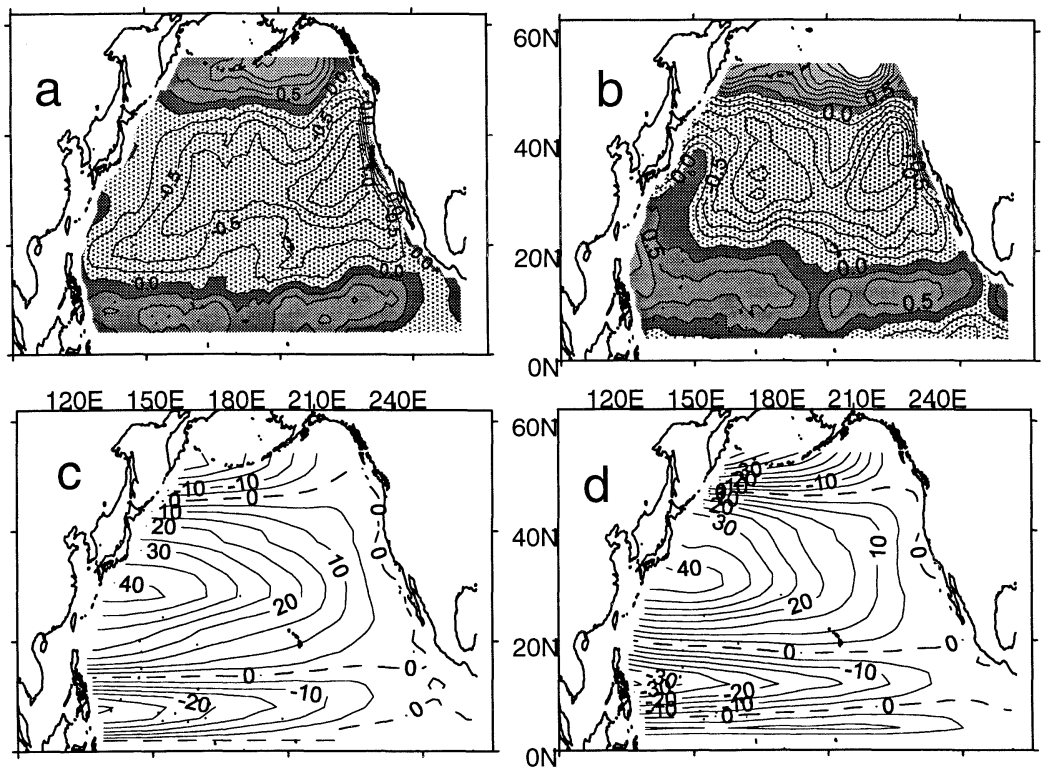

Fig. 1. Climatological wind stress curl from HERLLERMAN and ROSENSTEIN (1983) (CI=10^{-8} dyn/cm^3): (a) May and (b) October, and stream function from the Sverdrup Balance (CI=5×10^6 m^3/s): (c) May and (d) October.

respectively. Comparing the 60×10^6 m^3/s isoline in May with that in October, it is closer to Taiwan in May than in October. This means that the Kuroshio approaches the eastern coast of Taiwan with larger VT in May than in October, so that larger VT of the Kuroshio can flow into the Okinawa Trough through the ridge and cause a little larger VT of the Kuroshio on PN section in May than in October. This origin of this process is ascribed to the fact that NEC bifurcates at the southern latitude in May than in October. Therefore we propose that the wind stress curl and stratification are the main reasons of larger summer VT of the Kuroshio on PN section. When compared with the real measurement of VT of the Kuroshio, we shall be caution that the interannual changes also influence the VT of the Kuroshio significantly. KAWABE (1998) have reported that the variation of Kuroshio VT has 20-year period. QIU and LUKAS (1996) showed that the wind stress curl changing with the timescale of the El Niño Southern Oscillation (ENSO) can influence the Kuroshio VT.

3.4. South of Japan

There is a permanent anticyclonic eddy south of Japan. The VT reaches 115×10^6 m^3/s in winter (in January, not shown here) and 97.9×10^6m^3/s in October (Figure 4b). This is in consistent with the Sverdrup theory. SEKINE and KUTSUWADA (1994) has got the similar result by a 2-layer model.

4. Conclusions

In this paper, we have discussed the influence of the seasonal shift of wind stress curl to the Kuroshio VT variation on PN section. The seasonal shift of wind stress curl firstly causes the seasonal meridional shift of NEC bifurcation position, which can make the seasonal change in the Kuroshio VT east of Taiwain, and at last cause the seasonal change in the Kuroshio VT on PN section. It should be

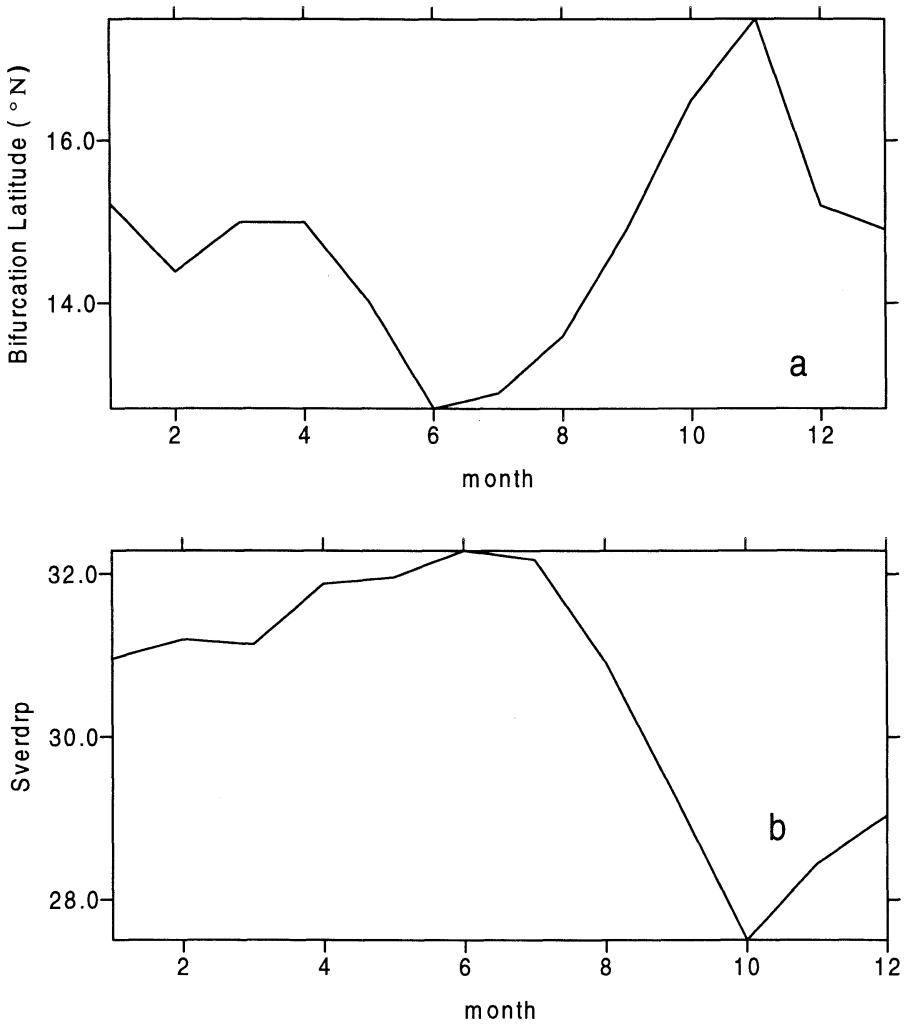

Fig. 2. (a) monthly change in the North Equatorial Current bifurcate position at the 125°E section, (b) monthly change in Volume Transport at PN Section (unit: $10^6 m^3/s$)

mentioned that the interannual changes influence the VT of the Kuroshio significantly (QIU and JOYCE, 1992; KAWABE, 1998), and the mesoscale eddies influence the Kuroshio path and its VT frequently (YANG *et al.*, 1999). We got the following conclusion in this study:

1) On the 125°E section the NEC bifurcates at the northernmost latitude in October and southernmost latitude in May. This is caused by the seasonal shift of zeroline of wind stress curl over the southern part of subtropical North Pacific. This seasonal shift also causes the variation of VT of the Kuroshio in the East China Sea.

2) The vertical velocity difference is larger in summer. This is caused by stronger stratification in summer. This is one of the main reason of larger Kuroshio VT in summer.

3) The Kuroshio VT on PN section is 31.0, 31.9, 32.1, 27.5×10^6 m^3/s in January, April, July and October respectively. The VT of the Kuroshio is strong in summer and weak in autumn.

4) The Kuroshio separates into the main branch and the eastern branch in the east of Taiwan.

Acknowledgement

This project was supported by the Youth

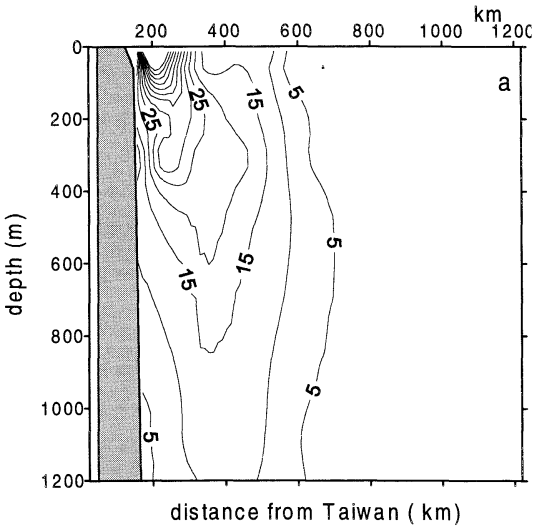

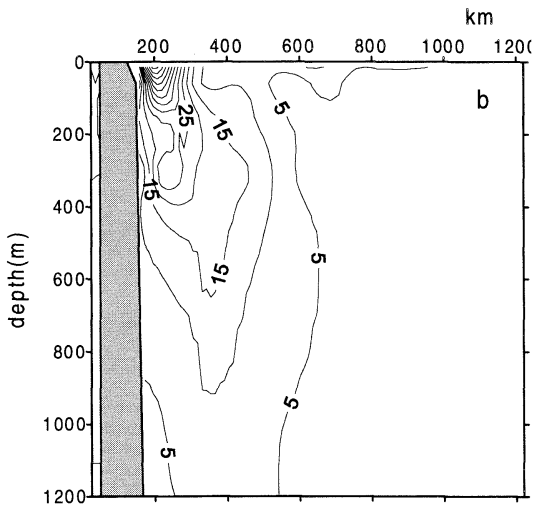

Fig. 3. Velocity structures at 23.125° N for 12 years integration: (a) May (Maximum velocity=92.1cm/s), (b) October (Maximum velocity=69.0 cm/s)

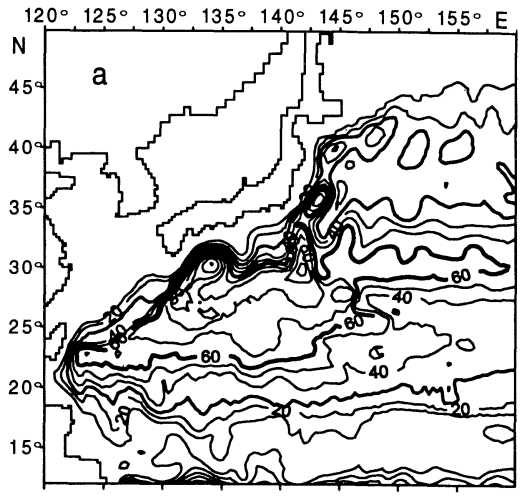

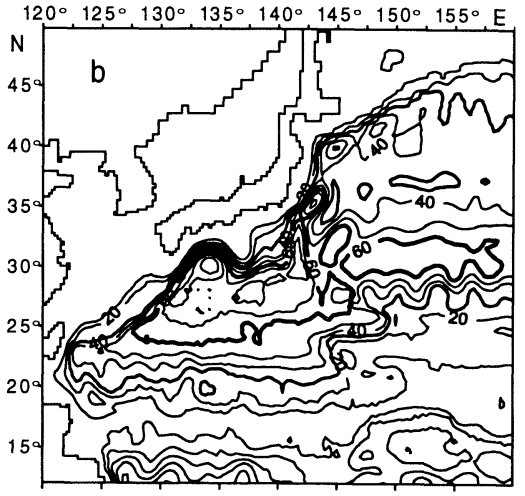

Fig. 4. Stream Function for 12-years integration (CI=10×10^6 m^3/s): (a) May, (b) October

Marine Science Foundation of State Oceanic Administration, P., R, China (No.98201), the Major State Basic Research Program (No.G1999043802), the National Natural Science Foundation of China (No.49776287), and the Youth Marine Science Foundation of Second Institute of Oceanography, SOA, China (No.9703).

References

ICHIKAWA, I. and R. C. BEARDSLEY (1993): Temporal and spatial variability of volume transport of the Kuroshio in the East China Sea. Deep Sea Research. **40**, No.3, 580–605.

KAGIMOTO, T. and T. YAMAGATA (1997): Seasonal transport variations of the Kuroshio: An OGCM simulation. J. Physical Oceanography. **27**, 403–418.

KAWABE M.(1998): How important is the monitoring of decadal variation of Kuroshio for the ocean and atmosphere climate? Joint GCOS–GOOS WCRP Ocean Observations Panel for Climate (OOPC) 3rd session, France.

HERLLERMAN, S., and M. ROSENSTEIN (1983) Normal monthly wind stress over the world ocean with error estimate. J. Physical Oceanography. **13**,

1093–1104.

LEVITUS, S., (1982): Climatological atlas of the World Ocean NOAA Professional Paper No. 13 U.S. Government Printing Office, Washington D. C 173PP.

LIU, K-K., G.-C. GONG, C.-Z. ZHYU S.-C. PAI C.-L. WEI and S.-Y. CHAO (1992): Response of Kuroshio upwelling to the onset of northeast monsoon in the sea north of Taiwan: Observations and a numerical simulation. J. Geophysical Research. **97**, 12511–12516.

National Oceanic and Atmospheric Administration (1988): Digital relief of the surface of the Earth, Data Announce. 88-MGG-02, http://www.ngdc.noaa.gov / mgg / global / selttopo.html, Natl. Geophys. Data Cent., Boulder, Colo.

QIU, B., and T. JOYCE (1992): Interannual variability in the mid and low latitude western North Pacific. Journal of Physical Oceanography, **22**, 1062–1079.

QIU, B., and R. LUKAS (1996): Seasonal and interannual variability of the North Equatorial Current, the Mindanao Current and the Kuroshio along the Pacific western boundary. J. Geophysical Research. **101**, 12315–12330.

SAKAMOTO, T. and T. YAMAGATA (1996): Seasonal transport variations of the wind-driven ocean circulation in a two-layer planetary geostrophic model with a continental slope. J. Marine Res. **54**, 261–284.

SEKINE, Y., and K. KUTSUWADA (1994): Seasonal variation in volume transport of the Kuroshio south of Japan. J. Physical Oceanography. **24**, 261–272.

SMAGORINSKY, J. (1963): General circulation experiments with the primitive equations: I. The basic experiment. Monthly Weather Review, **91**, 99–164

SUN, X., and I. Kaneko (1994), Variations of Kuroshio during the period of 1989–1991. Proceedings of China_Japan Joint Symposium of the Cooperative Research on the Kuroshio, China Ocean Press. 41–61.

YANG, Y., C.-T. LIU, J.-H. HU, and M. KOGA (1998): Taiwan Current(Kuroshio) and impinging eddies. J. Oceanography , 1999, **55**, 609–617.

YUAN, Y., Z. PAN, I. KANEKO, and M. ENDOH(1994): Variability of the Kuroshio in the East China Sea and the currents east of Ryukyu Islands., Proceedings of China-Japan JSCRK, Qingdao, China Press, 121–144.

XU, D.-F., and Y.-C. YUAN (1995): The calculation of the circulation east of Philippine Sea. Oceanography in China. Vol. 5, 84–97.

Received on February 10, 2000
Accepted on October 31, 2000

La mer 38 : 211-218, 2000
Société franco-japonaise d'océanographie, Tokyo

Water, heat and salt transports from diagnostic world ocean and north pacific circulation models

Zexun WEI* Byung-Ho CHOI** and Guohong FANG*

Abstract : Global and North Pacific robust diagnostic models are established based on MOM of GFDL to study the circulation in the world ocean and East Asian marginal seas respectively. The horizontal grid sizes are 1 degree for the global model and 1/3 degree for the North Pacific model, and the vertical water column is divided into 21 levels. The hydrographic data are taken from World Ocean Atlas 1994 (1994) and the wind stress from HELLERMAN and ROSENSTEIN (1983).

Based on the model result, the horizontal volume, heat and salt transports across some representative sections are calculated. The results show that: though the cross-equator volume transports in the Atlantic, Indian and Pacific Oceans are all small, the heat transports across equator in the Atrantic is northward. This is cleary a result of the southward flow of the North Atrantic Deep Water and the northward compensating warm flow in the upper layer. The annual mean of the cross-equator heat transport in the Pacific from the present model is significantly lower than that calculated by PHILANDER *et al.* (1987). This might indicate the importance of the Indonesian Throughflow in the heat transport in the Pacific. Our calculation shows that the heat transport through the Indonesian Archipelago is -1.0 PW, which is comparable with the poleward heat transport in the North Atlantic and Pacific Oceans. The difference in heat transports across the sections 4 (it separates the southern Atlantic and Indian oceans) and 5 (it separates the southern Pacific and Atlantic Oceans) demonstrates the importatn role of tha Agulhas current in the heat balance of the world ocean.

Key words : *Volume transport, heat transport, salt transport, world ocean*

1. Introduction

The rapid development of the computers has made it possible to simulate the ocean circulation using three dimension primitive numerical models, especially for the large margin with fine resolution. GFDL (Feophysical Fluid Dynamic Laboratory)'s Modular Ocean Model (MOM) is one of this kind of models. It is based on Kirk BRYAN (1969)'s work. As described by Bryan, the equations consist of the Navier Stokes equations subject to the Boussinesq, hydrostatic, and rigid lid approximations along with a nonlinear equation of state which couples two active tracers, temperature and salinity to the fluid velocity.

The diagnostic study on the world ocean circulation has been conducted by FUJIO *et al.* (1991, 1992). The resolution of their model was $2^\circ \times 2^\circ$, thus it was not able to resolbe the East Asian marginal seas adequately and the emphasis of their study was on the water movement.

In the present study, we established a $1^\circ \times 1^\circ$ resolution robust diagnostic model for the world ocean and $1^\circ/3 \times 1^\circ/3$ resolution robust diagnostic model for the North Pacific ocean based on MOM to study the circulation on the world ocean and East Asian marginal seas respectively. Based on the model results, the horizontal volume, heat and salt transports across some representative sections are obtained.

* Department of Physical Oceanography, Institute of Oceanology, Chinese Academy of Sciences, 7 Nanhai Road, Qingdao 266071, China (e-mail: weizx@ms.qdio.ac.cn)
** Department of Civil and Environmental Engineering, Sungkyunkwan University, Korea

2. Model description

The governing equations are as follows:

$$\frac{\partial u}{\partial t}+(u\cdot\nabla)u+w\frac{\partial u}{\partial z}+fk\times u$$
$$=-\frac{1}{\varrho_0}\nabla p+A_H\nabla^2 u \quad (1)$$
$$+A_v\frac{\partial^2 u}{\partial z^2}+minor\quad terms$$

$$\frac{\partial p}{\partial z}+\rho g=0 \quad (2)$$

$$\nabla\cdot u+\frac{\partial w}{\partial z}=0 \quad (3)$$

$$\frac{\partial \theta}{\partial t}+(u\cdot\nabla)\theta+w\frac{\partial \theta}{\partial z}$$
$$=K_H\nabla^2\theta+K_v\frac{\partial^2\theta}{\partial z^2}+\gamma(\theta^*-\theta) \quad (4)$$

$$\frac{\partial S}{\partial t}+(u\cdot\nabla)S+w\frac{\partial S}{\partial z}$$
$$=K_H\nabla^2 S+K_v\frac{\partial^2 S}{\partial z^2}+\gamma(S^*-S) \quad (5)$$

$$f=2\Omega\sin\phi \quad (6)$$

The damping terms $\gamma(\theta^*-\theta)$ and $\gamma(S^*-S)$ in the equations (4) and (5) were first proposed by SARMIENTO and BRYAN (1982), and the model was called as *robust diagnostic* model. These terms force the model-produced temperature ad salinity to approach the observed values.

The horizontal resolution is 1 degree for the global model and 1/3 degree for the North Pacific model, and the vertical water column is divided into 21 levels (see Table 1). The domain is 0°–360°, 80° S–87° N for the Global model and 99° E–75° W, 2° N–64° N for the North Pacific model. The topography is taken from DBDB5 data set (Natinal Geophysical Data Center, Boulder, Colorado). The hydrographic data is taken from World Ocean Atlas 1994 (1994) and the wind stress from HELLERMAN and ROSENSTEIN (1983).

The damping coefficient γ was taken:

$$\gamma=[\gamma_d+(\gamma_0-\gamma_d)*e^{\frac{z}{h}}]*|\sin\varphi| \quad (7)$$

where γ_0 and γ_d are the coefficients at the sea surface and abyss, set as $(100\text{day})^{-1}$ and $1/5\gamma_0$ respectively. z is the water depth, $h=500$ m, φ is the latitude. To restore the observed temperature and salinity quickly, we used larger γ during the first month integration.

As shown in FUJIO *et al.* (1992), the diagnostic model is not significantly influenced by the choice of eddy mixing parameters. Thus we used the following values:

$A_H=1.0\times10^8$ cm^2/s, $A_V=1.0$ cm^2/s,
$K_H=1.0\times10^7$ cm^2/s, $K_V=0.2$ cm^2/s.

In the global model, we used the cyclic boundary condition on the east and west boundaries, and the solid boundary conditons on the north and south boundaries. In the North Pacific model, we used the solid boundary conditions on the all boundaries. The Bering Strait lies on the north, but the volume transport is very small. The south boundary is open, but the current here is basically zonal, therefore, to simplify the problem, we neglect the meridional flows along these two boundaries.

For the global model, we made 11-year integration for each month and annual mean forced by steady hydrography and wind stress respectively. For the North Pacific model we

Table 1. Depths and Thickness of Model Levels

Level	Depth range(m)	Thickness (m)	Mid~depth (m)
1	0~20	20	10
2	20~40	20	30
3	40~80	40	60
4	80~120	40	100
5	120~180	60	150
6	180~250	70	215
7	250~350	100	300
8	350~450	100	400
9	450~550	100	500
10	550~700	150	325
11	700~900	200	800
12	900~1100	200	1000
13	1100~1400	300	1250
14	1400~1750	350	1575
15	1750~2250	500	2000
16	2250~2750	500	2500
17	2750~3250	500	3000
18	3250~3750	500	3500
19	3750~4250	500	4000
20	4250~4750	500	4500
21	4750~5750	1000	5250

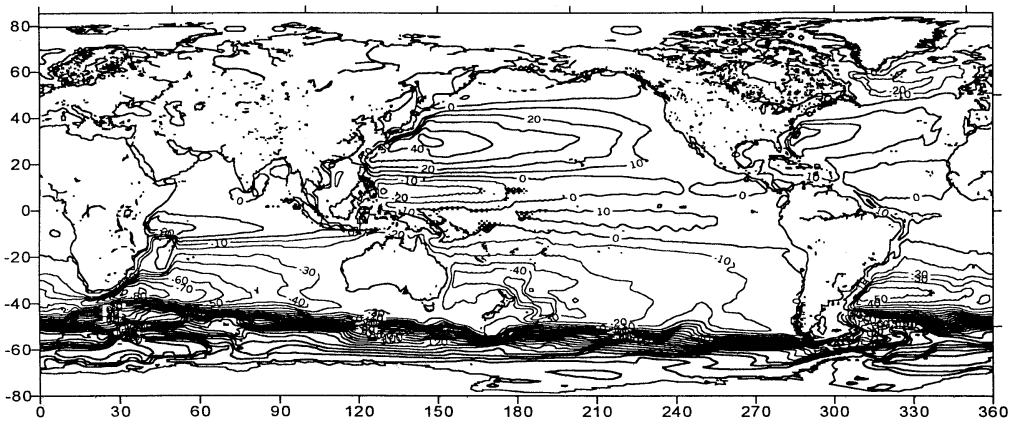

Fig. 1. Tranport stream function (unit: Sv) of the world ocean (annual mean)

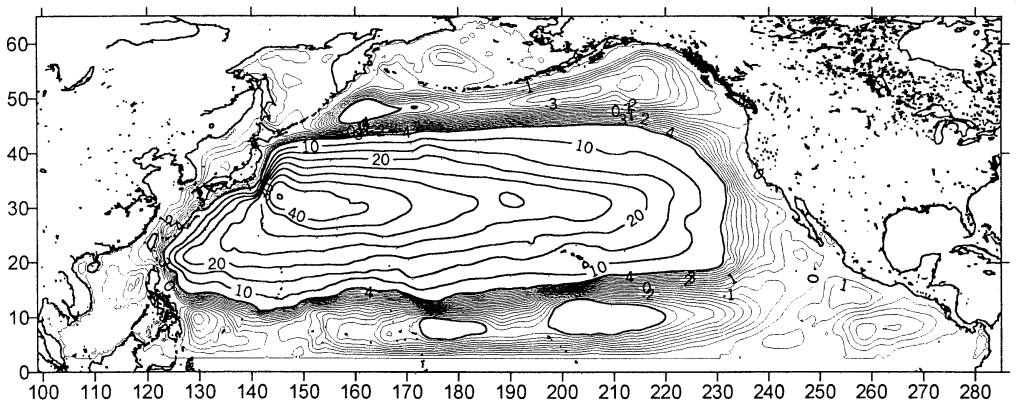

Fig. 2. Tranport stream function (unit: Sv) of the North Pacific (annual mean)

made 7-year integration. The results of the last year were saved for analysis.

3. Volume, heat and salt transports

The model-produced transport stream functions are shown in Figs. 1 and 2 respectively. From Fig. 1, we find that the basic pattern is quite similar to that of FUJIO *et al.* (1992), except that some improvement can be seen. For example, the western boundary currents are strengthened and thus more realistic, the Pacific equiatorial counter current and the Mindanao dome have been better reproduced. From Fig.2 we can see more detailed structures of the circulation near the western boundaries. These include the Mindanao dome southeast of Philippines, the NW Luzon Cyclonic Gyre in the South China Sea (FANG *et al.*, 1998), the Taiwan-Tsushima-Tsugaru Warm Current System in the East China Sea and Japan/East Sea (FANG *et al.*, 1991). These features were not resolved in FUJIO *et al.* (1992) due to its coarse grid.

To estimate the water volume, heat and salt transports in various regions we selected some representative sections in the oceans as shown in Fig. 3. The sections 1(C), 2(C) and 3(C) in the Pacific lie on the equator, 30° N and 30° S latitudes respectively. The transports across section 1(C) represent the energy and substance transfer between the North and South Pacific. These across section 2(C) represent energy and substance transfer between the northern and southern North Pacific. In particular, the heat transports here characterize the poleward heat flux in the Pacific. The

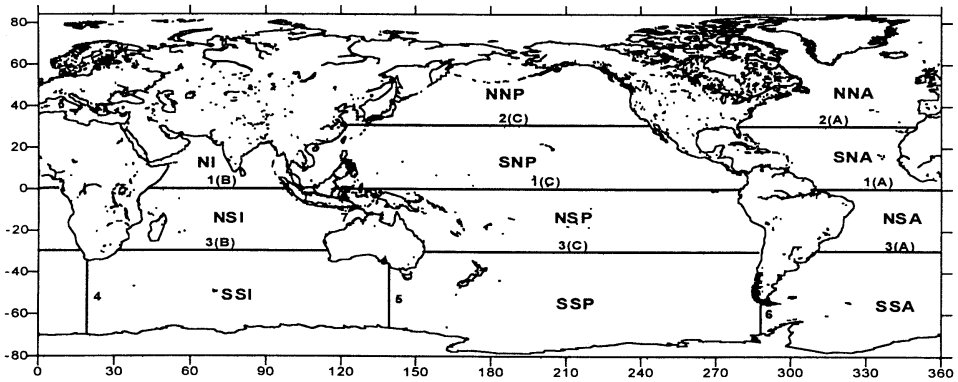

Fig. 3. The sections dividing the oceans into several regions

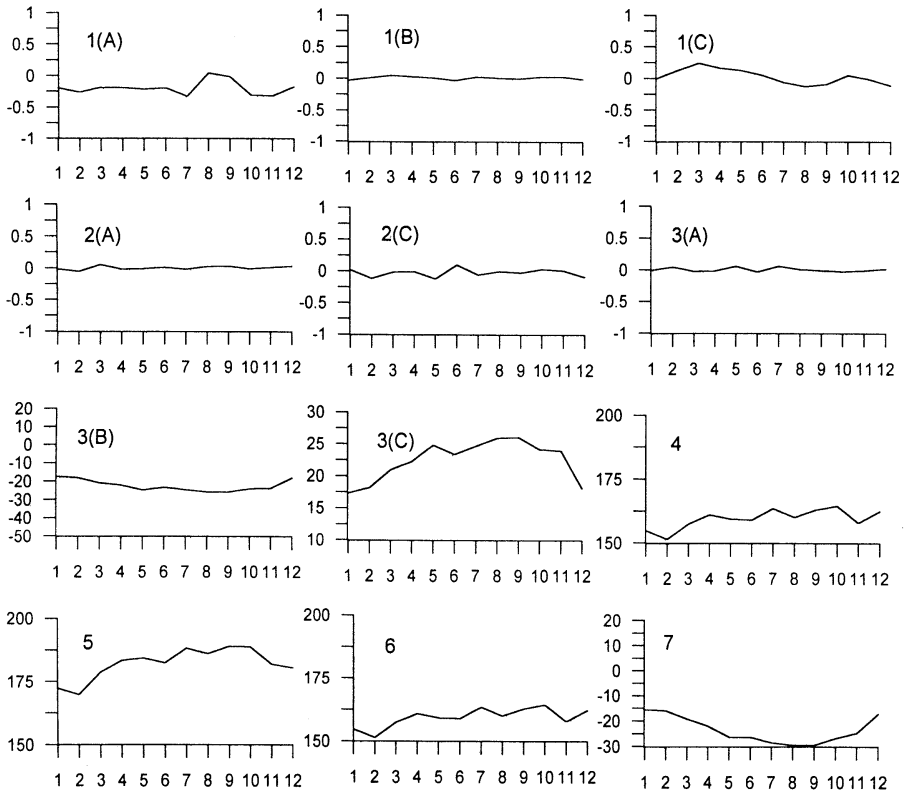

Fig. 4. The water volume transports (in Sv, 1 Sv=10^6 m^3/s) The abscissa denotes months

transports across section 3(C) represent the energy and substance transfer between the Pacific and the Southern Ocean. The sections in the Atlantic and Indian Oceans are similar. The sections 4, 5 and 6 separate the southern Atlantic, Indian and Pacific Oceans, while section 7 passes through the Indonesian Archipelago. For short, the regions separated by these sections are named as in Fig. 3.

Figures 4, 5 and 6 show the calculated water volume, heat and salt transports across the above representative sections. The unit is Sv(1 Sv=10^6 m^3/s) for the water volume transport, the unit for heat transport and salt transport

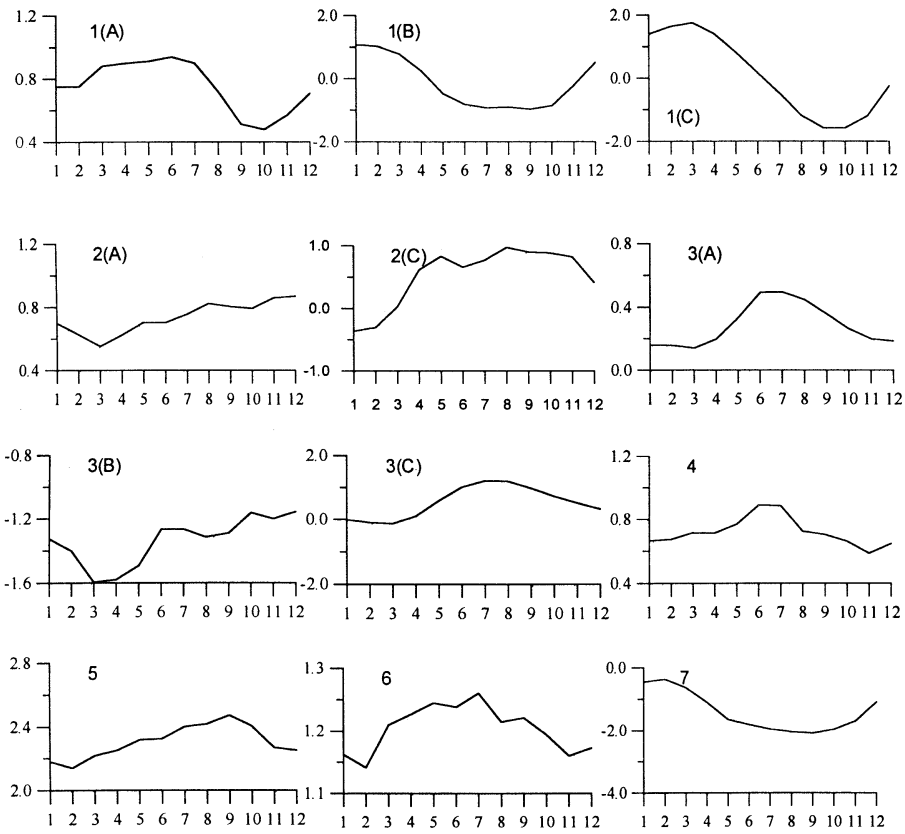

Fig. 5. The heat transports (in PW, 1 PW=10^{15} W) The abscissa denotes months

are PW (1 PW=10^{15} W) and Tg/s (Tera Grams /sec.) respectively. All these transports are denoted as positive if they are eastward and northward respectively.

The model result shows that: the Antarctic Circumpolar Current (ACC) has a volume transport of 170-220 Sv from the southern South Indian ocean (SSI) to the southern South Pacific (SSP), 150-180 Sv both from SSP to the southern South Atlantic (SSA) and from SSA to SSI. It indicates that there should be a pathway allowing the water to flow from the Pacific Ocean towards the Indian Ocean and then joining ACC and to return to the Pacific Ocean. By examining the transports across section 3(C), 7 and 3(B), we find that the transport from SSP to the northern South Pacific (NSP) is 17-26 Sv, the volume transport of the Indonesian Throughflow from the Pacific to Indian Ocean varies from 15 to 29 Sv, and that from the northern South Indian Ocean (NSI) to SSI is 17-26 Sv. This shows that the water volume transport is in balance. A rate of 15-29 Sv (with an average of 20 Sv) for the Indonesian Throughflow is rather close to the simulated result of GODFREY (1989) (16±4 Sv.) and the observational result of FIEUX *et al.* (1994) (18.6 ±7 Sv.).

Very small water flows across the equator in the Pacific, Atlantic and Indian Ocean, for that the northern boundaries of these oceans in the model are not connected to each other. For adjacent areas to the China, water is transported from the Pacific to the South China Sea through the Luzon Strait at rates of 0.6-2.1 Sv, and northward flows through the Taiwan Strait and east of the Taiwan Island are at 0.1 -1.9 Sv and 14-23 Sv respectively. Water flows from the East China Sea to the Pacific through the north of Ryukyu Island and to the East/

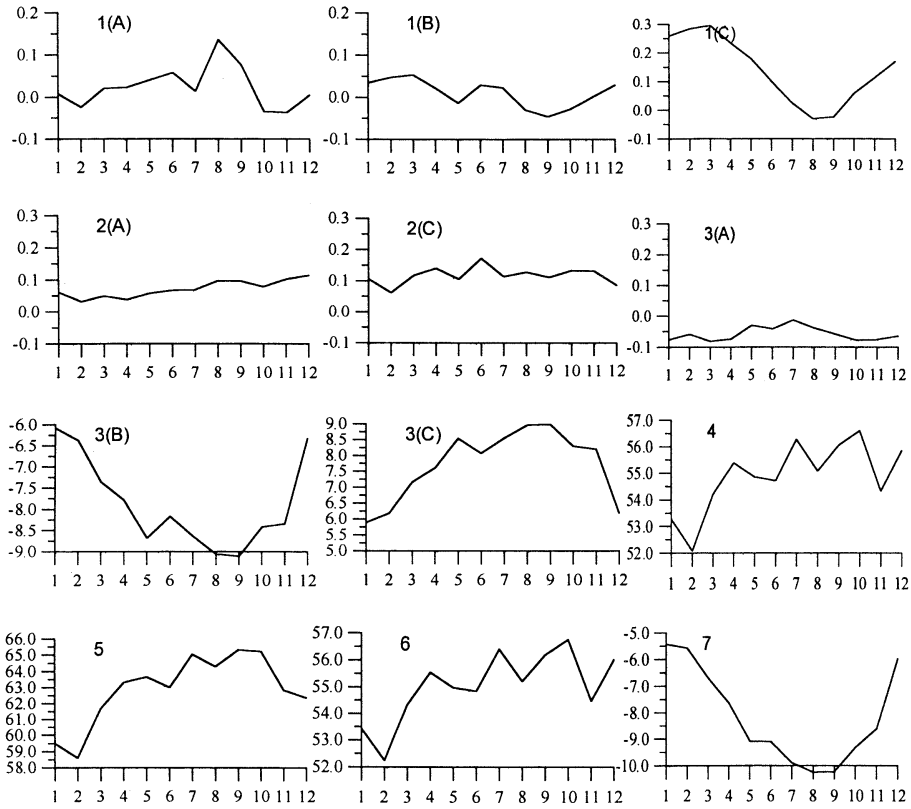

Fig. 6. The salt transports (in 10^{-1} Tera Grams/sec. (Tg/s)) The abscissa denotes months

Japan Sea through the Korea Strait are at 13–22 Sv and 1.6–2.1 Sv respectively. The volume transports from East/Japan Sea to the Pacific through the Tsugaru Strait and the Soya Stait are about 0.9 Sv and 0.5–1.0 Sv respectively.

The heat transport across the equator in the Atlantic Ocean is from 0.4 to 1.0 PW, and that in the Indian Ocean is from −1.0 to 1.0 PW. The heat transport across the equator in the Pacific Ocean varies from −1.5 PW in summer to 1.7 PW in winter. This seasonal characteristic is in agreement with the result of PHILANDER *et al.* (1987), who computed the seasonal variation of the zonally integrated meridional heat transport for the tropical Pacific Ocean. But our annual average of the cross-equator heat transport in the Pacific is lower than that calculated by PHILANDER *et al.* (1987). This is most likely a consequence of the negligence of the Indonesian Throughflow in the Philander's model. Across the latitude 30° N, the heat transport in the Pacific Ocean varies from −4.0 to 1.0 PW with an average of 0.5 PW. The heat transport in the Atlantic at 30° N varies from 0.5 to 0.9 PW with an average of 0.7 PW. YU and MALANOTTE-RIZZOLI (1998) calculated the heat transports in the North Atlantic using an inverse model. The annual average at 25° N is 0.7 PW, quite close to our result. In spite of large volume transport of ACC, the eastward heat transports of section 4, 5 and 6 are not accordingly large. The reason is that the temperature near the Antarctica is very low. The heat transport across section 5 is about 1 PW more than that across section 6. It indicates that a certian amount of heat in the SSP is lost. Checking the heat transport across the section 3(C), we find that about 1 PW is transferred from the Southern Ocean to the Pacific Ocean. Across the sections of 30° S, the heat transports in the Atlantic Ocean and Indian Ocean vary from 0.1 (in winter) to 0.5 (in summer) PW with an

average of 0.3 PW and −1.0 to −1.6 PW with an average of −1.4 PW respectively. It means that across the latitude 30° S, the heat is transported northward in the Atlantic and Pacific Ocean, while southward in the Indian Ocean. These differences can be mainly attributed to the Agulhas Current and Indonesian Throughflow. The heat transport through the Indonesian Archipelago ranges from −2.0 PW to −0.4 PW, with annual average of −1.0 PW.

The salt transport across the equator vary from −0.002 Tg/s (in summer) to 0.03 Tg/s (in winter) in the Pacific Ocean, from −0.003 (in winter) to 0.014 Tg/s (in summer) in the Atlantic Ocean, and from −0.005 (in summer) to 0.005 Tg/s (in winter) in the Indian Ocean. Across the latitude 30° N, the salt transport in the Pacific Ocean is about 0.01 Tg/s with a small seasonal variation, and that in the Atlantic Ocean is from 0.003 to 0.01 Tg/s with a small seasonal variation too. Across the latitude 30° S, the salt transports are from −0.001 to −0.008 Tg/s in Atrantic Ocean, from −0.6 (in winter) to −0.9 Tg/s (in summer) in the Indian Ocean, and from 0.6 (in winter) to 0.9 Tg/s (in summer) in the Pacific Ocean. For ACC, the eastward salt transports across sections 4, 5 and 6 are very large. They are from 5.2 (in winter) to 5.65 Tg/s (in summer) iacross section 4, from 5.86 (in winter) to 6.53 Tg/s (in summer) across section 5, and from 5.22 (in winter) to 5.68 Tg/s (in summer) across section 6, This seasonal variation may be partially attributed to the variation in volume transports and may also be related with melt of the ice near the Antarctica in boreal winter, when the salinity of the seawater may decrease.

4. Concluding remarks

The 1-degree diagnostic model of the present study can well reproduce the basic patterns of the general circulation in the world ocean, the 1/3-degree model can significantly improve the results, especially in producing the structures of the circulation in the Pacific-Asian marginal seas.

Though the cross-equator transports in the Atlantic, Indian and Pacific Ocean are all small, the heat transports across equator in the Atlantic is northward. This is clearly a result of the southward flow of the North Atlantic Deep Water and the northward compensative warm flow in the upper layer. The annual mean of the cross-equator heat transport in the Pacific from the present model is significantly lower than that calculated by PHILANDER *et al.* (1987). This might indicate the importance of the indonesian Throughflow in the heat transport in the Pacific. Our calulation shows that the heat transport through the Indonesian Archipelago is −1.0 PW, which is comparable with the poleward heat transport in the North Atlantic and Pacific Oceans. The difference in heat transports across the sections 4 and 5 demonstrates the important role of the Agulhas Current in the heat balance of the world ocean.

Nevertheless the present work did not well reproduce some observational features, for example, the position of the Kuroshio deviates eastward. This is likely a result of the coarse resolution in the available climatological hydrographic data. To better simulate the western boundary current diagnostically a refined temperature and salinity climatological dataset is resuired.

Acknowledgments

The present work was supported by the National Science Foundation of China Grants 49876010 and 49576280, the Major State Basic Research Program, No.G1999043808 and the Chinese Academy of Sciences Grant KZCX 2-202-01. The work was also partially supported by Natural Hazard Prevention Research (Critical Technology-21) Project, funded by MOST through KISTEP (Korea Institute of Science and Technology Evaluation Planning) and Daewoo Corporation, Korea for the second author.

References

BRYAN, K. (1969): A numerical method for the study of the circulation of the world ocean, Jaurnal of Computational Physics, **4**, 347-376.

FANG, G. *et al.* (1998): A survey of studies on the South China Sea upper ocean circulation. Acta Oceanographica Taiwanica, **37**(1), 1-16.

FANG, G. *et al.* (1991): Water transport through the Taiwan Strait and the East China Sea measured with current meters. Oceanography of Asian marnginal Seas (TAKAN, T. ed.) Elsevier, Holland,

345–358.

FIEUX, M. *et al.* (1994): Measurements within the Pacific–Indian oceans throughflow region. Deep Sea Res., Part I, **41**, 1091–1130.

FUJIO, S. and N. IMSASATO (1991): Diagnostic calculation for circulation and water mass movement in the deep Pacific. J. Geophys. Res, **96**, 759–774.

FUJIO, S. *et al.* (1992): World ocean circulation diagnostically derived from hydrographic and wind stress fields, 1. The velocity field. J. Geophys. Res, **97**, 11163–11176.

FUJIO, S. *et al.* (1992): World ocean circulation diagnostically derived from hydrographic and wind stress fields, 2. The water movement. J. Geophys. Res, **97**, 14439–14452.

GODFREY, J. S.(1989): A Sverdrup model of the depth integrated flow for the world ocean allowing for island circulations. Geophys. Astrophys. Fluid Dyn., **45**, 89–112.

HELLERMAN, S., and M. ROSENSTEIN (1983): Normal monthly wind stress over the world ocean with error estimates. Jpurnal of Physical Oceanography, **13**, 1093–1104.

PHILANDER, S., W. J. HURLIN and A. D. SEIGEL (1987): Simulation of the seasonal cycle of the tropical Pacific ocean. Journal of Physical Oceanography, **17**, 1986–2002.

SARMIENTO, J. L. and K. BRYAN (1982): An ocean transport model for the North Atrlantic. J. Geophys. Res, **87**, 394–408

SEMTNER, A. J. and R. M. CHERVIN (1988): A simulation of the global ocean circulation with resolved eddies. J. Geophys. Res., **93**, 15502–15522.

SEMTNER, A. J., Jr., and R. M. CHERVIN (1992): Ocean general circulation from a global eddy–resolving model. J. Geophys. Res. **97**, 54493–5550

YU, L. and P. MALANOTTE–RIZZOLI (1998): Inverse modeling of seasonal variations in the North Atlantic Ocean. J. Phys. Oceanogr, **28**, 902–922.

Received on May 23, 2000
Accepted on October 31, 2000

La mer 38 : 219-226, 2000
Société franco-japonaise d'océanographie, Tokyo

Coastal impacts of offshore meso-scale eddies through the Kuroshio variation

Kaoru ICHIKAWA* and Atsushi KANEDA**

Abstract : In order to assess the influence of offshore meso-scale eddies in coastal areas facing to the Kuroshio, temperature data in the Bungo Channel and altimetry sea surface height (SSH) data are analyzed. It is east of Okinawa, far away from the Bungo Channel, where the SSH variation is most strongly correlated with the coastal temperature changes with periods of several weeks to months. Complex empirical orthogonal function analysis of the SSH variation indicated strong coherency with the coastal temperature for a train of meso-scale eddies propagating northeastward from east of Okinawa to south of Shikoku, suggesting that variations of the Kuroshio in front of the Bungo Channel induce the coastal temperature changes. However, in areas other than east of Okinawa and south of Shikoku, larger SSH variations which would not correlate well with the coastal temperature variations are detected showing that cross correlation with the coastal temperature is not significant in these regions.

Key words : *meso-scale eddies, Bungo Channel, Kuroshio, Complex EOF analysis*

1. Introduction

Although oceanic conditions in coastal areas are subject to many factors, influences of offshore variations are known to be one of the major factors in southern Japanese coasts facing to the Kuroshio. Using abundant coastal observations, many past researches have examined coastal variations in connection with the Kuroshio (e. g., KANEDA *et al.*, 1996; MATSUYAMA *et al.*, 1999).

Recently, longer time series of satellite altimetry data are available, which provide good description of sea surface dynamic height variations in offshore regions. In the present paper, we used those good descriptive data, both coastal and ofshore, and related coastal temperature variations in the Bungo Channel (Fig. 1) to the offshore dynamic height variations by calculating their cross correlation. Furthermore, using complex empirical orthogonal function (CEOF) analysis of the altimetry data, distinct movement pattern of meso-scale eddies coherent with the coastal temperature variations are extracted, and influence of the offshore meso-scale eddies on the coastal temperature is discussed.

The present paper consists of 6 sections: Data sets of temperature in the Bungo Channel and altimetry sea surface height are described in the next Section 2. Then results of their cross correlations are shown in Section 3. In Section 4, simple introduction of CEOF analysis is first presented, followed by corresponding results for the altimetry data, which are then used to interpret movement patterns of meso-scale eddies affecting to the coastal temperature changes. Discussion and conclusions of the results are summarized in Sections 5 and 6, respectively.

2. Data

2.1. Coastal temperature data

Mooring stations have been deployed mainly by Ehime Prefectural Fisheries Laboratory and Ehime University to monitor water temperature along the eastern side of the Bungo Channel (Fig. 1). In the present analysis, 5m-depth water temperature record at the station K5 in

* Research Institute for Applied Mechanics, Kyushyu University, Fukuoka, Japan also, Frontier Observational Research System for Global Change, Tokyo, Japan
** Center for Marine Environmental Studies, Ehime University, Matuyama, Japan

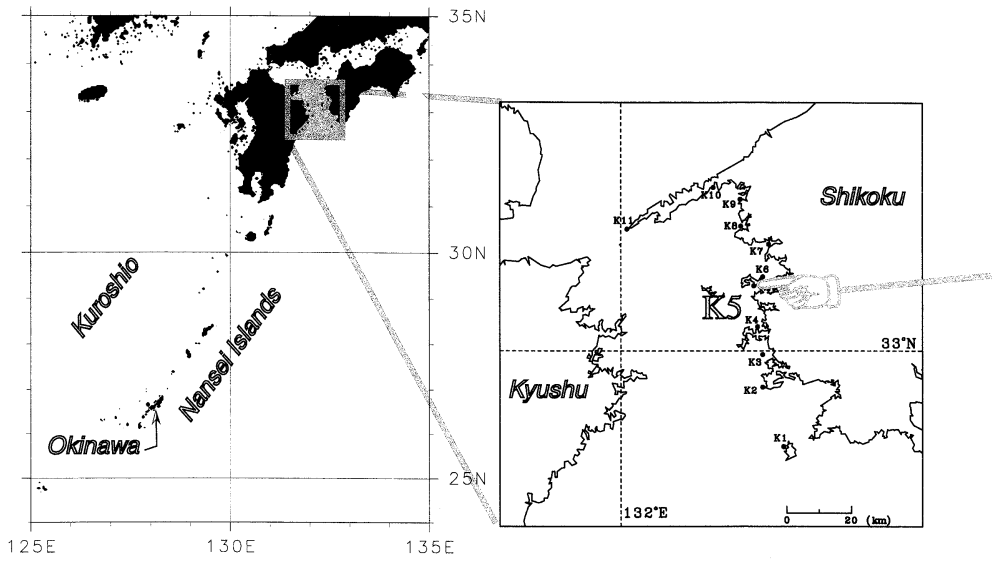

Fig. 1. Location of the Bungo Channel and mooring stations.

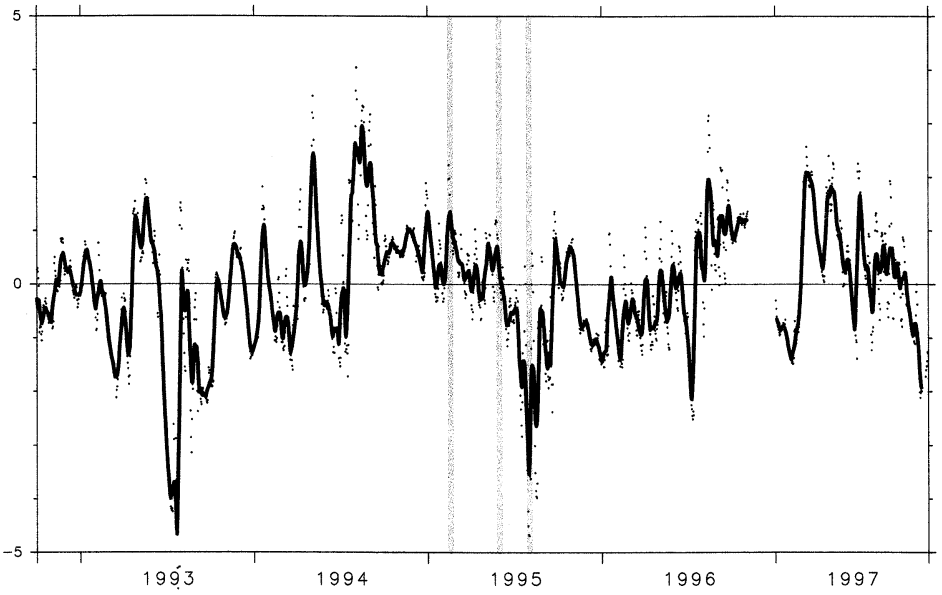

Fig. 2. Time series of daily temperature anomalies (dots) and their 10-day running means (line) at the station K5. Vertical lines indicate the dates corresponding to Fig. 6.

Shitaba Bay is used from October 1992 to November 1997 when the altimetry data are available.

The coastal temperature is obviously dominated by an annual cycle mainly determined by heat flux variations. In order to focus on temperature changes induced by meso-scale eddies, we should extract this annual variation. Sinusoidal temperature variation with an annual cycle is estimated by the harmonic analysis of 5 years of 30-minute temperature data and extracted to obtain temperature anomaly;

Figure 2 shows time series of daily-averaged temperature anomalies. In additon, for further comparizon with altimeter data, daily temperature anomaly data is averaged over same 10 day periods with altimetry data.

2.2. Altimetry data

For altimetry data, we use all TOPEX/POSEIDON, ERS-1 (phase C, E, F and G) and ERS-2 data which are provided by AVISO as CORSSH. The CORSSH products are supplied by the CLS Space Oceanography Division, Toulouse, France (AVISO, 1996; LE TRAON *et al.*, 1995; LE TRAON and OGOR, 1998).

From those data, sea surface height (SSH) deviation from the climatological mean (YI, 1995) is estimated at 0.5° grid pints in a study area south of Japan (125°-135°E, 24°-35°N; left panel of Fig. 1) for each 10-day period from October 1992 for 5 years by an optimal interpolation similar to ICHIKAWA and IMAWAKI (1996) with spatial and temporal scales to be larger than approximately 150 km and 17 day, respectively (see YASUDA *et al.* (2000) and ICHIKAWA (2000) for more description of the optimal interpolation method used). Areas are exclued in the present analysis when the estimated error exceeds 99% of the root-mean-squared magnitude of SSH variations, and they are generally on the coastal boundary where less altimetry data are available. For the consistency with the coastal temperature anomaly data, sinusoidal annual SSH variation estimated from 5-year data is removed for each grid point.

3. Correlation between coastal and offshore variations

Cross correlation between the coastal temperature anomaly and the offshore SSH anomaly is calulated fo 5 year (189 10-day cycles). Spatial distribution of the correlation coefficient is shown in Fig. 3. The stronger positive (or negative) correlation becomes, the more frequently temperature in the Bungo Channel changes warmer (or colder) when the SSH anomaly increases. In this figure, statistically insignificant correlation coefficients indicated by the Student-t test with 95% confidence level are masked.

Significant correlations are found to be positive south of Shikoku and east of the Tokara strait (132°E, 29°N), and negative east of Okinawa and Kyushu. Note that there exists no significant correlation in front of the Bungo Channel. Also the strongest correlation in the study area is located east of Okinawa island, more than 700 km away from the channel. These results would suggest that either the temperature anomaly in the Bungo Channel is remotely controlled by SSH variations east of Okinawa island, or there exists a coherent variation which affects both the temperature anomaly in the Bungo Channel and the SSH anomaly east of Okinawa, but it does not dominate the SSH variation in front of the channel.

In the next setion, we perform CEOF analysis on the SSH anomaly in order to separate a SSH pattern corresponding to the temperature anomaly variations in the Bungo Channel from the other SSH patterns. By studying the separated SSH pattern, we would be able to interpret the distribution characteristics of the cross

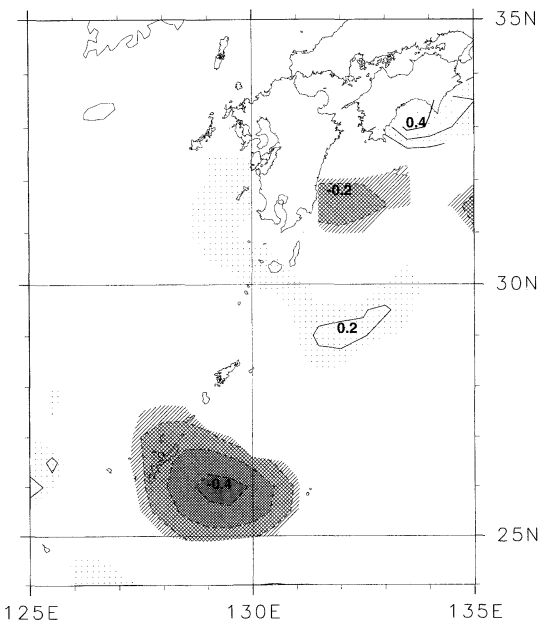

Fig. 3. Spatial distribution of cross correlation coefficient between the coastal temperature anomaly changes and the offshore SSH variations. Contour interval are 0.1 and positive (negative) correlations are shaded with dots (lines). Statistically insignificant values are masked in the figure.

correlation as shown in Fig. 3.

4. Decomposition by CEOF modes

4.1. CEOF analysis of offshore SSH variations

In CEOF analysis, SSH anomaly $z(x, t)$ at a given position x and time t is decomposed into orthogonal complex modes $C_j(x, t)$ as

$$z(x,t) \simeq \sum_{j}^{N} Re\{C_j(x,t)\}, \quad (1)$$

$$C_j(x,t) = A_j(x) e^{i\varphi j(x)} B_j(t) e^{i\varphi j(t)}, \quad (2)$$

where N is the number of significant modes, $A_j(x)$ spatial amplitude factor, $\phi_j(x)$ spatial phase distibution, $B_j(t)$ temporal mode amplitude, and φ_j (t) temporal phase variation (e. g. BARNET, 1983; WHITE *et al.*, 1987).

The value so-called contribution ratio, R_j, is often used to account for the contribution of a given mode j to explain overall variance of $z(x, t)$, and is defined by

$$R_j = \frac{\int\int |C_j(x,t)|^2 dxdt}{\int\int z^2(x,t) dxdt} \quad (3)$$

By adopting a normalization condition $\int A_j^2(x)dx = 1$ for any mode j, and by assuming that the sum of N CEOF modes in Equation (1) well represent the overall variance of $z(x, t)$, the above Equation (3) can be simplified as

$$R_j = \frac{\int B_j^2(t) dt}{\sum_k^N \int B_k^2(t) dt} \quad (4)$$

In addition, we can define "local contribution ratio", $R_j^L(x_0)$, for a given mode j at a given location x_0 as

$$R_j^L(x_0) = \frac{\int |C_j(x_0,t)|^2 dt}{\int z^2(x_0,t) dt}$$

$$= \frac{A_j^2(x_0) R_j}{\sum_k^N A_k^2(x_0) R_k} \quad (5)$$

The CEOF analysis is performed on the 5-year SSH anomaly in the study area. We select first 11 modes as significant CEOF modes ($N = 11$) such that their contribution ratio R_j exceed 2% and the sum of these modes explains more than 80% of total SSH variance. Contribution ratio R_j of each mode is shown in Fig. 4. One may noticethat there is no significant domination by a single mode. This is mainly because significant annual signals are removed before CEOF analysis, and also because movements of meso-scale eddies in this area are complicated due to interactions with the Kuroshio current.

4.2. Decomposition of coastal temperature data

Using temporal amplitude and phase variations of CEOF modes, $B_j(t)$ and $\varphi_j(t)$, time series of the coastal temperature anomaly, $T(t)$, can be decomposed by harmonic analysis. In other words, we would determine unknown amplitude factor F_j and phase constant θ_j in an estimate $\tilde{T}(t)$ by minimizing $\int (T(t)-\tilde{T}(t))^2 dt$, where

$$\tilde{T}(t) = \sum_{j}^{N} Re\{F_j B_j(t) e^{i(\varphi_j(t)+\theta_j)}\} \quad (6)$$

By replacing $A_j(x)$and $\phi_j(x)$ in Equation (2) by F_j and θ_j, ocntribution ratio of each CEOF mode for explaining the variance of the coastal temperature anomaly can be defined as

Fig. 4. Contribution ratio R_j of each CEOF mode to the SSH variance.

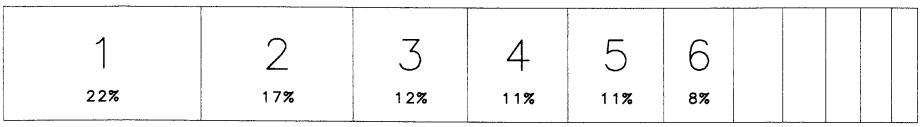

Fig. 5. Contribution ratio of each CEOF mode to decompose temporal variations of the temperature

$$R_j^T = \frac{F_j^2 R_j}{\sum_k^N F_x^2 R_k}, \quad (7)$$

similarly to the local contribution in Equiation (5).

Figure 5 shows values of R_j^T for all 11 modes. Clearly in the figure, contribution of the 8th mode R_8^T becomes significantly large, despite the fact that the SSH variation of that mode explains only 4% of the overall SSH variations (Fig. 4). This increase of contribution ratio of the 8th mode suggests that the coastal temperature is highly sensitive to the SSH variation pattern of that mode.

Examples of the SSH variation for the CEOF 8th mode, $Re\{C_8(x,t)\}$, in 1995 are shown in Fig. 6; vertical lines in Fig. 2 show corresponding dates. The temporal phase variation of this mode $\varphi_8(t)$ around these dates is plotted in Fig. 7. In this figure, unreliable phase estimates based on smaller mode amplitude $B_8(t)$ are marked by asterisks when area variance $\int |C_8(x,t)|^2 dx = B_8(t)^2$ becomes less than 1 cm^2. From east of Nansei islands to south of Shikoku, a train of cyclonic and anti-cyclonic eddies with the size of approximately 200-400 km is seen in Fig. 6, as indicated by "A" - "F". These meso-scale eddies seem to propagate northeastward, or in the downstream direction of the Kuroshio, at a speed of approximately 4 cm/s during this period (Figs. 6 and 7).

Comparing with the coastal temperature anomaly in the Bungo Channel in Fig. 2, cyclonic and anti-cyclonic meso-scale eddies agree well with the distribution pattern of the cross correlation coefficient between the SSH anomaly and the coastal temperature anomaly shown in Fig. 3. In Fig. 6c when the coastal temperature shows sharp harp decrease (Fig. 2), eddies with positive SSH anomaly are present in the east of Okinawa (F) and east of Kyushu (B), and those with negative SSH anomaly are found in the south of Shikoku (A) and east of the Tokara strait south of Kyusyu (C). Meanwhile, the sign of SSH anomaly becomes opposite in Fig. 6a when the coastal temperature anomaly is largely positive. The location of the eddies seems subtle since amplitude of the coastal temperature anomaly is not large when the position of these eddies is slightly shifted in Fig. 6b.

The existence of meso-scale eddies can be noticed in Fig. 6 in front of the Bungo Channel, which is not clear in the cross correlation analysis in Fig. 3. These eddies correspond to variations of the Kuroshio, and it seems to be physically more realistic to interpret that the coastal temperature variation is directly caused by variations of the Kuroshio, rather than being remotely controlled by meso-scale eddies east of Okinawa. Since the coastal temperature is largely affected by slight move-

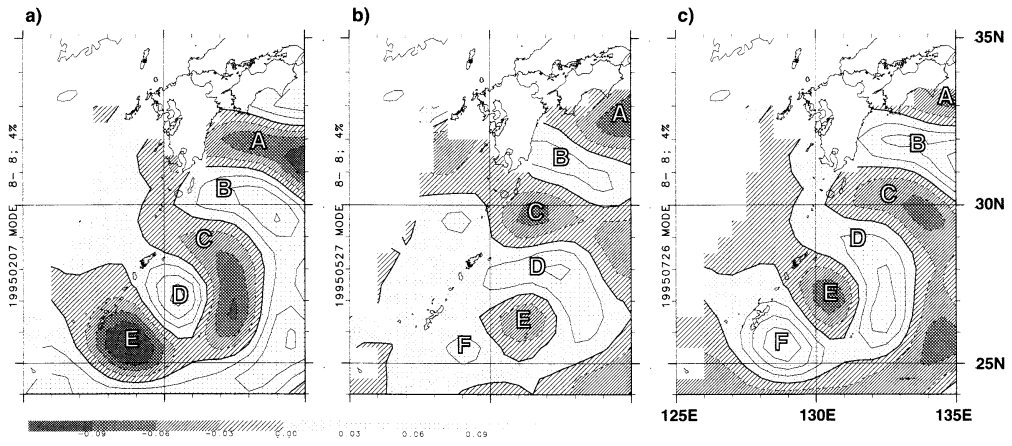

Fig. 6. The SSH anomaly of CEOF 8th mode on 7 Feburaly(a), 27 May(b) and 26 July, 1995(c). Contour intervals are 3 cm and negative values are heavily shaded. Characters "A" to "F" are shown for concenience of discussions.

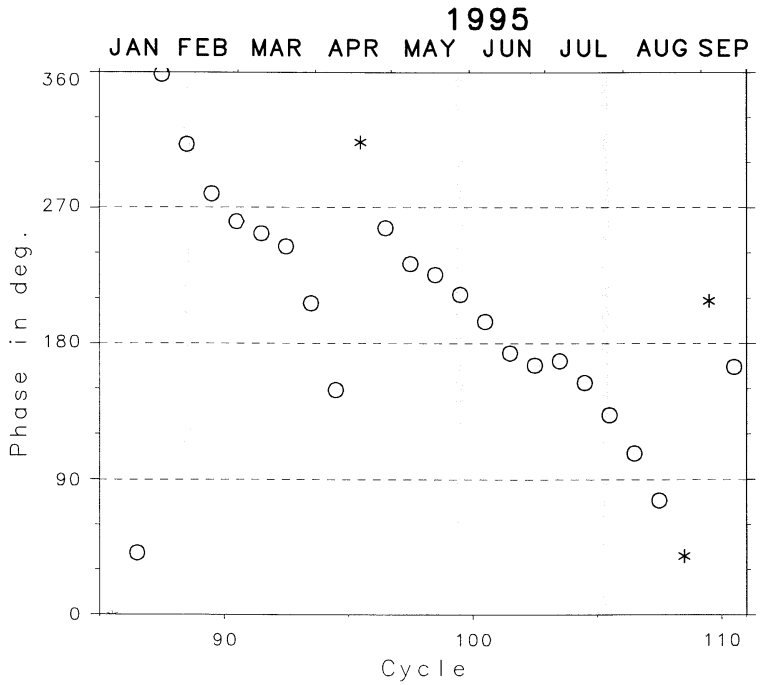

Fig. 7. Temporal phase variation of the CEOF 8th mode, $\varphi 8(t)$ in 1995. In this figure, asterisks indicate unreliable estimation. Vertical lines indicate the dates shown in Fig. 6. Numbers at the bottom indicate the altimetry 10-day cycles.

ment of the eddies as seen in Fig. 6, the idea, that the coastal temperature variation is directly caused by the eddies closer to the Bungo Channel, would be also circumstantially supported.

The reason why the meso-scale eddies in front of the Bungo Channel are not clearly seen in the cross correlation coeficient (Fig. 3) would be explained by referring to a map of local contribution ratio for the CEOF 8th mode R_8^T shown in Figure 8. The local Contribution ratio of the 8th mode R_8^T has largest valuse in areas east of Okinawa and south of Shikoku, meanwhile R_8^T is less than 5% in front of the Bungo Channel. In the areas with small R_8^T such as in front of the Bungo Channel, SSH variations of the other CEOF modes than the 8th would be present whose amplitudes surpass that of the 8th mode and which may not correlate with the coastal temperature variations. In such a case, cross correlation coefficient between the SSH and the coastal temperature would be statistically insignificant even

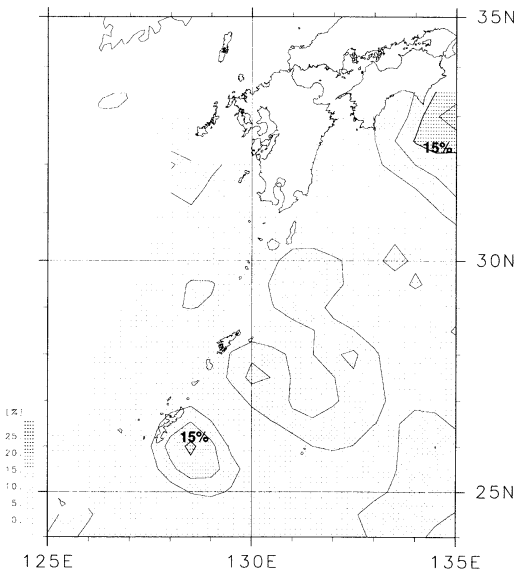

Fig. 8. Map of the local contribution ratio for the CEOF 8th mode, (χ). Areas with larger ratio are heavily shaded. Contour intervals are 5%.

though there may exist moderate SSH variations given by the CEOF 8th mode which correlate well with the coastal temperature changes. On the contrary, in the areas with larger R_6^T, the SSH variation would be more similar to that of the 8th mode alone seen in Fig. 6, so that the cross correlation coefficient would become statistically significant.

5. Discussions

Although the coastal temperature anomaly in the Bungo Channel is found sensitive to the SSH anomaly of the CEOF 8th mode, physical reasons are not considered in the present paper. The anti-cyclonic meso-scale eddy "B" in front of the channel in Fig. 6c, which is elongated in the direction normal to the Kuroshio axis, indicates that the Kuroshio axis is located slightly closer to the channel when the coastal temperature becomes cold. This relationship between the cloeser Kuroshio path and colder coastal temperature is consistent with hydrographic observations in the Bungo Channel in 1993, which indicate intrusion of offshore cold bottom water when the Kuroshio took a slightly closer path (KANEDA *et al.*, 1996). This intrusion may be induced by shoreward bottom Ekman transport enhanced by the near-shore Kuroshio path flowing over the shelf. Another interpolation, however, can be obtained from Fig. 6c that seaward surface velocity in the Bung Channel is accelerated when the coastal temperature decreases, which may also result in intrusion of cold bottom water by assuming simple mass conservation at the mouth of the channel. More in situ observational results are necessary to understand physical processes of water exchange in the channel.

Also in the present paper, physical interpretation of the CEOF 8th mode itself has not been discussed. One may notice that the eddies east of Nansei islands propagate northeastward, similarly in the Kuroshio region east of Kyushu and south of Shikoku where northeastward advection is strong. This may suggest the existence of strong northeastward current east of Nansei islands, although extensive observations are again necessary to study this possibility.

One may remind outstanding *kyucho* events in the Bungo Channel as an example of strong influences of the Kuroshio in the channel (e. g. TAKEOKA *et al.*, 1993). Unfortunately, *kyucho* is out of scope in the present analysis since spatial and temporal resolutions of the altimetry data are too coarse to detect *kyucho* events. We may define, however, frequency of *kyucho* occurrences during a certain period to cope with low resolutions of the SSH data, although we shall leave this for study in the future.

We used the temperature data at the station K5 only to represent variations of the whole Bungo Channel. This could be a severe problem for small-scale phenomena such as *kyucho* events, but it should be accepteble in the present analysis since our interest is limited to variations of larger scales. Rather, use of the data at the eastern side of the channel may induce some quantitative discrepancy from the area average, although apparent qualitative characteristics in Fig. 2 would not be altered (KANEDA *et al.*, 1996).

6. Conclusions

Temperature variations in the Bungo Channel are interpreted with respect to the offshore sea surface height (SSH) variations obtained from altimetry data. In order to focus on variations induced by meso-scale eddies, sinusoidal variations with an annual cycle are first removed from both the SSH and the coastal temperature data.

Cross correlation between these two data sets indicates that the SSH variation east of Okinawa, more than 700 km away from the Bungo Channel, shows the strongest correlation in the study area. On the contrary, correlation coefficient in front of the Bungo Channel is statistically insignificant.

Complex empirical orthogonal function (CEOF) analysis of the SSH anomaly is then performed to extract phase-propagating SSH patterns coherent with the coastal temperature variations. More than 30% of the variance of the coastal temperature changes are explained by the minor CEOF 8th mode, which is characterized by a train of meso-scale eddies propagating northeastward from east of Okinawa to south of Shikoku. Movements of these eddies in the CEOF 8th mode coincident well the

coastal temperature variation. This result would suggest that the temperature in the Bungo Channel is affected by the eddies close to the channel which corresponds to variations of the Kuroshio, rather than being remotely controlled by the far eddies. Distribution of the local contribution ratio of the CEOF 8th mode, however, indicates existence of SSH variations of the other CEOF modes in front of the channel whose amplitude is much larger than of the 8th mode and which may not correlate well with the coastal temperature variation, resulting in smaller cross correlation coefficient with the temperature in the Bungo Channel. Meanwhile, in the areas east of Okinawa and south of Shikoku, the SSH variation is more similar to that of the 8th mode alone, so that the cross correlation in these areas would remain evident.

Physical reasons of coherency between the coastal temperature variations and slight meanders of the Kuroshio in front of the Bungo Channel indicated by meso-scale eddies in the CEOF 8th mode are discussed. Also, possibility of a strong northeastward current east of Nansei islands is considered, referring to the northeastward propagation of the eddies both in the Kuroshio region and in the area east of Nansei islands.

Acknowledgments

We would like to thank Prof. H. TAKEOKA of Ehime University and Dr. Y. KOIZUMI of Ehime Prefectural Fisheries Experimental Station who kindly provided valuable temperature data set in the Bungo Channel. Mr. T. SAITO of National Research Institute of Fisheries Science contributed to discussions on interpretation of the results. Also, discussion with Dr. Y. MASUMOTO of the University of Tokyo were helpful. This research was supported in part by a Grant-in-Aid for Scientific Research from the Ministry of Education, Science, and Culture of Japan, and also by Core Research for Evolutional Science and Technology (CREST) of Japan Science and Technology Corporation (JST).

References

AVISO (1996): AVISO Handbook for Merged TOPEX /POSEIDON Products. AVI-NT-01-101-CN, Edition 3.0.

BARNET, T.P (1983): Interaction of the monsoon and Pacific trade wind system at internnual time scales. Part I : The equatorial zone. Mon. Wea. Rev., **111**, 756-773.

ICHIKAWA, K.(2000): Variation of the Kuroshio in the Tokara Strait induced by meso-scale eddies. submitted to J. Oceanogr.

ICHIKAWA, K. and S. IMAWAKI(1996): Estimating the sea surface dynamic topography from Geosat altimetry data. J. Oceanogr., **52**, 43-68.

KANEDA, A., H. TAKEOKA and Y. KOIZUMI (1996):Decrease of water temperature in the Bungo Channel is summer 1993. Bull. Coastal Oceanogr., **34**, 71 -78. (in Japanese with English abstract)

LE TRAON, P. Y., P. GASPAR, F. BOYUSSEL and H. MAKHMARA (1995): Using TOPEX / POSEIDON data to enhance ERS-1 orbit. J. Atm. Ocean. Tech, **12**, 161-170.

LE TRAON, P. Y. and F. OGOR (1998): ERS-1/2 orbit improvemnt using TOPEX/POSEIDON: the 2cm challenge. J. Geophys. Res., **103**(C4) 8045-8057.

MATSUYAMA, M., H. ISHIDOYA, S. IWATA, Y. KITADE and H. NAGAMATSU (1999): Kyucho induced by intrusion of Kuroshio water in Sagami Bay, Japan. Continental Shelf Res., **19**, 1561-1575.

TAKEOKA, H., H. AKIYAMA and T. KIKUCHI (1993): The Kyucho in the Bungo Channel, Japan-Periodic Intrusion of Oceanic Warm Water(1987): J. Oceanogr., **49**, 369-382.

WHITE, W. B., S. E. PAZAN and M. INOUE (1987): Hindcast/Forecast of ENSO events based upon the redistribution of observed and model heat content in the western tropical Pacific, 1964-86. J. Phys. Oceanogr., **17**, 264-280.

YASUDA, I., S. ITOH, Y. SHIMIZU, K. ICHIKAWA, K. UEDA, T. HONMA, M. UCHIYAMA, K. WATANABE, N. SUNO, K. TANAKA and K. KOIZUMI (2000): Cold-core anti cyclonic eddies south of Bussol' Straint in the north-western Subarctic Pacific. J. Physical Oceanogr., **30**, 1137-1157.

YI, Y. (1995): Determination of Gridded Mean Sea Surface from TOPEX, ERS-1 and GEOSAT Altimeter Data, Rep. 434, Dept. Geod. Sci. Surv., The Ohio State Univ., Colombus.

Recived on January 27, 2000
Accepted on August 2, 2000

La mer 38 : 227-231, 2000
Société franco-japonaise d'océanographie, Tokyo

The influence of the drag coefficient on the simulation of storm surges

Xiuqin WANG*, Chengchun QIAN* and Wei WANG*

Abstract : Wind stress plays a major role in the formation and propagation of storm surges. In numerical simulation of the storm surge, wind stress is expressed by empirical formula as a power law of wind speed, where the drag coefficient decides the rate of momentum transmission from air into water. Observations show that the drag coefficient increases gradually with the increase of wind speed and is a function of surface roughness and atomspheric stability. In this paper, sever proposed formulae of the drag coefficient varying with the increasing of wind speed have been examined by numerical simulation of the storm surge. The elevations simulated with varying drag coefficient coincide much better with the observed value than those for the constant drag coefficient. The best result is obtained when the formula proposed by SMITH(1980) is adopted.

Key words : *storm surge, drag coefficient, Bohai Sea, Yellow Sea*

1. Introduction

Wind stress plays a major role in the formation and movement of storm surges. In numerical simulation of the storm surge, wind stress is expressed by an empirical formula as 2-power law of wind speed, where the drag coefficient (C_d) decides the rate of momentum transmission from air into water. The drag coefficient in the empirical formula is usually considered as a constant, that is, the sea surface roughness does not vary during the process of a storm surge. In this condition, the results of numerical simulation cannot really reflect the process of a storm suge.

Numbers of observations showed that the drag coefficient increases gradually with the increase of wind speed and should be a function of surface roughness and atmospheric stability. In the present paper, several formulae proposed to represent the drag coefficient varying with the increase of wind speed have been examined by numerical simulation for the storm surge in the Bohai and Yellow Seas caused by Typhoon Rita(No.7203) in 1972.

* Ocean University of Qingdao, 5 Yushan Road, Qingdao, China

2. Numerical model

Two-dimensional storm surge model is employed. The goverining equations are:

$$\frac{\partial \zeta}{\partial t}+\frac{\partial}{\partial x}[(\zeta+h)U]+\frac{\partial}{\partial y}[(\zeta+h)V]=0,$$

$$\frac{\partial U}{\partial t}+U\frac{\partial U}{\partial x}+V\frac{\partial U}{\partial y}-fV = -g\frac{\partial \zeta}{\partial x}-\frac{1}{\rho}\frac{\partial P_a}{\partial x}+\frac{(\tau_{x,a}-\tau_{x,b})}{\rho(\zeta+h)},$$

$$\frac{\partial V}{\partial t}+U\frac{\partial V}{\partial x}+V\frac{\partial V}{\partial y}+fU = -g\frac{\partial \zeta}{\partial y}-\frac{1}{\rho}\frac{\partial P_a}{\partial y}+\frac{(\tau_{y,a}-\tau_{y,b})}{\rho(\zeta+h)},$$

where ζ is the surfece elevation relative to the undisturbed water depth h, (U, V) are the transport components in the (x, y) direction, f is Coriolis parameter, g is gravitational acceleration, P_a is the atmospheric pressure, ρ is the density of sea water, (τ_{xa}, τ_{ya}) are the components of wind stress $\vec{\tau}$ and $\vec{\tau}_a=C_d\rho_a\vec{W}|\vec{W}|$, in which $\vec{W}$ is the velocity of wind, ρ_a is the diensity of air, C_d is the drag coefficient of wind stress, (τ_{xb}, τ_{yb}) are the components of bottom stress $\vec{\tau}_b$ and $\vec{\tau}_b=C_f\rho\vec{V}|\vec{V}|$, in which $\vec{V}$ is the velocity of current, C_f is the friction coefficient of bottom.

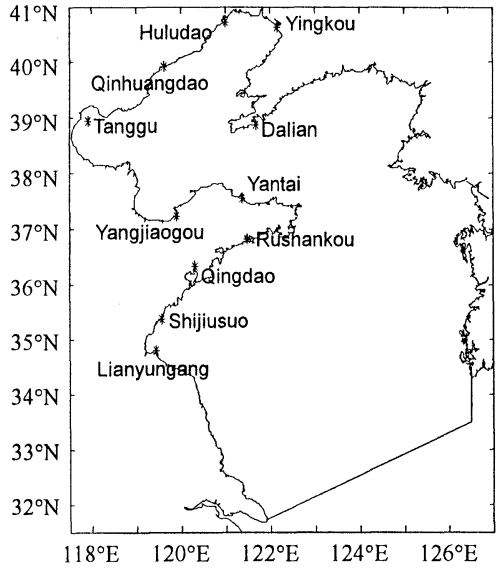

Fig. 1. Locations of the tide gauge stations

The numerical scheme is based on a finite difference used by LEENDERTSE (1967) on an Arakawa C-grid. This is an alternating direction implicit (ADI) technique, which generates solutions space and time. The computational domain is the Bohai Sea and the Yellow Sea (see Fig. 1) and the horizontal resolution is(1/12)°. The zonal distance (Δx) between two adjacent grid points is varying with the latitude, while the meridianal distance (Δy) is equal.

At the open boundary, the water levels are taken to bes$=(P_\infty - P_a)/\rho g$ in which P_∞ is the environmental pressure.

According to the feature of the wind field of Typhoon, the elliptical wind field model (WANG, 1999) is adopted, which is derived from JELESNIANSKI (1965) circle wind field model.

$$\vec{W}=\begin{cases}\dfrac{r}{R+r}(V_{ox}\vec{i}+V_{oy}\vec{j})+W_R(\dfrac{r}{R})^{3/2}\\ \cdot\dfrac{1}{r}(A\vec{i}+B\vec{j}),\ (r\le R)\\ \dfrac{r}{R+r}(V_{ox}\vec{i}+V_{oy}\vec{j})+W_R(\dfrac{R}{r})^{1/2}\\ \cdot\dfrac{1}{r}(A\vec{i}+B\vec{j}),\ (r>R),\end{cases}$$

$$P_a=\begin{cases}P_0+\dfrac{1}{4}(P_\infty-P_0)(\dfrac{r}{R})^3,\ (r\le R)\\ P_\infty-\dfrac{3}{4}(P_\infty-P_0)(\dfrac{R}{r})^3,\ (r>R),\end{cases}$$

where $A=\cos(\alpha+\varphi+\theta)$ and $B=\sin(\alpha+\varphi+\theta)$, in which α is the inclination angle of major axis against x axis, φ is the angle of tangent in calculated point, and θ is the inflow angle; (V_{ax}) are the x-and y-components of velocity at the typhoon center respectively; W_R is maximum wind velocity at the distance R from the typhoon center; $\vec{W}$ is wind speed at the distance r from the typhoon position; P_a is air pressure on sea surface; P_o is air pressure at the typhoon center. These parameters are obtained from annals of typhoon, and some properties are modified for some parameters.

3. Simulation and analysis of results of it

The numerical simulations are performed using Typhoon Rita (No.7203) that had strong influence on the Bohai and Yellow Seas; the path of Rita is shown in Fig. 2. Typhoon Rita originated in the Western Pacific Ocean near the Equator (9.5 N, 150.5 E) on 5 July 1972 and moved northwestward and reached to its peak intensity on 11 July with an estimated central

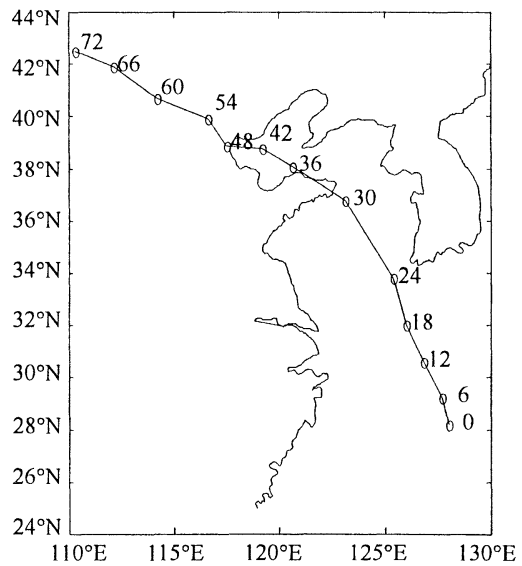

Fig. 2. Track of Typhoon Rita(No.7203) from 1972/7/25 08:00 to 1972/7/28 08:00

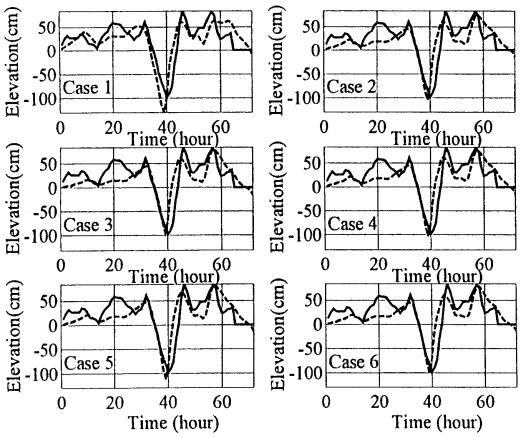

Fig. 3. Temporal change of observed elevation and that simulated at Lianyungang (Solid line: Observed value; dash line: Simulated value; Time: 1972/7/25 08:00 to 07/28 08:00)

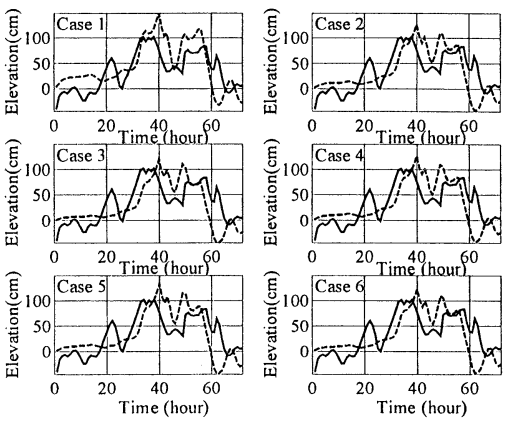

Fig. 5. Temporal change of observed elevation and that simulated at Yangjiaogou (Solid line: Observed value; dash line: Simulated value; Time: 1972/7/25 08:00 to 07/28 08:00)

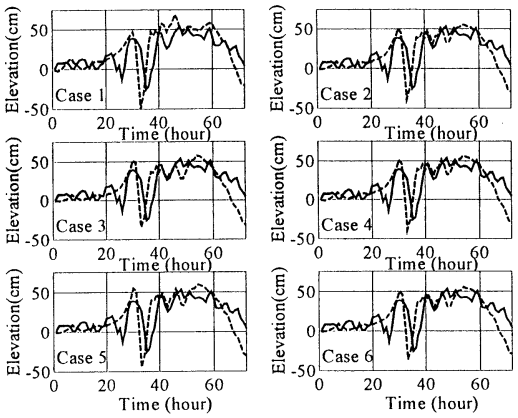

Fig. 4. Temporal change of observed elevation and that simulated at Rushankou (Solid line: Observed value; dash line: Simulated value; Time: 1972/7/25 08:00 to 07/28 08:00)

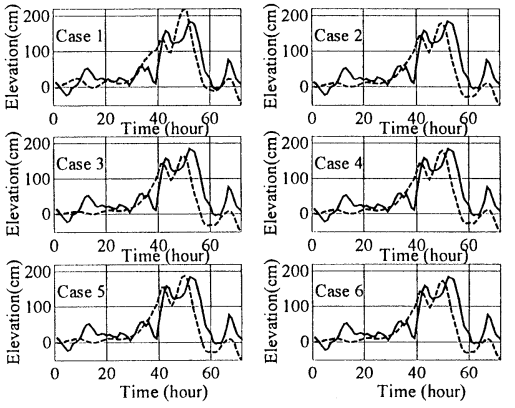

Fig. 6. Temporal change of observed elevation and that simulated at Tanggu (Solid line: Observed value; dash line: Simulated value; Time: 1972/7/25 08:00 to 07/28 08:00)

pressure of 911hPa and a maximum wind speed of 65 m s^{-1}. About 25 July it got into the Yellow Sea with a central pressure of 957hPa with a maximum wind speed of 35 m s^{-1}. It crossed the eastern coast of the Bohai Sea on 27 July and then weakened as it moved to the inland.

In numerical simulation, the different fromulae of the drag coefficient are examined. The formulae are as follows:

case 1 : $C_d = 0.0026$ (Const),

case 2 : $C_d = (0.8 + 0.0065 \times U_{10}) \times 10^{-3}$
$0 < U_{10} < 50$ (WUJING, 1982),

case 3 : $C_d = (0.61 + 0.063 \times U_{10}) \times 10^{-3}$
$6 < U_{10} < 22$ (SMITH, 1980),

case 4 : $C_d = (0.75 + 0.067 \times U_{10}) \times 10^{-3}$
$3 < U_{10} < 21$ (GARRATT, 1977),

case 5 : $C_d = (0.577 + 0.085 \times U_{10}) \times 10^{-3}$
$4 < U_{10} < 24$ (GEERNAERT, 1987),

case 6 : $C_d = (0.8 + 0.0065 \times U_{10}) \times 10^{-3}$
$0 < U_{10} < 6$
$(0.29 + 3.1/U_{10} + 7.7/U_{10}) \times 10^{-3}$
$3 < U_{10} < 21$
$(0.6 + 0.07 \times U_{10}) \times 10^{-3}$
$6 < U_{10} < 26$ (MARGARET, 1996),

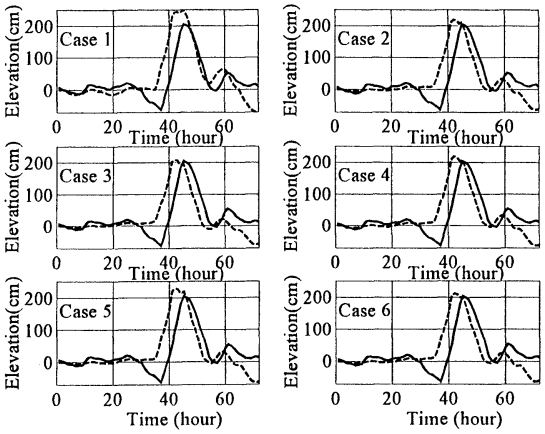

Fig. 7. Temporal change of observed elevation and that simulated at Huludao (Solid line: Observed value; dash line: Simulated value; Time: 1972/7 /25 08:00 to 07/28 08:00)

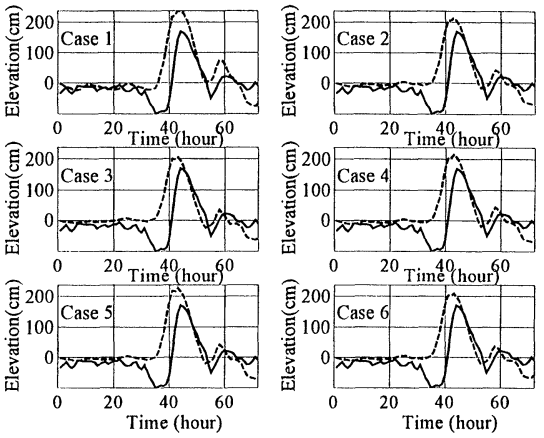

Fig. 8. Temporal change of observed elevation and that simulated at Yingkou (Solid line: Observed value; dash line: Simulated value; Time: 1972/7 /25 08:00 to 07/28 08:00)

Table 1. The maximum elevations at 11 tide gauges in the Bohai and Yellow Seas

	The maximum elevations of the storm surge at 11 tide gauge stations											
Tide gauges	Lian	ShiJS	Qing D	RuSK	YanT	YangJG	TangG	QinHD	HuLD	YingK	DaLian	SD
Observation	84	59	64	53	118	101	183	181	204	168	127	
Case 1	53.8	61.9	62.4	68.6	103.2	149.0	218.6	256.9	250.3	236.0	149.1	32.33
Case 2	75.4	70.7	59.8	56.0	100.6	126.7	178.9	221.7	218.4	213.8	145.8	20.23
Case 3	73.4	68.6	57.1	54.4	93.7	117.2	163.9	204.8	205.3	200.5	136.7	**17.57**
Case 4	75.8	71.0	59.7	56.2	100.7	126.2	178.0	220.9	218.0	213.4	145.9	20.03
Case 5	80.9	75.6	63.3	59.5	109.3	133.2	187.4	234.0	229.1	224.8	157.0	22.22
Case 6	77.7	72.3	60.4	55.7	98.6	122.5	171.6	214.4	213.1	208.4	143.2	18.61

Table 2. Standard deviations between observed and simulated elevations at 11 tidal stations.

Case	Standard deviations of the storm surge at 11 tide gauge stations											
	LianYG	ShiJS	QingD	RuSK	YanT	YangJG	TangG	QinHD	HuLD	YingK	DaLian	Mean
1	25.74	23.43	16.14	20.05	19.35	34.35	37.91	43.24	53.95	58.45	23.65	32.39
2	24.85	21.71	15.76	18.62	20.36	35.30	38.63	41.39	52.92	57.51	22.92	31.82
3	25.26	21.90	16.21	18.02	20.01	34.82	38.34	39.52	52.13	56.58	22.37	**31.38**
4	24.92	21.76	15.83	18.63	20.43	35.39	38.72	41.46	53.00	57.58	22.97	31.88
5	25.31	22.21	16.16	19.51	21.53	36.71	40.10	44.44	54.82	59.49	24.22	**31.14**
6	25.14	21.95	16.25	18.48	20.39	35.21	38.94	41.19	53.16	57.70	22.96	31.94

here U_{10} is the wind speed at 10m over sea surface. In these models, if the U_{10} is out of the range of these formulae, the drag coefficient is considered as a constant corresponding to the general value of $C_d=0.0026$. In this paper we adopt $C_f=0.0016$, $P_\infty=1020$ hPa and $\theta=20°$ for the case of Typhoon Rita.

The temporal changes of elevation observed at 6 tide gauges in the Bohai and Yellow Seas and the corresponding results of simulation for the case 1～case 6 are shown in Fig. 3～Fig. 8, respectively. From these figures, we can see

that the simulated results in the case 2~case 6 are more in agreement with the real processes of the storm surge than that in case 1.

The results of simulations are analyzed by two methods. The first is comparison of the maximum elevations due to the surge between observations and simulations at 11 tide gauges along the coast of the Bohai and Yellow Seas. The results of comparison are listed in Tabel 1. The last column (SD) is the standard deviation of the difference between observed and simulated maximum elevations at these stations. The Table 1 indicates that the best results are obtained by adopting the Smith's formula. The second is to examine the standard deviation (SD) of the difference between observed and simulated elevations; the SD values are listed in Table 2. The mean values of SD are lowest in the case 5 and secondary lowest in the case 3.

4. Conclusion

By comparison of the results simulated by different C_d formulae, it has been clarified that the Smith's formula works better than others. Thus we conclude that the Smith's formula is the better selection for the numerical simulation of a storm surge.

Reference

GARRATT, J. R. (1977): Review of drag coefficients over oceans and continents. Mon. Weather Rev., **105**, 915–929.

GEERNAERT, G. K., LARSSEN and S. E. HANSEN, J. (1987): Measurements of the wind-stress, Heat flux, and turbulence intensity during storm conditions over the North Sea. J. Geophys. Res., **98**, 16571–16582.

JELESNIANSKI, C. P. (1965): A numerical computation of storm tides induced by a tropical strom impinging on a continental shelf. mon. Wea. Rev., **93**, (16), 343–358.

LEENDERTSE, J. J. (1967): Aspects of a computational model for long-period water wave propagation, the Rand Corporation, RM-5294-PR.

SMITH, S. D. (1980): Wind stress and heat flux over the ocean in gale force winds. J. Phys. Oceanogr., **10**, 709–726.

WANG, X., C. QIAN and W. WANG (1999): The elliptic typhoon wind field model. The proceedings of the Ninth Chinese Coastal Engineering Symposium(in chinese).

WUJING (1982):Wind-stress coefficients over sea surface from breeze to hurricane. J. Geophys. Res. **87**, 9704-9706.

Received on January 11, 2000
Accepted on October 23, 2000

La mer 38 : 233-243, 2000
Société franco-japonaise d'océanographie, Tokyo

Several aspects of the simulated response of the Japan (East) Sea to synoptic atmospheric forcing due to siberian cold air outbreaks

Christopher N.K. MOOERS*, HeeSook KANG*, and Shuyi S. CHEN**

Abstract : The Japan (East) Sea (JES) is influenced by synoptic-scale Siberian cold air outbreaks during the winter season. The response of JES to two cold-air outbreaks in early January 1997 is explored with numerical simulations using synoptic winds from ECMWF, NSCAT, and MM5 to drive a mesoscale eddy-admitting JES circulation model (JES-POM). The importance of the associated low level wind jet (and the consequent high heat loss region) off Vladivostok is demonstrated. The simulated response includes cooling in the upper layer and low-order, barotropic, basin-scale divergence and vorticity modes. The net response is not very sensitive to the spatial and temporal resolution of the wind-forcing; however, the synoptic sequence of the response is quite sensitive.

Key words : *ocean circulation, semi-enclosed sea, cold air outbreak, atmospheric forcing*

1. Introduction

The circulation of the Japan (East) Sea (JES) is driven mainly by the throughflow of the Tsushima Warm Current and atmospheric forcing, including Siberian cold air outbreaks associated with the passage of extratropical cyclones and fronts, on a 4-to-10 day timescale, during the winter season (typically late November through early March). The response of the JES to cold air outbreaks is anticipated to be complex, ranging from increased sea states to wind-driven setup (along the Japanese coast) and setdown (along the Korean and Russian coasts) of coastal sea level; to intense mixing, cooling, and evaporation on the Asian side of the JES, plus adjustment to intense precipitation on the Japanese side; and to generation of transient open ocean and coastal upwelling/downwelling, near-inertial motions, and mixed-layer deepening. However, most previous studies (a notable exception is BANG *et al.* (1996)) of JES oceanic responses to atmospheric forcing have used climatological monthly or mean fields which, of course, do not include the synoptic effects of individual winter storms that dominate the mean fields as well as the variability. The availability of high resolution surface winds from satellite scatterometer measurements and mesoscale numerical weather prediction models now allows addressing these response issues in new ways, as described below.

The interaction of the cold air outbreak driven JES transient response with the JES general circulation is thought to be essential for wintertime ventilation of the JES and the annual formation of intermediate water and occasional formation of deep water (cf. SENJYU and SUDO, 1996). Observational evidence suggests that the center of intense air-sea interaction and ventilation is located off Vladivostok (cf. SEUNG and YOON, 1995) (though there are alternative candidate sites and mechanisms), where a low-level jet (associated with cold air outbreaks) flows seaward through a prominent coastal valley north of Vladivostok. This hypothesis and related issues are explored by

* OPEL/AMP/RSMAS/University of Miami
4600 Rickenbacker Causeway
Miami, FL 33149-1098 USA
Email: cmooers@rsmas.miami.edu
** MPO/RSMAS/University of Miami
4600 Rickenbacker Causeway
Miami, FL 33149-1098 USA

driving a regional ocean circulation model (JES-POM) with various surface wind datasets derived from a standard operational NWP model (ECMWF), a spaceborne scatterometer (NSCAT/ADEOS), and an atmospheric mesoscale circulation model (the PSU/NCAR MM5). Examples are presented of the simulated responses, and of their sensitivity to the various atmospheric forcing fields utilized. This study complements an earlier analysis (KAWAMURA and WU, 1998) of somewhat similar issues (but for mean conditions over the entire month of January) with air-sea transfer estimates (using NSCAT winds) and satellite-sensed sea surface temperature (SST) fields.

The JES response to the cold air outbreaks is simulated with JES-POM (KANG, 1997), an implementation of the Princeton Ocean Model (POM, BLUMBERG and MELLOR, 1987) for the JES. POM is a primitive equation model with a free seasurface, as well as many other important attributes. The version of JES-POM used here has 26 sigma levels and ca. 10 km horizontal resolution; it uses a value of HORCON = 0.1 in the Smagorinsky lateral turbulence parameterization. The model was spun-up for 4,200 days with the Na climatological mean winds (NA *et al.*, 1992), relaxation (time scale = 100 days) of surface temperature and salinity to the LEVITUS climatological means (LEVITUS, 1982), and specified throughflow of 2.8 Sv. (Note: the model was usefully in statistical equilibrium at that stage; otherwise, there was no particular reason for starting the synoptic forcing simulations at that time.) For the MM5 case, the wind-forcing and surface thermal forcing were replaced with MM5 winds and heat flux by ramping-up over five inertial periods (i.e., a total of 85 h) to the MM5 forcing of 00Z/1 JAN 97. For the NSCAT and ECMWF cases, the NSCAT and ECMWF winds, respectively, were used with the MM5 heat flux.

The PSU/NCAR (nonhydrostatic) atmospheric mesoscale model MM5 (DUDHIA, 1993) was implemented with a triply nested domain. The outer domain covers Northeast Asia and has 45-km horizontal resolution; the intermediate domain covers JES and its coastal areas and has 15-km resolution; and the inner domain covers an area off Vladivostok and has 5-km resolution. This implementation has 26 sigma levels between the surface and the 50 mb isobaric surface. MM5 is forced by the ECMWF global analysis fields on its lateral boundaries. A mesoscale analysis dataset including additional station observations is assimilated into the outer domain. The MM5 simulation has been verified by independent datasets; e.g., the GMS-5 satellite visible and infrared imagery and the JMA meteorological buoy near Oki Is. In the present study, fields from the intermediate domain (with 15-km resolution and no additional data assimilation) are used to force JES-POM.

2. Synoptic atmospheric conditions, 1 to 10 January 1997

Two extratropical cyclone (storm) passages occurred in JES during 1 to 10 January 1997 (Fig. 1). The first cyclone developed in association with a strong upper-level disturbance moving from Northeast Asia across the northern JES during 1 to 2 JAN, intensified, and

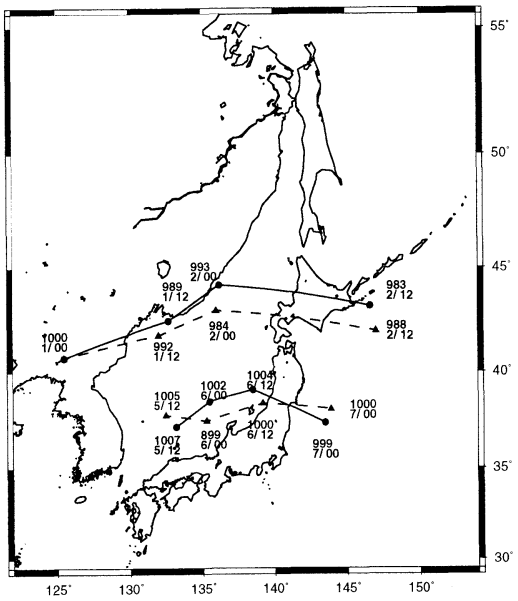

Fig. 1. Tracks of the cyclone centers associated with the two cold air outbreaks, 1 to 10 JAN 97. Centers are plotted every 12 hours from two sources: MM5 model (dashed line) and composite (solid line) of satellite visible and infrared imagery. (Center positions are labelled with central pressure (mb), day in JAN, and time (hours/GMT).)

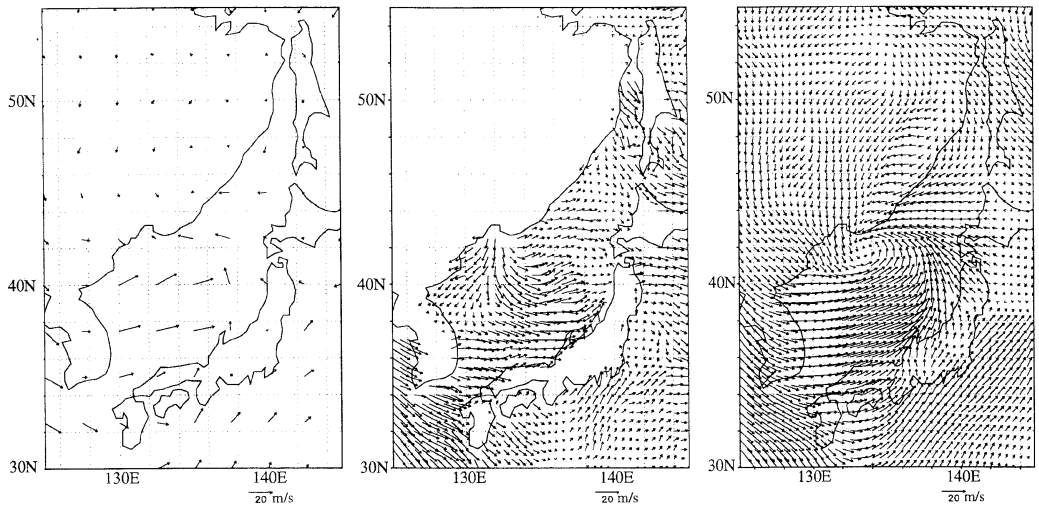

Fig. 2. Synoptic surface windfields for 12Z, 1 JAN 97 (left: ECMWF wind; center: NSCAT wind; right: MM5 wind).

moved rapidly more or less along the western side of the JES before crossing over northern Japan. The second cyclone developed in the southern JES during 5 to 6 JAN, intensified to a lesser degree, and moved slowly more or less along the eastern side of the JES (along a track ca. 500 km to the south of the first, and parallel to it) before crossing over central Japan. While the first storm can be categorized as a classical "cold air outbreak", the second storm lacked a strong outflow of cold air from Siberia and provided mostly wind-forcing.

3. The atmospheric forcing

Three sources of synoptic surface winds (noted above) were utilized for forcing JES-POM. Simultaneous "snapshots" of the three surface wind fields (Fig. 2) serve to indicate their differing attributes. For example, the ECMWF product has a resolution of 12 hrs and ca. 275 km; NSCAT has a resolution of 12 hrs and ca. 50 km; and MM5 has a resolution of 1 hr and 15 km. The three wind fields generally agree on the basin-scale; however, while the ECMWF wind field broadly indicates a cyclonic feature over the central JES, it (understandably) does not depict the seaward wind jet streaming from Vladivostok as indicated by NSCAT and MM5 fields. Further, the NSCAT field does not depict the low-level cyclonic circulation associated with the first storm that MM5 indicates, which has been validated independently with satellite visible and infrared imagery. The flow pattern of the nine-day mean surface wind stress fields (Fig. 3) of MM5, ECMWF, and NSCAT appear largely in agreement, and the maximum stress (ca. 0.2 N/m^2 in each case) occurs south of Vladivostok. However, from their difference fields (not shown) there are patterned differences with typical maximum magnitudes of 0.1 N/m^2 south of Vladivostok. The ECMWF and MM5 mean wind stress fields generally disagree significantly only within ca. 200 km of the coast due to MM5's superior resolution of coastal orography. Their significant differences with NSCAT wind stress are more widespread but greatest off Vladivostok. Also, their standard deviation fields (Fig. 4) are indicative of substantial differences in the underlying six hourly synoptic fields. The consequences for JES circulation of these differences in the forcing fields will be examined below.

The MM5 heat flux pattern is also of interest because it is used in the present simulations and is critical to water mass transformations. The 9-day mean heat flux (Fig. 3) indicates regions in excess of 900 W/m^2 oceanic heat loss off Vladivostok, in the southernmost JES, and along the coast of Honshu. The 9-day standard deviation of the heat flux (Fig. 4) indicates values of about 300 W/m^2 in the areas of

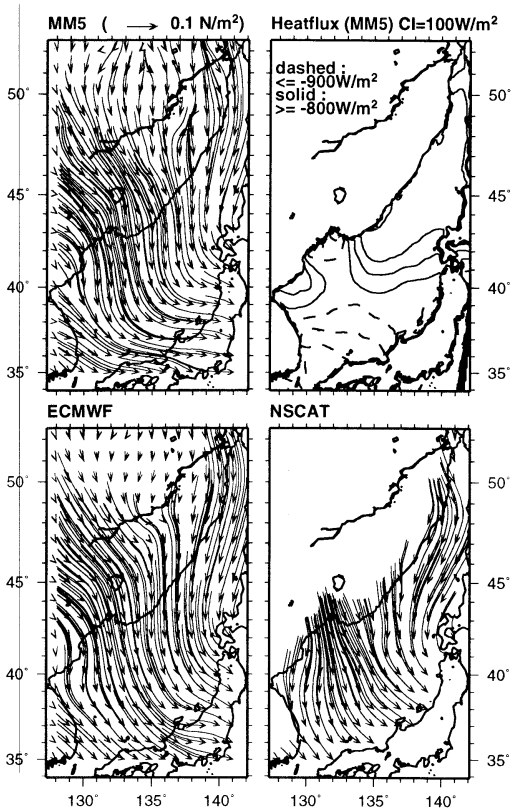

Fig. 3. Mean (1 to 10 JAN 97) of wind stress (N/m^2) from MM5, ECMWF, and NSCAT and of heat flux (W/m^2) from MM5.

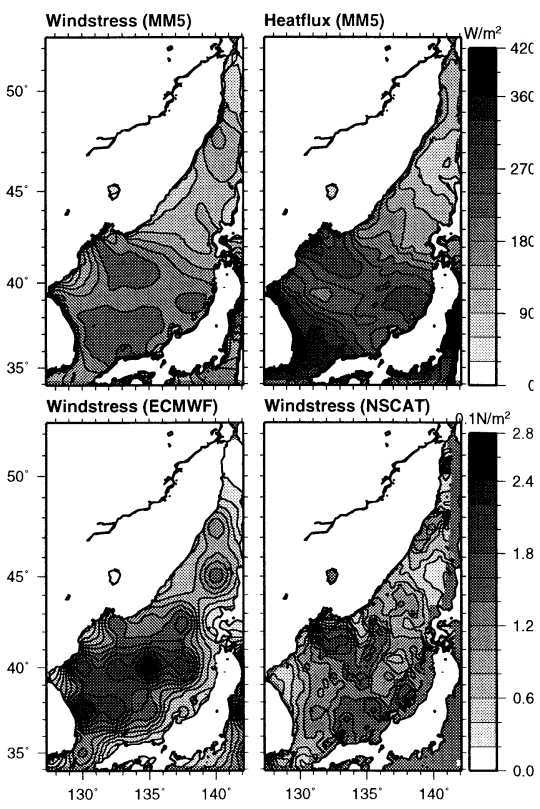

Fig. 4. Standard deviation (1 to 10 JAN 97) of wind stress (N/m^2) from MM5, ECMWF, and NSCAT and of heat flux (W/m^2) from MM5.

maximum heat loss, reflecting the intense synoptic variability.

4. The simulated JES response

Here, the focus is on the changes in seasurface height (SSH) and transport stream function (TSF) fields. The SSH field represents the barotropic divergence field, and the TSF field represents the barotropic vorticity field. Thus, the temporal variations of the SSH and TSF fields are related to the barotropic divergence and vorticity modes, respectively, of the JES basin.

The simulated 9-day mean SSH with MM5 forcing (Fig. 5) indicates the several main features of the upper layer general circulation of the JES: the East Korean Warm Current (EKWC) and its separation at 37.5 N, the meandering Subpolar Jet, the Nearshore Branch off Honshu, the cyclonic recirculation gyre off Wonsan Bay, the large recirculation cyclonic gyre over the Japan Basin, and a cyclonic gyre in the northern JES. The 9-day SSH standard deviation (Fig. 5) has a primary maximum in the northernmost JES and a secondary maximum in the southernmost JES, with typical values in the southern JES of 2 to 4 cm. The 9-day mean TSF (Fig. 5) indicates the throughflow transport from Korea Strait to Tsugaru and Soya Straits, plus the cyclonic recirculation gyres off Wonsan Bay and over the Japan Basin. The 9-day TSF standard deviation (Fig. 5) has a maximum (in excess of 3 Sv) over Yamato Rise and Japan Basin. Consequently, the spatial distribution of variability in TSF is opposite to that in SSH; i.e., high in the center and high in the north and south, respectively.

To assess the difference in the JES responses, the changes in SSH and TSF between 1 and 10

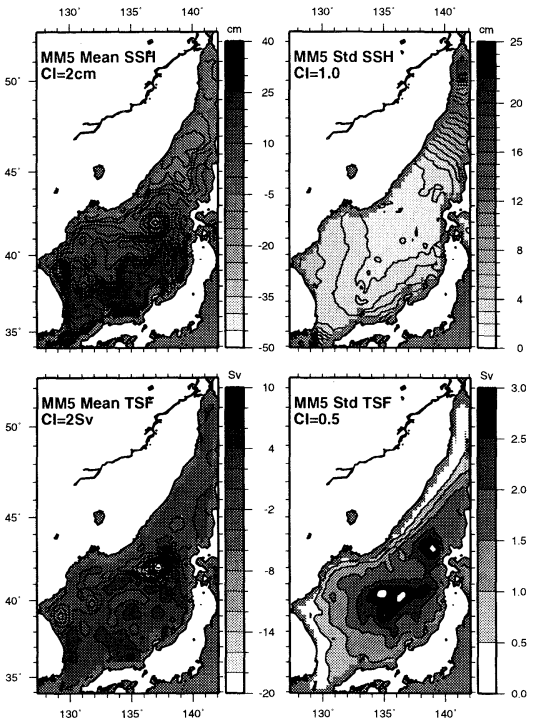

Fig. 5. Mean and standard deviation (1 to 10 JAN 97) of SSH and TSF for the MM5 case.

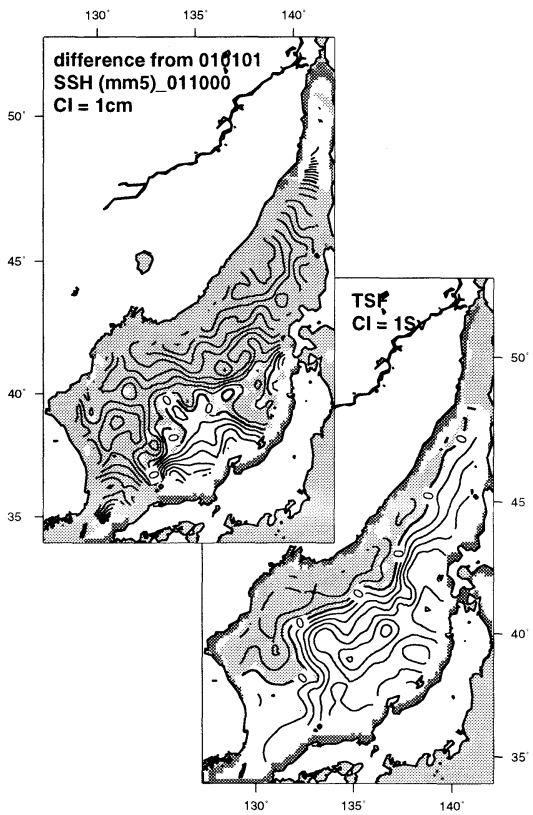

Fig. 6. SSH and TSF difference fields for 10 JAN -1 JAN 97 for the MM5 case. (Shaded area represents negative values)

January 1997 are compared for the three wind forcing fields. For conciseness, only the MM5 case is shown (Fig. 6). The SSH is setup and setdown by ca. 0.1 m in the south and north, respectively, in all three cases. However, the ECMWF and NSCAT (not shown) cases indicate a setup along the coast of North Korea and southern Russia, while the MM5 case indicates a setup along the coast of southwestern Japan, as expected. The TSF is increased and decreased by a few Sverdrups in the east and west, respectively, in all three cases. Moreover, their basin-scale patterns are very similar and suggestive of a response composed of basin scale modes, and they are each characterized by numerous mesoscale features. The temporal evolution of SSH and TSF needs further scrutiny, as given below.

To explore the nature of the dynamical response, tendencies in the barotropic divergence (SSH) and barotropic vorticity (TSF) fields are examined. The SSH and TSF difference fields (between several fiducial times given below) for the MM5 case (Figs. 7 and 8, resp.) indicate a finer temporal resolution analysis of the simulated fields, as given in the next section with EOFs, to characterize better the nature of the temporal variability. These fields were evaluated for the beginning of storm 1 minus start of synoptic run (12Z/1 JAN-01Z/1 JAN), end of storm 1 minus beginning of storm 1 (00Z/3 JAN-12Z/1 JAN), beginning of storm 2 minus end of storm 1 (06Z/5 JAN-00Z/3 JAN), end of storm 2 minus beginning of storm 2 (00Z/7 JAN-06Z/5 JAN), and stop of synoptic run minus end of storm 2 (00Z/10 JAN-00Z/7 JAN).

As measures of the sensitivity of the simulated response to the wind-forcing, the SSH and TSF difference fields for the NSCAT minus MM5 cases (Figs. 9 and 10, respectively) and ECMWF minus MM5 cases (not shown) are examined for the fiducial times utilized above.

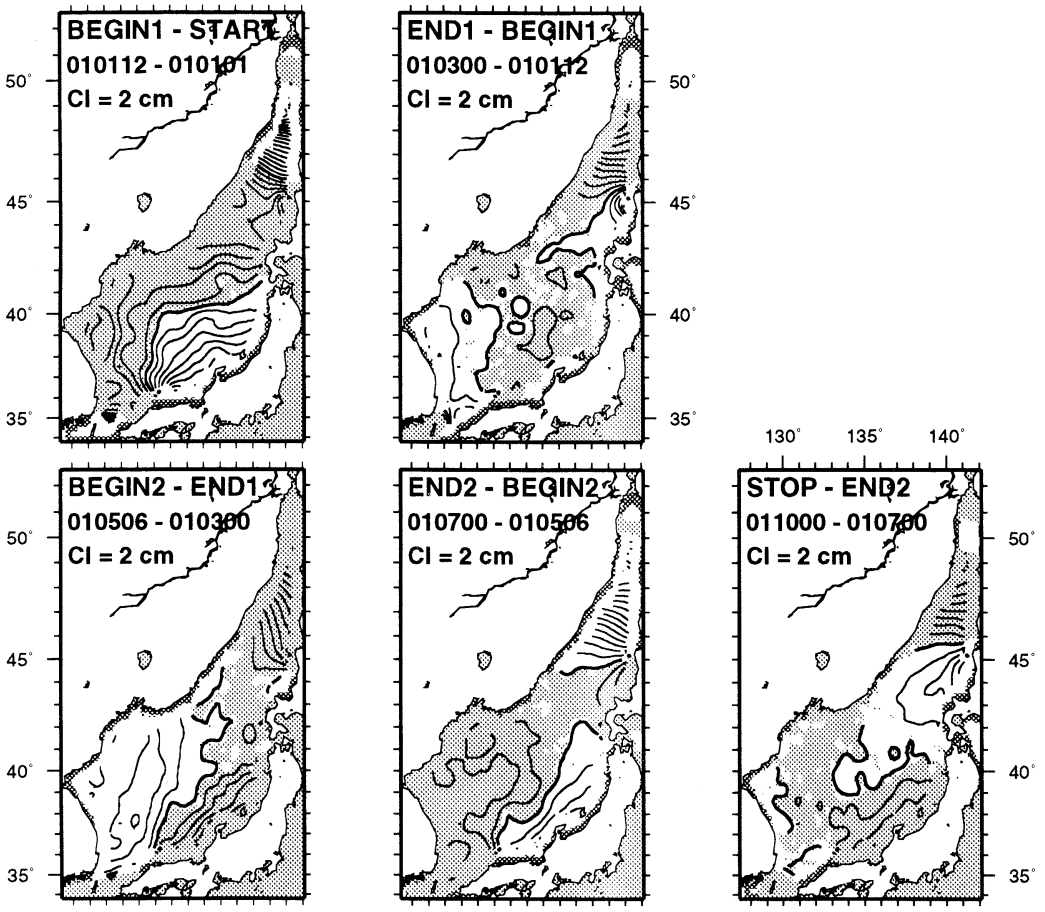

Fig. 7. SSH difference fields for the MM5 case. (Shaded area represents negative values)

Clearly, there are instantaneous basin-scale differences of order ±0.1m in SSH and ±6 Sv in TSF which, however, are substantially attenuated by the end of the calculations. (The patterns and magnitudes of the differences for the ECMWF minus MM5 cases (not shown) are very similar to those of NSCAT minus MM5 cases.) Thus, the calculated responses are very sensitive to the synoptic forcing used, though the "correct" forcing and response are not known and the attributes of ECMWF and NSCAT that lead to these differences have not been isolated.

While the emphasis here is on some aspects of the dynamical response, one aspect of the thermohaline response is examined, too, viz., the upper ocean thermal response at 41.5 N, 133.0 E. This position is located in the hypothesized Japan Sea Proper Water formation region (SENJYU and SUDO, 1996) and the designated "flux center" (KAWAMURA and WU, 1998), i.e., north of 41 N and between 132 and 134 E, as highlighted by previous authors (e.g., SEUNG and YOON, 1995). The temperature anomaly of the upper 100 m (Fig. 11) for the MM5 case indicates a rapid cooling in the upper 40 m during passage of the first cyclone and gradual cooling during the remainder of the period. While the SST decreased by a total of 0.9 C, the cooling depth increased to nearly 100 m, which is consistent with previous estimates for cooling due to cold air outbreaks in this region (e.g., KAWAMURA and WU, 1998). The cooling at this location for the NSCAT and ECMWF cases (not shown) was similar in SST decrease (also ca. 0.9 C). However, the cooling

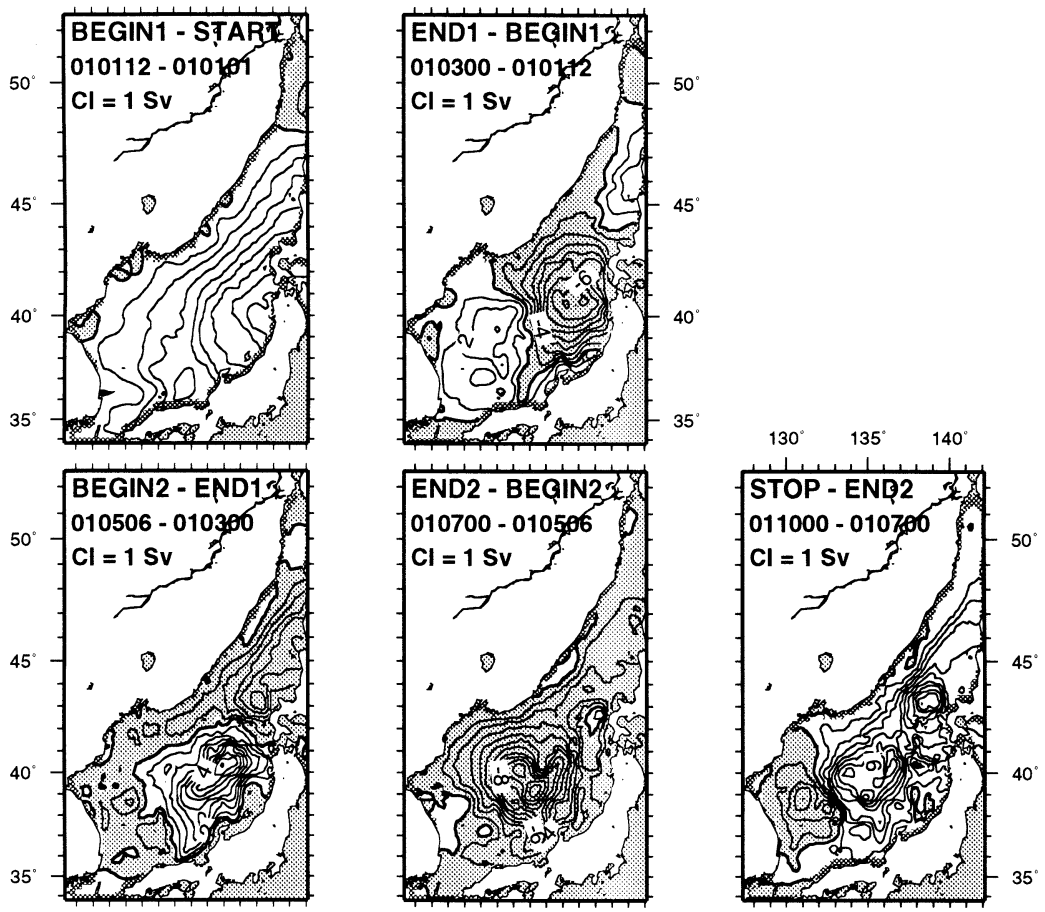

Fig. 8. TSF difference fields for the MM5 case. (Shaded area represents negative values)

depth was nearly 150 m for NSCAT and more than 150 m for ECMWF cases. These case-dependent differences in cooling response may become significant for longer integrations. The cooling response was highly spatially dependent (not shown) in the "flux center"; for example, at 42.5 N, 133.0 E, the cooling penetrated to 300 m while it was mainly confined to the upper 50 and 30 m at 41.5 N, 135.0 E and 42.5 N, 135.0 E (not shown), resp., in the MM5 case. The spatial variations in cooling response of the NSCAT and ECMWF cases were qualitatively similar to those of the MM5 case at these locations.

5. EOF Analyses

To efficiently characterize the space-time dependence of the transient response to the two cold air outbreaks, EOF analyses of 6-hourly gridded (subsampled by 1/3) SSH and TSF fields are presented for the MM5 case.

For SSH, the first four EOFs account for 70.8% of the variance. The spatial patterns of EOF1 and 4 (Fig. 12) are similar in the southern JES: when SSH is high along the Korean and southern Russian coasts, it is low along the Honshu coast; thus, they are basically zonal modes. The amplitudes (Fig. 13) are dominated by the weekly time scale and are in quadrature. Similarly, the spatial patterns of EOF 2 and 3 (Fig. 12) are similar throughout the JES except in the Korea (Tsushmia) Strait: when SSH is high in the southern basin it is low in the northern basin; thus, they are basically meridional modes. The amplitudes (Fig. 13) are dominated by the daily time scale,

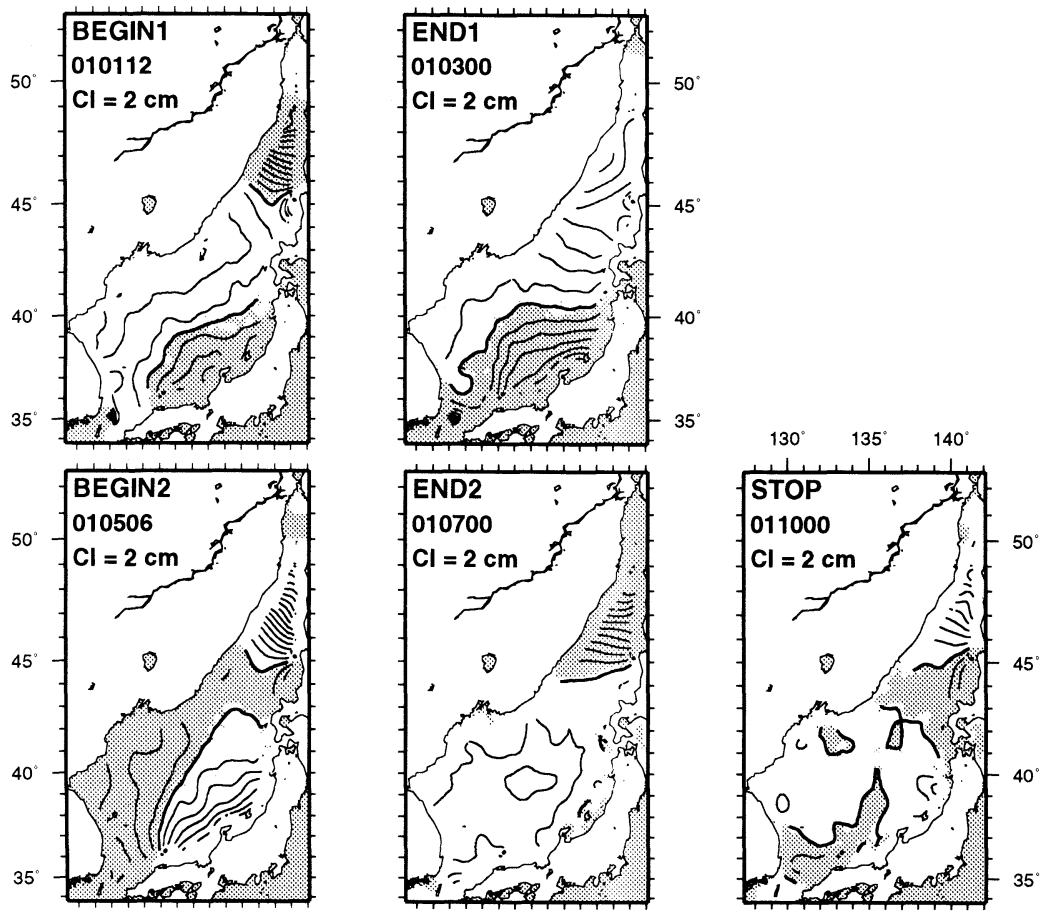

Fig. 9. SSH difference fields for the MM5-NSCAT cases. (Shaded area represents negative values)

which is due to aliasing of near-inertial energy. There is not a simple phase relation between their amplitudes except immediately after the passage of the first and second storms when they are in-phase.

For TSF, the first four EOFs account for 84.5% of the variance. The spatial patterns of EOF 1, 2, 3, and 4 all have a different character (Fig. 14). EOF 1 is in-phase throughout the basin, with an antinode over the Yamato Rise and Japan Basin; EOF 2 is basically a meridional mode, EOF 3 is basically a zonal mode, and EOF 4 is a sub-basin-scale mode. The EOF 1 amplitude (Fig. 15) is dominated by a strong reversal (change of sign) event associated with the passage of the second cyclone. There is a secondary fluctuation associated with the aliased near-inertial motion. The EOF 2 and 3 amplitudes are dominated by impulses of opposite sign associated with the passages of the two cyclones, and they are in quadrature. The EOF 4 amplitude is dominated by positive pulses associated with each cyclone passage and a strong reversal event during the final relaxation phase.

6. Summary

While the net change in barotropic vorticity (TSF) over nine days is not very sensitive to the differences in the three wind-forcing fields, the net change in barotropic divergence (SSH) is more sensitive to the choice of forcing. The synoptic response includes several basin-scale, barotropic vorticity and divergence modes. The modal amplitudes primarily vary with the timescale of the cold air outbreaks, but some

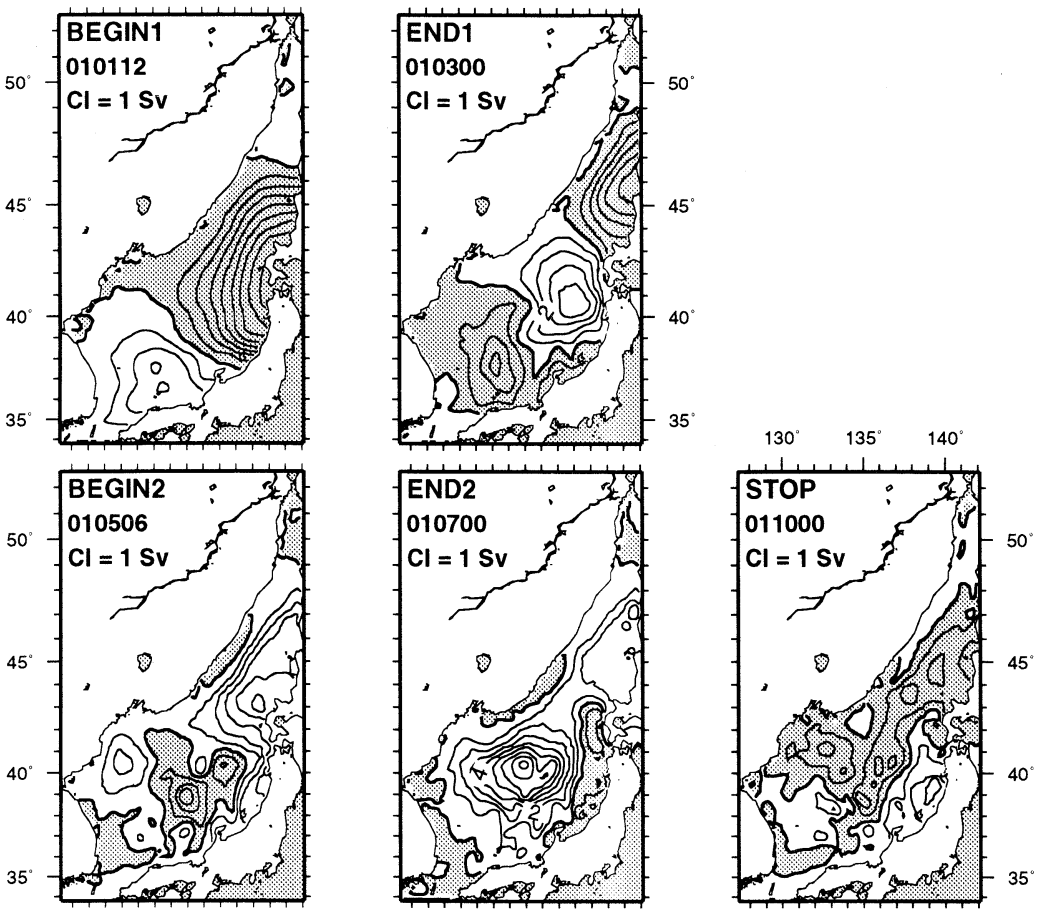

Fig. 10. TSF difference fields for the MM5-NSCAT cases. (Shaded area represents negative values)

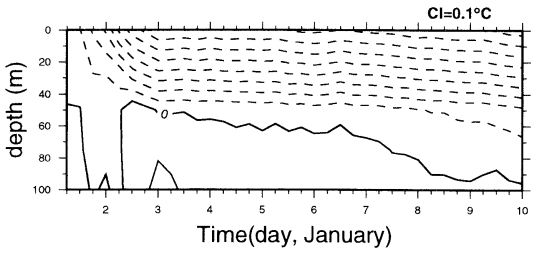

Fig. 11. Time-depth plot of temperature differences relative to the first temperature profile at 41.5N, 133E, 1 to 10 JAN 97 for the MM5 case. (Dashed lines represent negative values, cooling)

secondarily vary with a near-inertial period. These modes are intense enough that they should be detectable in time series of observations and synoptic maps. The cooling response of the upper ocean in the "flux center" off Vladivostok is consistent with this being a region where the seasonal succession of cold air outbreaks produces significant convection and ventilation. These issues will be pursued further with longer simulations. Overall, the sensitivity in temporal evolution for different forcing fields indicate that it is useful to utilize a data-assimilative atmospheric mesoscale model (e.g., the PSU/NCAR MM5) for accurate estimations of the atmospheric forcing associated with cold air outbreaks and the simulation of the response of JES to them.

Acknowledgement

This research was sponsored by the Navy Ocean Modeling and Prediction (NOMP) Program and the Departmental Research Initiative

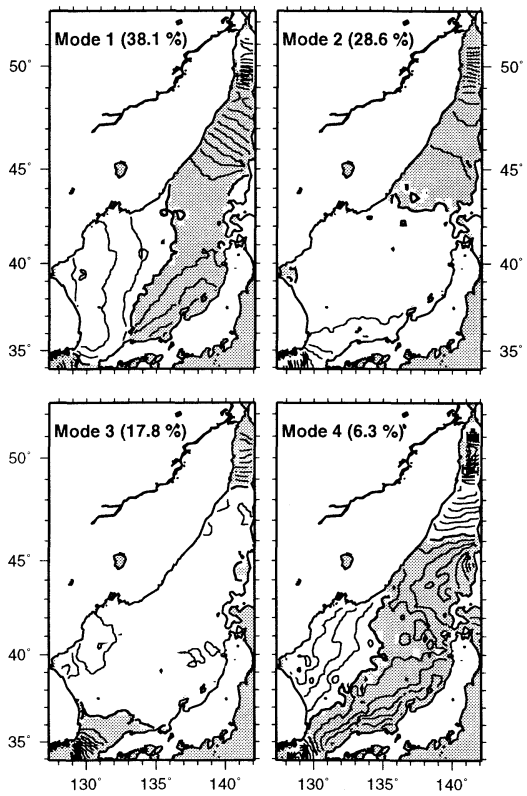

Fig. 12. Spatial patterns for first four SSH EOFs for the MM5 case. (Shaded area represents negative values)

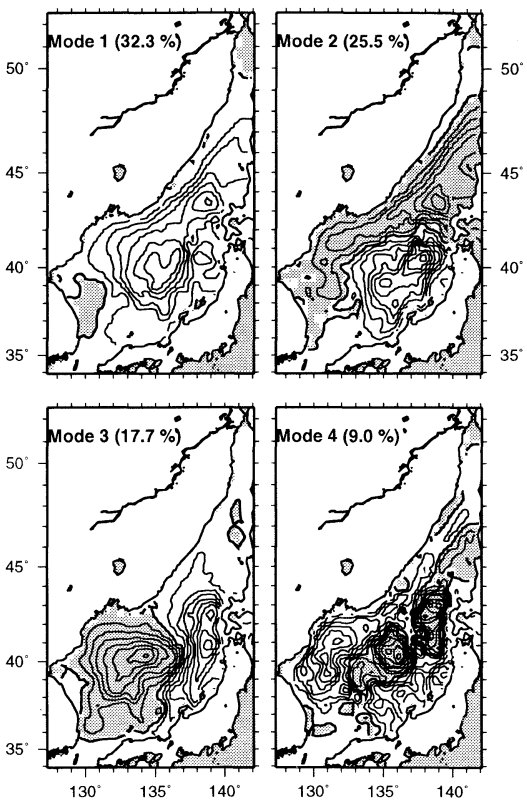

Fig. 14. Spatial patterns for first four TSF EOFs for the MM5 case. (Shaded area represents negative values)

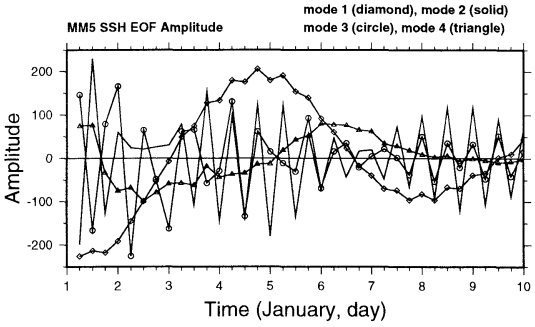

Fig. 13. Time-varying amplitudes (1 to 10 JAN 97) for first four SSH EOFs for the MM5 case.

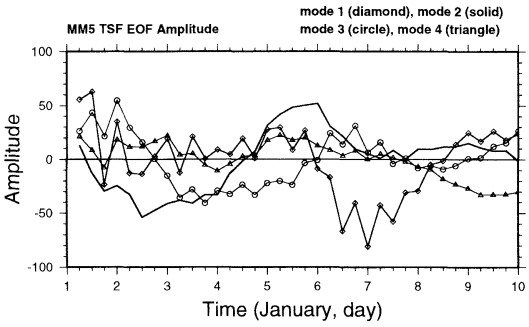

Fig. 15. Time-varying amplitudes (1 to 10 JAN 97) for first four TSF EOFs for the MM5 case.

(DRI) for the Japan (East) Sea (JES) of the U.S. Office of Naval Research. Dr. W. Timothy LIU, JPL provided the NSCAT wind analysis. Constructive comments by Academician Artem S. SARKISYAN, INM/RAS are gratefully acknowledged.

References

BANG, I., J. -K. CHOI, L.KANTHA, C.HORTON, M.CLIFFORD, M. -S. SUK, K. -I. CHANG, S. Y. NAM, and H. -J. LIE (1996): A hindcast experiment in the East Sea (Sea of Japan). La Mer, **34**: 108-130.

BLUMBERG, A. F. and G. L. MELLOR (1987): A

description of a three-dimensional coastal ocean circulation model. In: Three - Dimensional Coastal Ocean Models (Ed., N. S. HEAPS), Coastal and Estuarine Sciences, **4**: 1-16.

DUDHIA, J. (1993): A nonhydrostatic version of the Penn State-NCAR mesoscale model: Validation test and simulation of an Atlantic cyclone and cold front. Mon. Wea. Rev., **121**: 1493-1513.

KANG, H. S. (1997): Implementation, sensitivity testing, and evaluation of a numerical model for the East/Japan Sea circulation. University of Miami Technical Report, No. RSMAS-97-008, 174 numb. leaves.

KAWAMURA, H. and P. WU (1998): Formation mechanism of Japan Sea Proper Water in the flux center off Vladivostok. J. Geophys. Res., **103** (C10): 21, 611- 21,622.

LEVITUS, S. (1982): Climatological Atlas of the World Ocean. NOAA Prof. Paper 13, NOAA / ERL / GFDL, Princeton, NJ, 190 pp.

NA, J. -Y., J. -W. Seo and S. -K. Han (1992): Monthly mean sea surface winds over the adjacent seas of the Korea Peninsula. J. Oceanogr. Soc. Korea, **27**: 1-10.

SENJYU, T. and H. SUDO (1996): Interannual variation of the upper portion of the Japan Sea proper water and its probable cause. J. Oceanogr., **52**: 27-42.

SEUNG, Y. H. and J. H. YOON (1995): Some features of winter convection in the Japan East Sea. J. Oceanogr., **51**: 61-73.

Revised on February 5, 2000
Accepted on October 2, 2000

賛助会員

アレック電子株式会社	神戸市西区井吹台東町７－２－３
株式会社イーエムエス	神戸市中央区多聞通３－２－９
有限会社英和出版印刷	文京区千駄木４－20－６
株式会社内田老鶴圃 内田　悟	文京区大塚３－34－３
財団法人海洋生物環境研究所	千代田区内神田１－18－12　北原ビル
株式会社川合海苔店	大田区大森本町２－31－８
ケー・エンジニアリング株式会社	台東区浅草橋５－14－10
国土環境株式会社	世田谷区玉川３－14－５
三洋測器株式会社	渋谷区恵比須南１－２－８
株式会社高岡屋	台東区上野６－７－22
テラ株式会社	世田谷区代田３－41－８　代田ウエスト５Ｆ
日本海洋株式会社	北区栄町９―３
株式会社三菱総合研究所（社会システム部）	千代田区大手町２－３－６
渡邊機開工業株式会社	愛知県渥美郡田原町神戸大坪230

日仏海洋学会入会申込書

（正会員・学生会員）

	年度より入会	年　月　日申込
氏　名 ローマ時		年　月　日生
住　所　〒 勤務先　機関名 電　話		
自　宅　住　所　〒 電　話		
紹介会員氏名		
送付金額　円	送金方法	
会誌の送り先（希望する方に○をつける）	勤務先　自　宅	

（以下は学会事務局用）

受付	名簿 原簿	会費 原簿	あて名 カード	学会 記事

入会申込書送付先：〒150-0013 東京都渋谷区恵比寿 3-9-25

（財）日仏会館内

日 仏 海 洋 学 会

郵便振替番号：00150−7−96503

2000年12月25日印刷
2000年12月28日発行

うみ　第38巻 第4号

定価 ¥1,600

編集者　山口征矢
発行所　日仏海洋学会
　　財団法人　日仏会館内
　　東京都渋谷区恵比寿3-9-25
　　郵便番号：150-0013
　　電話：03（5421）7641
　　振替番号：00150-7-96503
印刷者　佐藤一二
印刷所　㈲英和出版印刷社
　　東京都文京区千駄木4-20-6
　　郵便番号：113-0022
　　電話：03（5685）0621

本雑誌に関する問い合わせ　電話番号 03(5463)0462

Tome 38 N° 4

SOMMAIRE

The Proceedings of the 5th International Marine Science Symposium on the Physical, Biological, Chemical and Geological Processes in the Pacific Ocean and Asian Marginal Seas (The tenth PAMS/JECSS Workshop) 7-9 October 1999, Kagoshima, Japan